DEPARTMENT OF BIOCHEMISTRY AND MOLECULAR BIOLOGY

CYCLE XXIX

UNIVERSITY OF SIENA

New technology platforms applied to the profiling of gene and protein expression at the single T-cell level

PhD thesis · 2016

M.Sc. Trine Meldgaard

New technology platforms applied to the profiling of gene and protein expression at the single T-cell level

PhD thesis · 2016

M.Sc. Trine Meldgaard

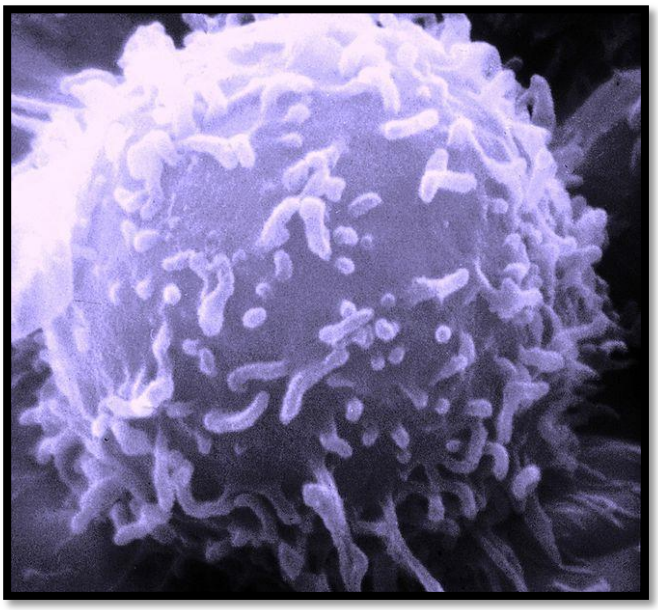

Siena University Supervisor: Prof. Cosima Tatiana Baldari

GSK Vaccines S.r.l. Supervisor: Dr. Sylvie Bertholet

Submitted: October 2016

This thesis is dedicated to my family and friends

who have always been there no matter what

Thank you ☺

Table of content

Acknowledgements

First of all, I would like to thank my supervisor Sylvie Bertholet without whom this project would have never existed. You are one tough lady, but I have learnt so much and have grown considerably in your company! Secondly, I would like to thank my university supervisor Cosima Tatiana Baldari and the entire HOMIN (Host-Microbe Interactions under ITN Marie Curie) team for support, ideas and guidance (and funding). Roland Kratzer, for setting up the project and helping me physically in the lab the first 3 months, and for the rest of the stay through lots and lots of emails. Fabiola Blengio and her supervisor Emilio Siena - without her great work, none of this would have ever happened, I thank you from the bottom of my heart and back. The Flow-Cy-TOF Core Facility: Chiara Sammicheli & Simona Tavarini, for their endless effort in the lab and outside, on the single-cell sorting, mass spectrometry experiments and everything in between. I would also like to thank their boss, Sandra Nuti, for support. Many thanks to the formulation team and animal facility staff for always providing great services and tremendous helpfulness. My fellow PhD students for the endless coffees, complaining sessions and success celebrating – you guys rock.

And last but definitely not least, a thanks to the people important in my life, my family and friends – you know who you are - for yet again understanding why I had to travel, this time not to the other side of the world, but still far for my studies and career, for being there when I needed you and for always listening and giving me supportive backup. Without you I would never have made it. Finally, to my dearest hubby Niklas, thank you for believing in me, even when I do not believe in myself, thank you for bringing light into my very confusing world and thank you for being you. You make this world much brighter, and you mean the world to me!

Abbreviations

$^{191/193}$Ir	Iridium 191/193
^{103}Rh	Rhodium 103
Ab	antibody(is)
aMIV	MF59^{TM}-adjuvanted Monovalent Influenza Vaccine
APC	allophycocyanin
BSA	bovine serum albumin
CFSE	carboxyfluorescein succinimidyl ester
CMTMR	5-(and-6)-(((4chloromethyl)benzoyl)amino) tetramethylrhodamine
CNE	cationic nano-emulsion
CXCR	chemokine receptors
CyTOF	mass cytometry time-of-flight
cRPMI	complete Roswell Park Memorial institute medium
CSM	cell staining medium
CSM-S	cell staining medium-saponin
Cq	quantification cycles
D10p1	day 10 post first immunization
D3p2	day 3 post second immunization
D9p2	day 9 post second immunization
D10p2	day 10 post second immunization
d.nm	diameter nanometer
DEG	differentially expressed genes
FACS	fluorescence activated cell sorting
FAM	6-carboxyfluorescein
FasL	Fas Ligand
FBS	fetal bovine serum
FDR	false discovery rate
FISH	fluorescent *in situ* hybridization
FITC	fluorescein isothiocyanate
GOI	gene of interest
HA	Hemagglutinin
HIV	human immuno-deficiency virus
HLA	human leukocyte antigen
IFC	integrated fluidic circuits
IFN	interferon
IL	interleukin
KLR	killer cell lectin-like receptors
LRT	likelihood ratio test
MGB	minor groove binder
MHC-I	major histocompatibility complex class I
NA	neuraminidase
NaN_3	sodium azide
NFQ	non fluorescente quencher
NaCl	natrium chloride
PBS	phosphate buffered saline
PCA	principle component analysis
PDI	polydispersity dndex
PE	phycoerythrin
RNA	ribo-nucleic acid
RNAseq	RNA sequencing
Rpm	revolutions per minute
RT	room temperature

RT-qPCR	reverse transcription- quantitative real-time polymerase chain reaction
SAM	self-amplifying mRNA
SAM(H1)	self-amplifying mRNA encoded with H1
SDS-PAGE	sodium dodecyl sulfate polyacryl aqmide gel electrophoresis
SLEC	short lived effector cells
SPAN	sorbitan trioleate
t-SNE	t-distributed stochastic neighbor embedding
T_{CM}	central memory T cells
TE	tris-EDTA
T_{EFF}	effector T cells
T_{EM}	effector memory T cells
TET	tetra-chloro-fluorecein
T_H	T-helper
TNF	tumor necrosis factor
TUMM-II	TaqMan universal PCR master mix II with UNG
TWEEN	polysorbate 80
UNG	uracil-n-glycosylase
w5p1	week 5 post first immunization
w6p1	week 6 post first immunization
w6p2	week 6 post second t immunization
wRPMi	wash roswell park memorial institute medium
WFI	water for injection

Abstract

Priming of antigen-specific $CD8^+$ T cells by vaccination is key for subsequent viral clearance. However, to date, $CD8^+$ T-cell characterization is performed under the assumption that cells of a particular type are identical, and not acknowledging their heterogeneous nature. It has recently been proven, in many different studies, that cells do differ quite significantly and can drive different responses. In order to characterize the heterogeneity of vaccine-induced $CD8^+$ T cells, we performed gene expression profiling and protein characterization at the single-cell level, after delivery of influenza RNA-based vaccine (SAM (H1) (A/California/07/2009 (H1/N1)) or MF59^{TM}-adjuvanted Monovalent Influenza Vaccine (aMIV (A/California/07/2009 (H1N1)). $CD8^+$ T cells were isolated from mouse splenocytes, stained with MHC class-I $HA_{533-554}$ pentamer and either single-cell sorted, lysed, and processed for reverse transcription- quantitative real-time polymerase chain reaction (RT-qPCR) analysis of 96 individual genes, or characterized by mass cytometry for the expression of 32 biomarkers. In parallel, the functionality of the $CD8^+$ T cells was assessed in an *in vivo* cytotoxic assay.

$CD8^+$ T cells induced by the SAM(H1) vaccine showed increased antigen-specific lysis activity *in vivo*, compared to cells induced by aMIV. *Ex vivo*, higher frequencies of $HA_{533-541}$-pentamer$^+CD8^+$ T cells were induced by SAM(H1) compared to aMIV at all time points tested, and pentamer$^+$ cells were single-cell sorted for gene expression analysis. Refined analysis of T_{EFF} (*il-7rα*$^{-}$ *cd62l*$^{-}$), T_{EM} (*il-7rα*$^{+-}$*cd62l*$^{-}$) and T_{CM} (*il-7rα*$^{+-}$*cd62l*$^{+}$)) highlighted significant differences in gene expression profiles between and within the vaccines. Overall, SAM(H1) induced mostly T_{EM} cells, while aMIV induced equal number of T_{CM} and T_{EM} cells. Both vaccines induced few T_{EFF} cells, and only $CD8^+$ T cells from SAM(H1) showed T_{EFF} terminally differentiated short-lived effector cells (SLEC) (*klrg1*$^{+}$*il-7rα*$^{-}$*cd62l*$^{-}$*cxcr3*$^{-}$*tbet*$^{+}$*blimp-1*$^{+}$). Ten days after the second immunization, T_{EM} cells, unlike T_{CM} cells, showed a transcriptional difference between the vaccines. SAM(H1) and aMIV, with up regulation of members of the cytolytic/Fas Ligans (FasL) and tumor necrosis factor (TNF) Superfamily pathways, respectively. A specific molecular signature of 12 differentially expressed genes (DEG) was identified and further evaluated at the protein expression level using mass cytometry. Most of the proteins corresponding to the 12 DEG list were also expressed.

The aim of this study was to apply state-of-the-art technology platforms to the study of gene and protein expression by immune cells in response to vaccination. With this approach, we identified distinct $HA_{533-541}$-pentamer$^+CD8^+$ T-cell subsets elicited by RNA- and adjuvanted protein-based vaccines, which revealed a particular biomarker signature associated to each vaccine. In conclusion, our results showed that these novel technology platforms might be extremely useful for the in-depth characterization of immune responses to vaccination and can be extended to other medical applications.

Chapter 1: Introduction

1.1. Aim and rationale of the thesis

Many biological experiments are to date performed under the assumption that all cells of a particular "type" are identical. This bulk analysis, although informative, assumes ensemble averages that reflect the dominant biological mechanism operating within the entire population, and ignores essential cell-to-cell differences. To fully understand if cellular heterogeneity contributes to biological function or contains relevant information, a single-cell approach must be applied. Recent data suggests that individual cells within a single population may differ quite considerably and these differences can drive function of the entire cell population. Even within what seems to be a homogeneous population, there are considerable differences between individual cells and multiple studies have shown the individualism of single cells[1–7].

Current available techniques used to study cells are performed on bulk samples or with limitation in the number of biomarkers evaluated simultaneously. In microarray, the expression of thousands of genes are measured instantaneously, however, the technique is limited to the analysis of cells at the bulk population level in which cells are assumed to behave in a constant manner, or on single cells where transcripts in low abundance, as single cells indeed are, have limited accuracy of expression[8,9]. Moreover, techniques such as fluorescence activated cell sorting (FACS) are performed on the single-cell level, but have a limited number of biomarkers, which can be expressed within a single experiment[10–12]. This does not indicate the very complex structure of cell populations, and subtle subpopulations might be ignored. All cells are unique in their expression pattern. Each individual cell has a function to carry out, whether it is thermoregulation, nerve signaling or immune functions. Cell populations, especially in the immune system, are highly heterogeneous[13,14]. By dissecting this heterogeneity, one could reveal subsets of cells functionally different and clearly understand the mechanism(s) of protection after infection or vaccination. Single-cell approaches can be used to study the immune responses to new vaccines or to compare the effect of different vaccine adjuvants.

Newly emerging approaches enable high dimensional profiling of the molecular components in individual cells, and have the potential to complement existing work. In this thesis, we focus on two of these emerging single-cell analysis platforms: reverse transcription- quantitative real-time polymerase chain reaction (RT-qPCR) (BioMark (Fluidigm) HD system)[4–7] and mass cytometry time-of-flight (CyTOF-1 mass cytometer (Fluidigm))[15–17], allowing the detection of (>100) or (>30) biomarkers in a single-cell, respectively. Expression of specific combinations of biomarkers gives the opportunity to identify new correlates of immunogenicity and further understand the immune cellular mechanisms of action following vaccination. Emerging single-cell profiling strategies enable the direct assessment of molecular mechanisms that have conventionally been obscured in bulk samples. These new single-cell approaches will refine our cellular classification schemes, potentially revealing new and functionally distinct subsets of cells of the immune system, but could also be applied for the use in other medical fields such as immunotherapy and drug discovery.

In this thesis, we focused on the single-cell characterization of antigen-specific $CD8^+$ T cells, which play a key role in immunological functions. In order to induce antigen-specific CD8+ T cells, mice have been vaccinated with either an adjuvanted protein vaccine or a ribo-nucleic acid (RNA)-based vaccine. Cells were hereafter characterized by three methods: i) Cells were analyzed for their cytotoxic activity in an *in vivo* killing assay. Here, peptide-labeled naïve cells were adoptively transferred into vaccinated mice, and the level of specific killing was estimated. ii) Alternatively, antigen-specific T cells were single-cell sorted based on their $CD8^+$ phenotype and antigen-specificity, and levels of gene expression was assessed using a high-throughput RT-qPCR technique. A set of specific biomarkers were selected from the literature and applied to this fluorescent RT-qPCR, allowing the identification of antigen-specific $CD8^+$ T-cell subpopulations elicited by the different vaccine candidates, and biomarker signatures between the vaccines were revealed. iii) This molecular signature was further validated at the protein level from antigen-specific cells using mass cytometry.

1.2. Model of single-cell analysis – vaccine induced lymphocytes

The immune system work through complex processes that allow the formation, activation, and maintenance of many different cell types[13,18]. Development of immune resistance to any infection is based on proper priming of immune cells after infections or with vaccinations. Vaccination is the most cost-effective way to prevent a primary infection, through the induction of appropriate cellular immune responses combined with the production of protective antibodies (Ab). Many licensed influenza vaccines are available today (live attenuate, inactivated, subunit) with numerous new vaccine candidates under development, such as vectored, DNA or RNA vaccines, to help target the desired immune response. However, there is a need to understand in depth the cellular response in order to design vaccines that target the correct immune cells, something that can be done with novel single-cell techniques.

In order to decrease primary infection rate and symptoms, and to prevent secondary and further infections with the same pathogen, immune cells are stimulated and activated. The immune cells, also called leukocytes, are derived from one multipotent hematopoietic stem-cell in the bone marrow and can differentiate into diverse types of immune cells depending on the stimulatory signal received (figure 1.1). There are mainly two division groups: myeloid (granular) and lymphoid (non-granular) cells[18]. Myeloid progenitor gives rise to red blood cells (erythrocytes), platelets (blood clotting) and innate cells (first line of defense such as monocytes/macrophages, dendritic cells and granulocytes). The lymphoid progenitor gives rise to the adaptive immune response with lymphoid lineage of white blood cells or leukocytes; natural killer cells, B and T lymphocytes. One of the key players of the adaptive immune response is the T lymphocytes. There are two main populations of T cells based on the expression of membrane glycoprotein CD4 ($CD4^+$ T cells) and CD8 ($CD8^+$ T cells), and the latter is the focus of this thesis.

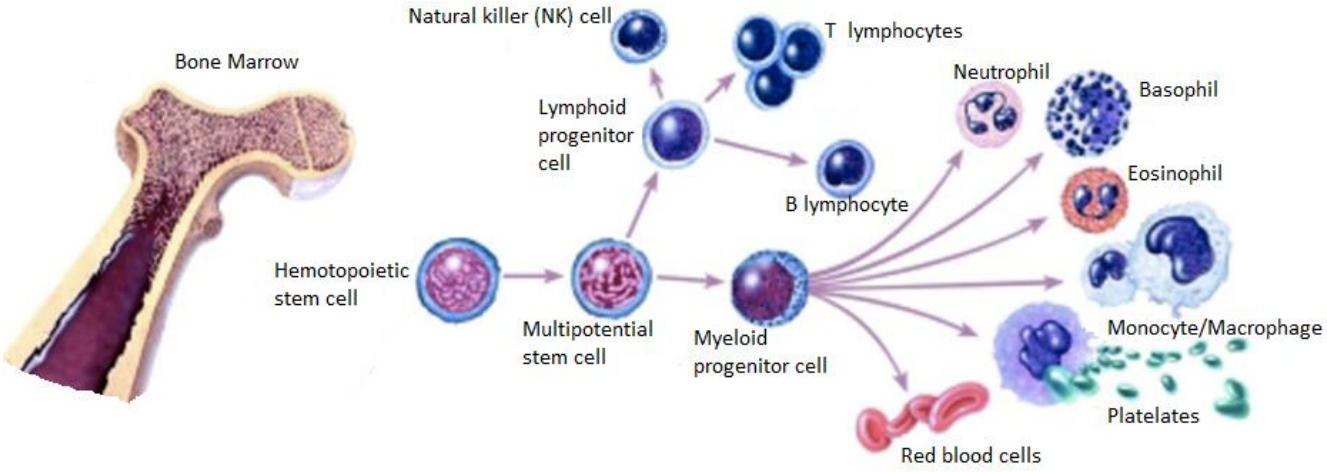

Figure 1.1: Cells of the Immune System. Cells of the immune system are developed within the bone marrow, and arise from a pluripotent hematopoietic stem-cell. These pluripotent cells are normally divided into two types of stem cells: A common lymphoid progenitor which gives rise to the lymphoid lineage of white blood cells or leukocytes (B-, and T-cell lymphocytes and natural killer cells) or a common myeloid progenitor gives rise the rest of the leukocytes (red blood cells (erythrocytes), platelets (produce platelets for blood clotting), monocytes/macrophages, dendritic cells and granules (neutrophils, eosinophils, basophils)). Source: adapted from www.NIH.gov.

1.2.1. $CD8^+$ T-cell mediated immunity

1.2.1.1. $CD8^+$ T cells

$CD8^+$ T cells are one of the key players in the adaptive immune response, found during cytotoxic viral clearance and as memory for a fast recall of immunity with a secondary infection. They are stimulated by Antigen-Presenting Cells presenting pathogen-derived peptides bound to major histocompatibility complex class I (MHC-I) molecules. $CD8^+$ T-cells are stimulated by intracellular pathogens or during viral infection[18] and are mainly considered of cytotoxic nature. Priming of antigen-specific CD8+ effector T cells (T_{EFF}) cells in response to infection or vaccination followed by development into different memory T-cell subsets are key factors for subsequent fast immune responses and viral clearance in case of secondary infections see figure 1.2.A[1,19–22].

The kinetics of the $CD8^+$ T-cell response is important and each single-cell is unique. After stimulation, which initiates in lymphoid organs, antigen-specific $CD8^+$ T_{EFF} cells will expand and be recruited to the site of infection, where they will kill virus-infected cells expressing MHC-I/peptide complexes. Upon

antigen-specific recognition, $CD8^+$ T cells will release cytotoxic molecules at the site of cell contact, ultimately leading to the target cell undergoing DNA fragmentation and apoptosis, with no further spread of the intracellular pathogen. The $CD8^+$ T cells then migrate to a new target and repeat the process until the infection is cleared. Some of the cytotoxic molecules that can be considered as biomarkers of cytotoxicity are perforin[18,23] (pore forming protein that ensures the delivery of granules contents into the cytoplasm of target cells), granzymes[18,23,24] (a family of serine proteases that activate apoptosis of target cell), Fas Ligand (FasL)[18,25] (proliferation of CD8+ T cells and induction of DNA degradation and membrane blebbing), interferon (IFN)-γ[18,26] (cytokine that inhibits viral replication and induces MHC-I expression on infected cells) and tumor necrosis factor (TNF)-α[18,27] (cytokine important for regulation of lymphocyte and maintaining homeostasis during antiviral T-cell response, and inflammation by being an endogenous pyrogen inducing apoptosis and inhibit viral replication). There will also be an upregulation of inflammatory homing receptors such as chemokine receptor (CXCR)3[18,28] (viral inflammatory homing for destruction of virus infected cells), CX3CR1[18,29] (antiviral homing) and CXCR6[18] (memory trafficking of cells into inflamed tissue such as lungs, place of influenza viral infections), and spi6 (a molecule found in the cytoplasm, inhibiting cytotoxic $CD8^+$ T cells from releasing cytotoxic content from within themselves to prevent self-apoptosis)[18,30]. Killer cell lectin-like receptors (KLR) are also important receptors upregulated during infection: KLRC[18,31] (Prevent apoptosis, preserve $CD8^+$ T cells), KLRD[18,32] (Regulate antiviral CD8+ T cells), KLRG18,33 (terminally differentiated short lived effector cells (SLEC) subpopulation) and KLRK[18,34] (activation of cytotoxic $CD8^+$ T cells). After resolution of an acute infection most antigen-specific $CD8^+$ T cells undergo apoptosis. PD1 is a normal suppression marker and indicator of exhausted cells[35,36], however, it was recently described as having more a role of controlling functional aspects of exhausted cells and to prevent terminal differentiation[37]. After infection, about 10% of $CD8^+$ T cells acquire a memory phenotype, and are found as tissue resident memory T cells or circulate in the blood, screening the body for a subsequent pathogen infection (figure 1.2.B)[18]. A specific homing to the bone marrow as a reservoir has also been described for antigen-specific memory $CD8^+$ T cells[38,39]. Many different long-term protective immune cells have been identified, mainly two broad subsets; effector memory T cells (T_{EM}) cells are defined as interleukin (IL)-$7R^{high}CD62^{low}CCR7^{low}$, and considered to be fast

producers of cytotoxic proteins, and central memory T cells (T_{CM}) defined as IL-7R^{high}CD62^{high}CCR7^{high} which have a high and robust recall rate with production of IL-2[40–44].

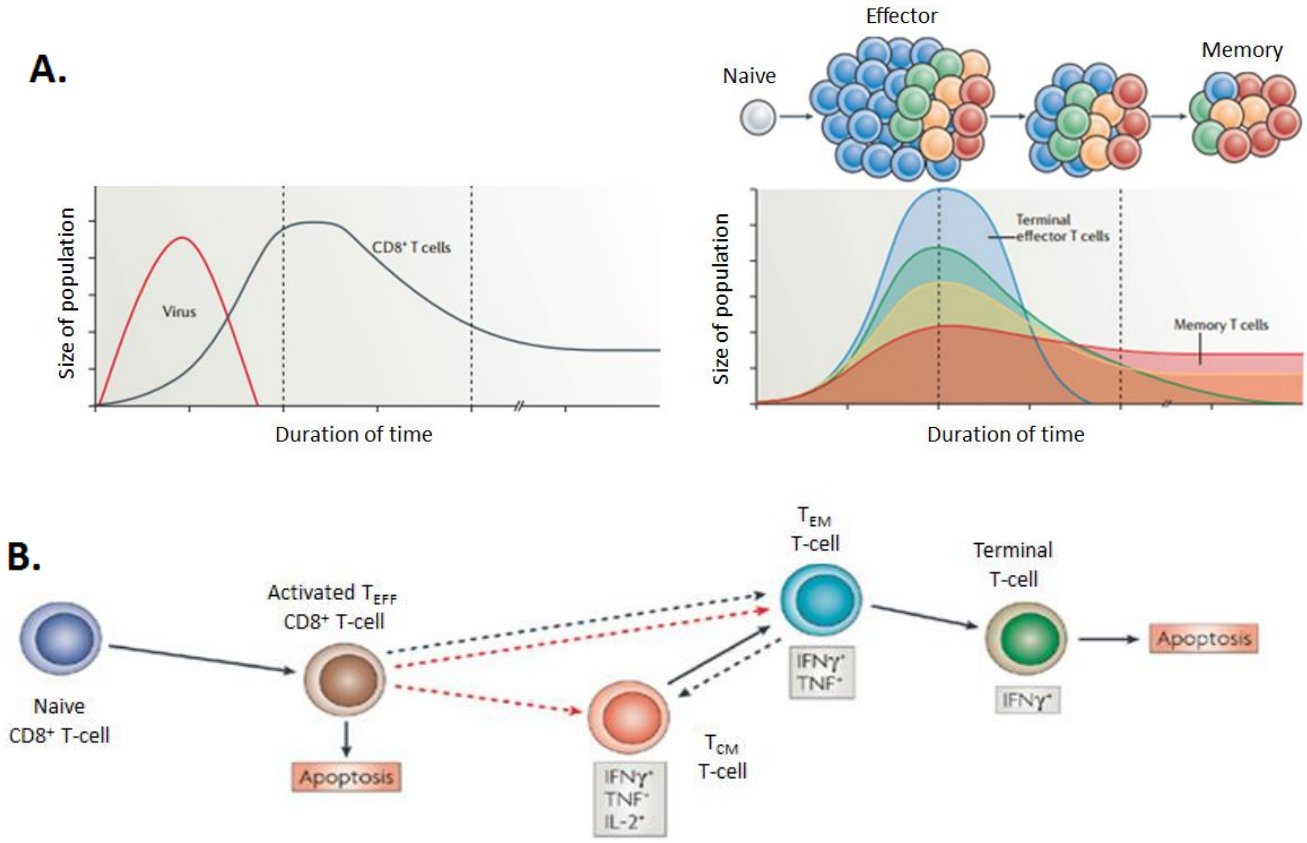

Figure 1.2: CD8$^+$ T cells. A. Kinetics of CD8$^+$ T-cell responses after viral infections and the transformation from one single naive T-cell to different cell types. **B.** After stimulation, naive CD8$^+$ T cells differentiate into a effector T-cell (T_{EFF}) response. After the initial infection, the T_{EFF} either undergo terminal differentiation with apoptosis and cell death, or develop into effector memory T cells (T_{EM}) or central memory T cells (T_{CM}). Source: A: adapted from Kaech *et al.,* 2012[44], B: adapted from Seder *et al*., 2008[42]

1.2.1.2. CD8$^+$ T-cell responses to vaccination: influenza vaccines as a model

The influenza virus is an eight segmented, negatively sensed RNA virus of the *Orthomyxoviridae* family. Five different genera are found, nevertheless, only influenza virus A, B and C are capable of infecting humans[45]. The virus undergoes seasonal genetic reassortment through antigenic drift (point mutations) or antigenic shift (genetic exchange between heterologous strains, with emergence of potential pandemic strains) resulting in altered strains capable of evading/escaping the host immune

response[45]. The structure of the virion (figure 1.3) is a spherical particle about 100 nm in diameter46. Influenza strains are characterized by two glycoproteins on the surface: hemagglutinin (HA) and NA, with 18 subtypes of HA and 11 subtypes of neuraminidase (NA) found currently[45,47,48]. HA and NA are important for viral entry by attachment to and release from the host cell, respectively. Occurrence of frequently mutating viruses by antigenic drift and shift, and the increasing resistance to drugs, are the leading challenges in influenza prevention and treatment, leading to the need of a universal influenza vaccine[49]. Large populations are at risk annually, as seasonal influenza infections can cause serious illness and hospitalization of 3-5 million individuals worldwide[50], especially in infants due to the naïve immunological state. Neutralizing Ab which neutralize the virus are very important for protection against infection, in addition, the complexity of virus-specific $CD4^+$ and $CD8^+$ T cells immune responses play a significant role in stimulating B cells and facilitating the clearance of the virus, respectively.

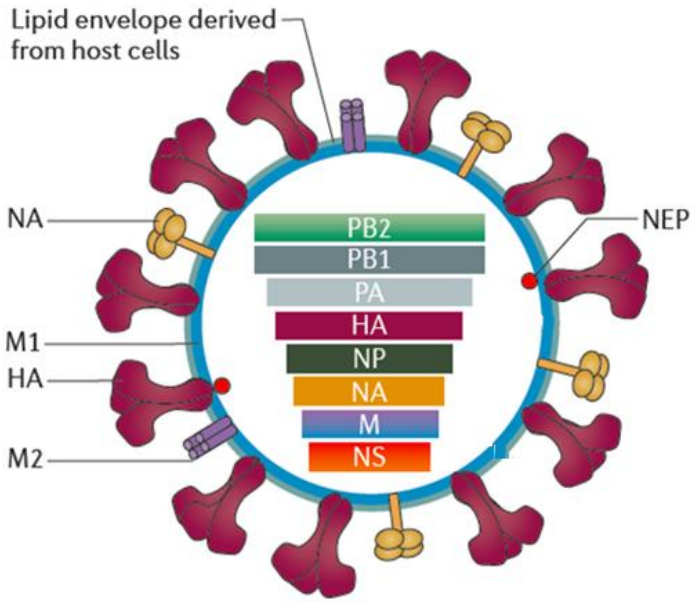

Figure 1.3: The influenza A virus. The eight stranded RNA enters target cells by the receptor binding hemagglutinin (HA) protein, and is released by acid-destroying neuraminidases (NA). The RNA-dependent RNA polymerase complex is composed of protein PB1, PB2 and PA, bound to the nucleoprotein (NP), in which the eight viral segments are wrapped around. Structural integrity is provided by the matrix protein (M1), and homeostasis is provided by the ion channel (M2). The non-structural proteins (NS1, PB1-F2 and N40) are host antiviral response, pro-apoptotic function and unknown function, respectively. The last, is the nuclear export protein (NEP). Source: adapted from Medina & García-Sastre, 2011[45].

The best and most cost-effective prevention is through vaccination. The first influenza vaccine licensed in humans was in 1945 in the USA. The vaccine was produced from an inactivated whole virus chemically inactivated[51]. Nowadays, there are several vaccines against influenza licensed for human use[49]. The seasonal trivalent/quadrivalent influenza vaccine target each year three or four influenza virus strains (two influenza A (H1N1 and H3N2) and one/two influenza B strains (Victoria or Tamagata lineages)). They are delivered as inactivated split/subunit or live-attenuated influenza vaccines[49,51,52]. Most adults have already an immunological memory against influenza antigens, meaning that the existing pool of memory cells can expand appropriately in response to the disease and vaccine. However, adjuvants such as MF59^{TM} (figure 1.4.A) are licensed to improve their immunogenicity in the elderly and in infants, who do not develop a strong enough immune response against seasonal influenza vaccines[53–55]. With this adjuvant, there is the possibility to stimulate the production of neutralizing Ab in the elderly and in infants[50,56–58]. MF59 is an oil-in-water emulsion that interacts with the antigens through electrostatic charges, and stimulates an immunogenic favorable environment for the easier uptake of the antigens at the site of injection [58,59]. Production of neutralizing Ab in response to vaccination is critical to reduce the rate of infection, but vaccines should also stimulate a robust T-cell response, especially $CD8^+$ T cells, for viral clearance after infection[21,22,38,39,60]. MF59-adjuvanted subunit vaccines induce $CD4^+$ T helper T cells for the stimulation of B cells and Ab production[22,58,59]. These current vaccines, however, still suffer from some limitations. Firstly, traditionally available egg-based influenza vaccines are complex to produce, and might induce allergic responses among some individuals[61–63], although they are slowly being replaced by cell-culture based vaccines. Moreover, the strains in the seasonal vaccine need to be updated every year with a formulation corresponding to the circulating viruses due to mismatch between vaccine strains and prevalent circulating subtypes of influenza, with production and delivery of the vaccines for the fall-winter period in the northern hemisphere. There is a wish for more broad and cross protective vaccines.

Other than adjuvanted protein vaccines, different platforms are being used for universal vaccines in pre-clinical development[49,52,64]. One approach is using a non-viral synthetic Self-Amplifying mRNA (SAM) vaccine. This approach has been successful to express antigen for a long time and to stimulate a robust T-cell response compared to conventional licensed vaccines[22,65,66]. The nucleic acids are

formulated with different delivery systems, one being a cationic nano-emulsion (CNE), which is composed of squalene, hydrofobic/hydrofilic surfactants and a cationic lipid called DOTAP. The DOTAP allows the attachment of the nucleic acid, and binds this tightly to the formulation (figure 1.4.B). The RNA/CNE formulation prevents RNAse-mediated degradation and helps deliver the replicons which contain gene of interest (GOI) to the target cell[67]**.** The current theory is that mRNA is transported to the cytoplasm by endocytosis, with an endosomal release due to the low pH in the endosomal pocket. The replicons will engage the ribosomes and launch translation of the GOI and replication of the replicon, resulting in antigen production at the immunization site ongoing for weeks (figure 1.4.B). SAM vaccines have been shown to increase the duration of antigen expression and immunogenicity *in vivo* without the need of a viral delivery system[65]. This novel vaccine technology elicited broad, potent and protective immune responses that were comparable to a viral delivery technology, but without the inherent limitations of viral vectors. In ferret studies, a decrease of virus titers was seen after vaccination with SAM encoding H1 (SAM(H1)), with an increase of total IgG-, HA inhibition- and viral-neutralizing titers[22]. After infection, SAM(H1)-vaccinated ferrets were healthier than protein alone or protein+MF59 vaccinated animals (indicated as a loss of less than 10% of weight relative to weight on the day of challenge). In addition, SAM(H1) immunization of BALB/c mice resulted in cytokine^{+}CD4^{+} T cells with a T-helper $(TH)_1$ phenotype (IFN-γ, TNF, IL-2), while protein and protein+MF59 induced cytokine^{+}CD4^{+} T cells with a TH_2 phenotype[22]. Only in SAM(H1) vaccinated mice, a cytotoxic TH_1 type cytokine^{+}CD8^{+} T-cell phenotype was found (CD107, IFN- γ, TNF, IL-2)[22]. Both after homologous and heterologous challenge, mice vaccinated with SAM(H1) showed an increased survival, with influx of different immune cells in the lung post infection. The vaccine platform has been shown safe and effective, and will soon enter clinical trials.

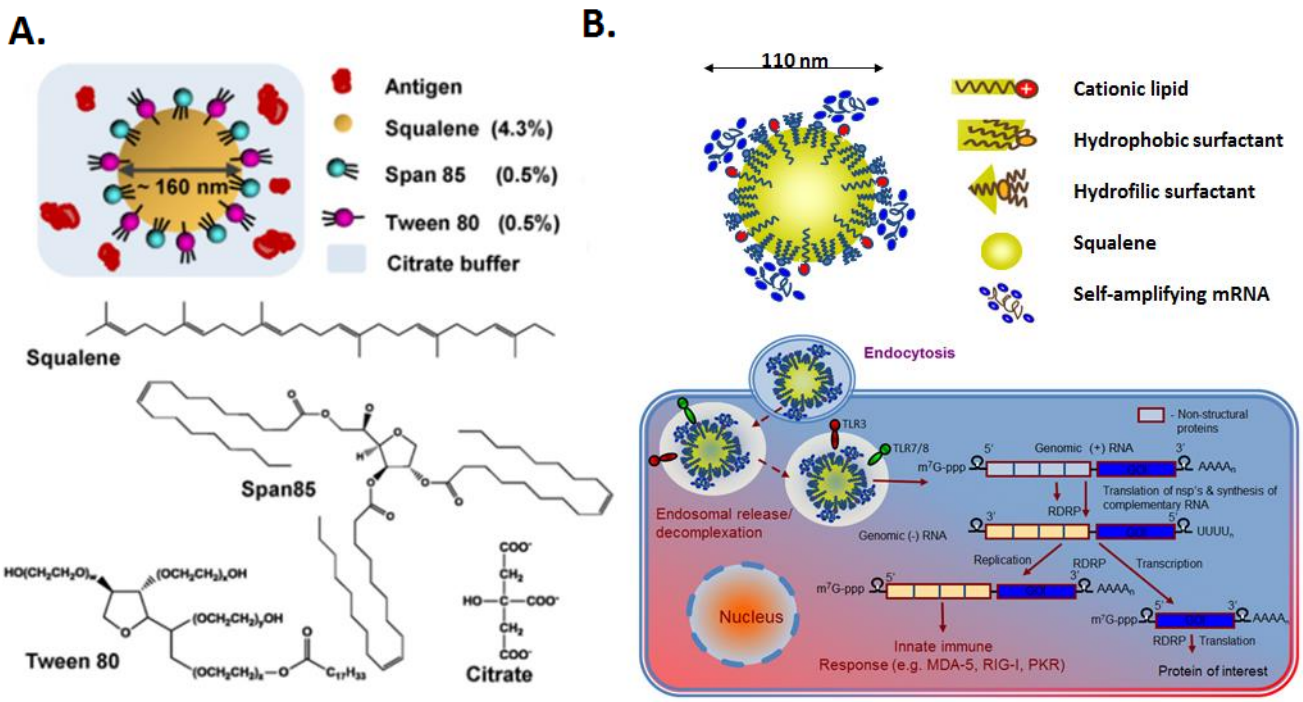

Figure 1.4: Influenza vaccines. A. On the market vaccine composed of the antigen of interest adjuvanted with MF59^{TM}. MF59 is approximately 160 nm and is composed of Tween80, Span85 and squalene formulated in citrate buffer. The antigen is not attached directly, but MF59 is believed to create an immuno-dominant environment at the injection site for the uptake of antigens. **B.** Self-Amplifying mRNA (SAM) and cationic nano-emulsion delivery system – the CNE/RNA complex is approximately 110 nm and is composed of cationic lipid (DoTAP), hydrophobic/hydrophilic surfactant, the SAM squalene formulated in citrate buffer. The SAM is directly attached by the cationic lipid. The replicons complexed to the delivery system are transported to the cytoplasm of the target cell via endocytosis. Within the target cell, the replicon will engage ribosomes and launch viral RNA dependent RNA polymerase (RDRP), permitting the self-replication of gene(s) of interest (GOI) inserted into the replicon. Proteins translated will be secreted as antigens in the area of immunization and will provoke an immune response. Source; adapted A: Calabro *et al.,* 2013[68], B: adapted from Brito *et al.,*2015[67].

1.3. Single-cell assays

To characterize in detail the behavior of cell populations, here T cells, there is a need for new methods that measure mRNA and protein expression. Cell populations are heterogeneous, and this heterogeneity can only be measured by assays analyzing biomarkers at the single-cell level, instead of averaging expression data at the cell population level[1–6,69–72]. Hence, single-cell heterogeneity is important for the development of proper cellular memory after vaccinations. With understanding of single-cell transcriptional differences after vaccination, it is possible to refine the understanding of immune responses to vaccination, possibly unraveling novel antigen-specific immune signatures correlating with protection in new vaccine designs.

Single-cell transcripts analysis can help to characterize expression heterogeneity; however, it is not a straightforward process. Firstly, eukaryotic transcription occurs in pulses, where a burst of transcript synthesis interspersed with intervals of inactivity during which transcript levels decay. There is then a stochastic variation in both burst duration and interval of inactivity, which means that bimodality of expression values are, so a gene can be ON or OFF (figure 1.5.A). This generates large cell-to-cell variation in transcript levels, 10- to 100-fold variation among cells, even in homogeneous population (figure 1.5.B)[2,4–6]. Single-cell gene expression is intrinsically noisy, so enough cells need to be analyzed to characterize the population, and to investigate multiple genes to get robust molecular signatures. Firstly, the eukaryotic transcription occurs over time. To take real advantage of single-cell transcripts analysis, it is important to set up a correct experimental design. Secondly, one can only understand changing kinetics of gene expression after vaccination at the single-cell level, by tracing individual lymphocytes on closely located timepoints. If kinetics of gene transcription needs to be understood after vaccination, the experimental design has to take into consideration that eukaryotic transcription occurs within a few hours, hence the monitoring needs to be complete with closer experimental timepoints. In this study, timepoints were selected based on early and late timepoints both after first (prime) and second (boost) immunization, which has been documented in previous reported studies[22]. Information on transcription kinetics can be lost with this approach of using distant time points. The reason for this loss is that genes appearing in OFF mode either may be missing or in a state of decay and the kinetic development of the lymphocytes cannot be thoroughly understood. Thirdly, a final issue with single-cell high throughput multiplexed RT-qPCR is the quantity of material one can analyze in single cells, as with other methods to date. The quantities of mRNA in single cells are extremely low, and even with novel techniques the mRNA needs to be pre-amplified[73].

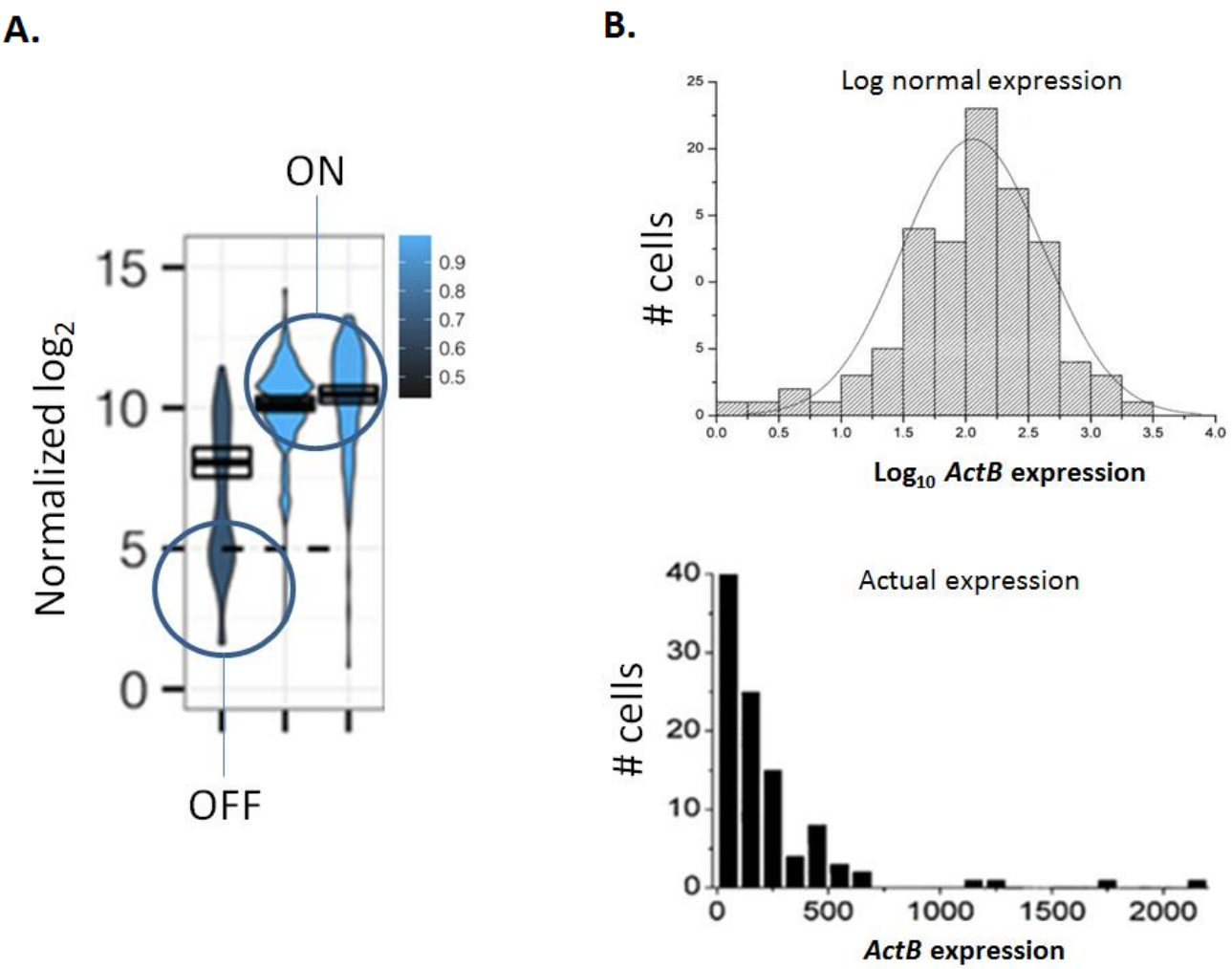

Figure 1.5: Single-cell analysis. A. Bimodular expression of genes, which can be ON or OFF. **B.** *ActB* (house-keeping gene) expression within 96 single cells is shown in a log scale (grey) and a linear scale (black). Single-cell transcripts levels are log-normally distributed (bell shape on the log scale). The average expression level in a population of cells is biased by a few cells, and with a very high number of transcript, logarithms of transcript levels are described by a lognormal distribution centered on the geometric mean. There is large cell-to-cell variation in transcript levels and there could be up to 10- to 100-fold variation within what appears to be a homogeneous population. Source; A: adapted from McDavid *et al*., 2014[3], B: adapted from Bengtsson *et al*., 2005[74].

1.4. Current and novel methods for transcript analysis

1.4.1. Current methods for transcript identification

Characterizing the gene expression profile of single cells can help the discovery of sub-populations that cannot be identified using a bulk approach. Fluorescent in situ hybridization (FISH), microarray, RNA sequencing (RNAseq) and qPCR are current assays used for single-cell analysis[8,70,71,75]. Each individual technique has both advantages and disadvantages when it comes to transcripts analysis[71].

FISH probing system is a method normally used to detect chromosomal abnormalities but can be used in gene mapping as well as single-cell transcriptomics[70,76]. The fluorescent reporter molecule is attached to a probe, which will, under a fluorescent microscope, emit light when attached to the specific region or the sequence of the target mRNA transcript. Multicolor probing technique exists for multiplex FISH, and is simple and effective[76]. The disadvantages with single-cell mRNA-FISH are as follows; they can only simultaneously measure up to 32 genes, and there is a need of a super-resolution microscope. This process is not high throughput.

Microarray is a technology that enables the gene expression profiling of over 47,000 transcripts using custom or pre-made gene arrays. This is a good technique for the screening of samples, where the genes important for certain diseases or drug targets are unknown. RNA samples are first reverse transcribed into cDNA, then transcribed and labeled, and hybridized to the corresponding probe on the gene array[8]. Microarray suffers from background hybridization, limited accuracy of expression for transcripts in low abundance, and signal saturation for highly abundant transcripts. Furthermore, microarray analysis of single cells may not be a good approach as the amount of cRNA loaded to the array is at least 100 ng (Affimetrix), while single cells have as little as 20 pg of RNA, where 5% is mRNA[74]. The extremely low amount of RNA from a single-cell requires multiple rounds of cDNA pre-amplification to reach the quantity needed, which produces both systematic biases and random errors in gene representation[8,77].

RNAseq is a technology platform that simultaneously lets one quantify the expression of most genes in one single-cell[71], by preparing a library (fragments of a given RNA/cDNA) and then run a sequencing of the library. The read is aligned to the genome, found on a database (NCBI) within the analysis. Unlike microarray, RNAseq can detect novel transcripts, single nucleotide variants, insertions and deletions. This method offers increased specificity and sensitivity. Sequence coverage can easily be increased to detect rare transcripts, single transcripts per cell, or weakly expressed genes. RNAseq gives a global profiling with no need of pre-knowledge as you run the entire genome. It is expected that once the high cost barrier of RNAseq has been overcome, this technique will become the predominant tool for single-cell transcriptome analysis, however, depending on the biological

question that needs to be answered. This technique still needs validation of genes of interest, with another technique, such as RT-qPCR.

RT-qPCR is the gold standard for validating a few genes in a sample. This is a quick way of quantifying gene expression[75,78]. Low throughput single-cell analysis with RT-qPCR is available with chemistry platforms such as SYBR Green (Qiagen) or TaqMan (Life Technologies). SYBR Green is a cyanine dye, binding mostly double stranded DNA. This method is not multiplexed, and hence of low throughput. TaqMan probes are highly sensitive dyes, but the low throughput and non-multiplexed issues are still a concern, and the probing system is greatly expensive to design.

Single cells have an extremely low amount of mRNA and none of the above techniques are, to date, equipped to provide the quality or quantity the experiments require within a reasonable cost range. The measurements are either low throughput, not available for single-cell analysis (bulk analysis are needed) or expensive, and there is a need to increase the number of single cells through high throughput analysis, which is fundamental to understand cellular responses at transcripts levels.

1.4.2. Single-cell transcripts analysis with 96 biomarkers (BioMark (Fluidigm) platform)

BioMark is presented by Fluidigm Corporation as “a production-scale throughput with exquisite single-cell sensitivity and consistent results”[79]. This novel multiplexed RT-qPCR technique consists of a chip-based array with the possibility of analyzing up to 9216 data points in one run (96 biomarkers vs 96 single cells). This method is, with its flexible design and high quality, an easy and sensitive single-cell approach. Diverse sample types and different probing chemistry (TaqMan, EvaGreen) selections can be chosen for many applications for the detection of molecular signatures or rare cell populations. The platform is fast and high throughput with an automated workflow and can be used as a validation technique or fast throughput screening, which brings the BioMark in front of other current techniques[3,21]. This single microfluidic device is based on PCR reactions in nanoliter volumes, and as such only a small amount of samples is required. The samples are loaded on a dynamic array together with the primer/probe system (figure 1.6.A), and by using automated integrated fluidic circuits (IFC), the primers/probe systems and the unique samples are mixed on a chip controlled by pressurized valves.

There are two main chemistry systems: Taqman and EvaGreen. EvaGreen is a DNA-binding dye, which is very simple, flexible and inexpensive, relative to probe-based assays. The drawbacks are that all double-stranded DNA are detected, with the possibility of primer-dimer detection. There is also a need to manually estimate the melting curve, which may introduce errors. Taqman probing system is, however, a gene-specific probing system used in multiplex qPCR. The probe design is difficult and highly expensive, but it is the most sensitive technique to date, with gene-specific product.

The TaqMan are dual labeled chemical probing systems, with oligonucleotides labeled with a fluorescent reporter dye on the 5’ end and a non fluorescente quencher (NFQ) located on the 3’ end, and hybridize to a complementary region of the cDNA (figure 1.6.B). The probe is flanked by an upstream and downstream primer pair that generates the PCR product. After polymerization, if the reporter dye has not found a cDNA to bind with and hence is in close proximity to the NFQ, the reporter dye transfers the energy to the NFQ instead of emitting light – this is called Fluorescence Resonance Energy Transfer. Conversely, when the probing system binds complementary regions, the 5' exonuclease activity of the DNA polymerase will, during the PCR product extension, cleave the probe. This separates the reporter dye and NFQ, inhibiting Fluorescence Resonance Energy Transfer. The intensity of fluorescent expression will therefore be proportional to the number of probe molecules cleaved. Two reporter dye systems are present, 6-carboxyfluorescein (FAM) and tetra-chloro-fluorecein (TET). FAM is a fluorescent dye with an absorption wavelength of 495 nm and an emission wavelength of 517 nm, used for this study, with a minor groove binder (MGB) NFQ. The analog data is converted by the program into Quantification cycles (Cq) values (defined as the number of cycles required for the fluorescent signal to cross a pre-defined threshold) (figure 1.6.C), and can be further analyzed (figure 1.6.D).

The biomarkers chosen for multiplexed single-cell RT-qPCR can comprise activation and memory markers, adhesion receptors, transcription factors, cytokines, homing molecules and/or cell fate differentiation markers. The 96 gene expression biomarkers chosen for this study are all markers that in literature have shown importance for T-cell stimulation, activation, regulation and function (appendix 1).

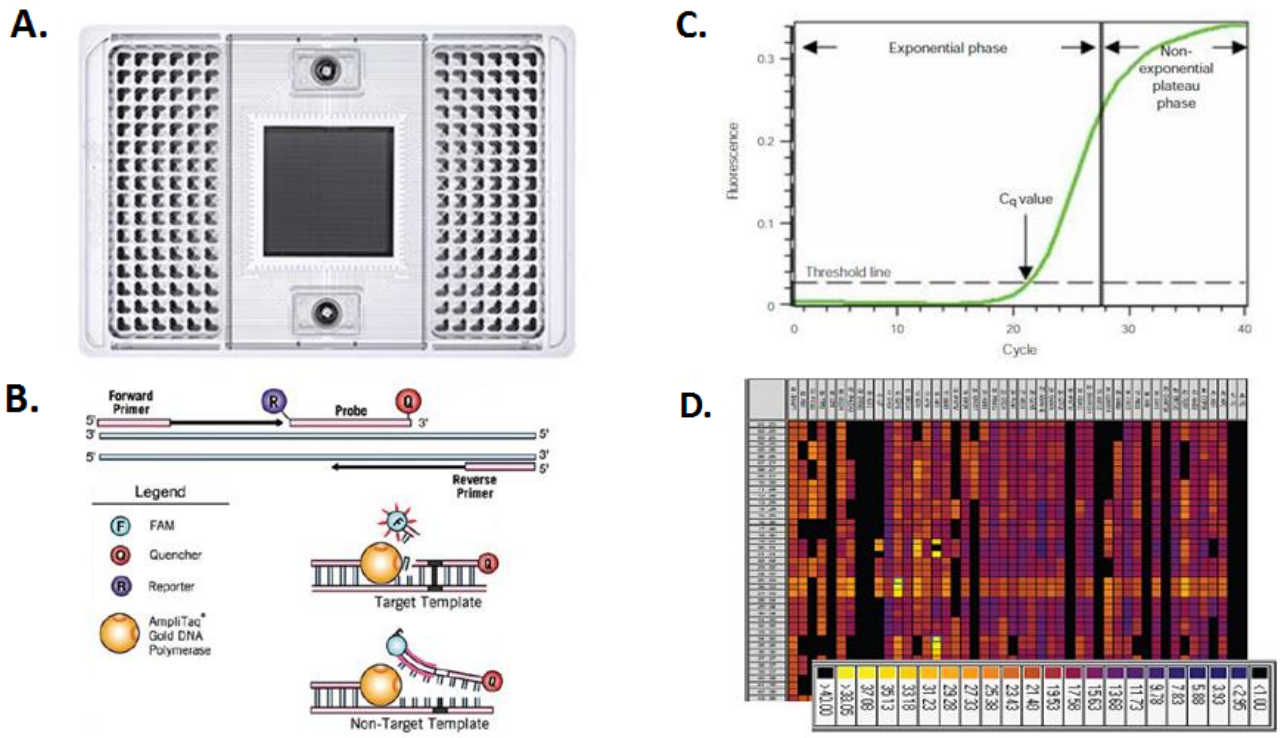

Figure 1.6: RT-qPCR BioMark (Fluidigm) platform. The sample cDNA is loaded **A.** on the left side of Fluidigm's 96.96 dynamic arrays, while the TaqMan gene expression assays (Life Technologies) are loaded on the right. 1 individual cell meets 1 individual TaqMan assay on the chip, controlled by integrated fluidic circuits (IFC), with 9216 total reaction individual chambers. **B.** The TaqMan probe process, composed of a probe containing a reporter dye (FAM) and non fluorescent quencher (NFQ), and the forward/reverse primer of the gene of interest. **C.** In a real time PCR assay, a positive reaction is detected by accumulation of a fluorescent signal. The Cq (quantification cycle) is defined as the number of cycles required for the fluorescent signal to cross the threshold (exceeds background level). Cq levels are inversely proportional to the amount of target nucleic acid in the sample. **D.** The raw output and Cq values from the digital data program. Source; A+B: http://www.Fluidigm.com, C: http://Technologyinscience.com, D: Raw data from the author.

1.5. Current and novel methods for protein analysis

1.5.1. Current methods for protein identification

Flow cytometry has dominated the field of single-cell analysis for the past 30 years. This technology is built on visualizing cell components, through staining with fluorescently-labeled Ab. After staining, the cells are pushed through a nozzle by a stream of fluid that aligns the cells in a single line and further broken into droplets. Here a laser light source provides information about the cell size and internal complexity by forward/side scatter light, and excites the fluorophore from the stained cells to emit light at various wavelengths. The light is filtered through different photo-multiplying tubes, which

detect the specific wavelength. This is converted to a voltage pulse known as an event and detected by a computer for analog-to-digital conversion.

Flow cytometry has abundant applications in basic and clinical research, and in clinical practices. Fluorochrome development has continuously evolved since the 1970', and there are approximately 40+ fluorescent dyes currently available on the market. The development of flow cytometry has improved over the years; however there is a constant prerequisite for new chemistry (dye), hardware and software development. With the fast increases of novel high throughput techniques and extraordinary demand for high throughput data, there is a need for higher level of multiparametric analysis, which simply cannot be met with current fluorescence technologies, due to limitation of the number of spectrally resolvable fluorochromes[17].

1.5.2. Single-cell proteins analysis with 32 biomarkers (CyTOF (Fluidigm) platform)

Mass spectrometry has revolutionized single-cell multi-parametric protein analysis[15–17,71,80–82]. Ab are tagged with isotopically pure and rare lanthanides elements, instead of fluorochromes, increasing the parameters to >30 for deep cell profiling[17,82]. Mass cytometry is very similar to flow cytometry, however since it is not using fluorescence, but metal isotopes this could allow the detection for more parameters simultaneously. There is a high level of choices for metal isotopes with very little signal overlap, which decreases the noise, giving the possibility of adding various biomarkers, containing different atomic mass, in the same experiment. Many elements have been described for single-cell mass cytometry[17], and labeling technologies such as the Maxpar metal labeling tools makes it easy to target, detect and quantify cellular responses by using the TOF mass cytometry. The methodology of cell data acquisition is seen in figure 1.7.; after staining cells with marker-specific metal isotope-conjugated Ab, they are introduced into the nebulizer, with hundreds of cells passing per sec, creating an aerosol. The aerosol of single cells is passed through the plasma torch, where cells are vaporized, leaving only ionized metals. The ion clouds enter the TOF chamber, where the metals are separated based on the mass to charge ratio as they accelerate towards the detector. This will identify isotopes that were once bound to proteins on the cells, and single cells will be identified and protein quantified based on the isotopic markers, generated into FSC files, and analyzed by a third party software (FlowJo, Cytobank[83]). This method will reveal the phenotype of each individual cell, and the

technique is progressing within different fields such as T-cell analysis, and is comparable to conventional methods such as flow cytometry[16,80]. This method will be an important tool for future studies. The 32 biomarkers chosen for this study are a subset of the 96 individual biomarkers chosen for the transcripts analysis (appendix 1 and 2).

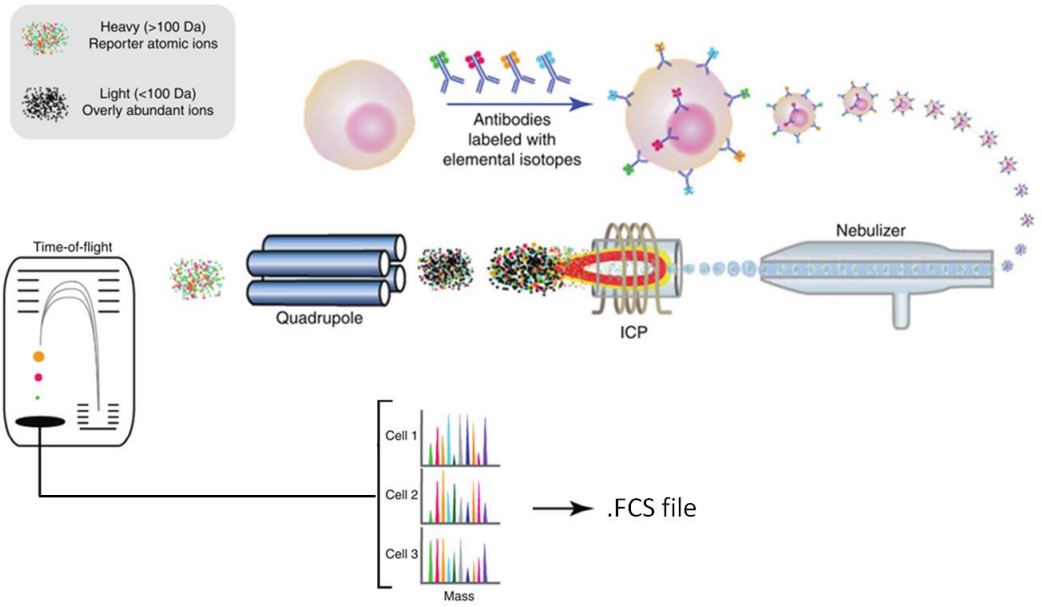

Figure 1.7: Mass cytometry by CyTOF-1 Mass Cytometer (Fluidigm) platform. Mass cytometry is a technique that allows the analysis of single cells by measuring the atomic mass of heavy elemental isotopes. Cells are stained with metal-labeled antibody (Ab), injected into the nebulizer, which produces droplets. The droplets then pass through the ICP (individual Coupled Plasma), where each cell is atomized, and the element composition is determined by their mass within the Time-of-Flight chamber. The data output can be extracted and analyzed by conventional cytometry platforms. Source; adapted from Bendall *et al.,* 2012[17].

1.6. Significance of the study and main objectives

This project will identify the presence of subpopulations of T cells that could confer protection after immunization with an antigen combined with different adjuvants, or with seasonal influenza vaccine compared to SAM(H1) vaccines. This approach will identify distinct antigen-specific $CD8^+$ T-cell subsets elicited by different vaccines. The three main objectives are:

1. Physico-chemical characterization of vaccine formulations and characterization of antigen-specific adaptive immune responses comparing two different systemic deliveries. Cytotoxicity of the cells, priming of antigen-specific T cells, and homing of memory cells will be analyzed (FACS)
2. Identify antigen-specific $CD8^+$ T cells which will be sorted using MHC-I HA-pentamers, and characterized in depth at the single-cell level using multiparametric quantitative single-cell multiplex RT-PCR by state-of-the-art immunological assays (BioMark)
3. Confirm and validate the findings based on markers identified in 2, with MHC-I HA-pentamers for in-depth characterization at the protein level using cutting edge single-cell mass cytometry phenotype profiling (CyTOF). Phenotypes identified in 2) and 3) will be compared.

At the end of this project, we will have gained a better understanding of single-cell antigen-specific $CD8^+$ T cells induced by vaccination. Two different vaccines will be formulated, delivered and the resulting $CD8^+$ T cells induced will be compared. The $CD8^+$ T cells will provide us with a unique transcript signature based identified by high-throughput RT-qPCR. This molecular signature will be validated at the protein level using mass cytometry, and correlated in an *in vivo* functional assay. This single-cell analysis platform will be the beginning of high profiling of pre-clinical vaccines research.

Chapter 2: Methodology

2.1. Characterization and single-cell sorting of antigen-specific $CD8^+$ T cells

In this study two influenza vaccines were used as models, and the phenotype of single $HA_{533-541}$-specific $CD8^+$ T cells induced by seasonal MF59-adjuvanted Monovalent Influenza Vaccine (aMIV) (A/California/07/2009 (H1N1) – corresponding to the 7th isolate of an H1N1 subtype virus isolated in humans in California in 2009) or RNA-based SAM encoding H1 from the same virus and formulated with CNE56 were compared.

2.1.1. Formulation of MF59-adjuvanted H1N1 monovalent antigen and CNE56-adjuvanted SAM

2.1.1.1.H1N1 antigen and MF59 formulation

Monovalent H1N1 subunit and MF59 adjuvant were for laboratory use only and were not final commercial products intended for human use. MF59 is a trade mark of Novartis, used under licence by the GSK group of companies. Production of Influenza A/California/7/2009 (H1N1) monovalent vaccine: the specific strain was injected into the allantoic cavity of embryonated chicken eggs and grown for 10 days. Allantoic fluids were harvested, and virions concentrated by centrifugation. Virions were chemically inactivated and disrupted by detergent. Subunit H1N1 proteins were purified, and the individual monovalent pool stored at 4 °C. On the formulation day, 3 µg of H1N1 antigen were freshly prepared alone (MIV) or with 50% (vol:vol) of oil-in-water MF59 nano-emulsion (aMIV[58,84]) per mouse dose. The size of MF59 was 160 nm and composed of polysorbate 80 (Tween), sorbitan trioleate 85 (Span) and squalene. The formulation was prepared by mixing each component (water for injection (WFI), PBS, MF59 and antigen) in sequential order (starting from left) as illustrated;

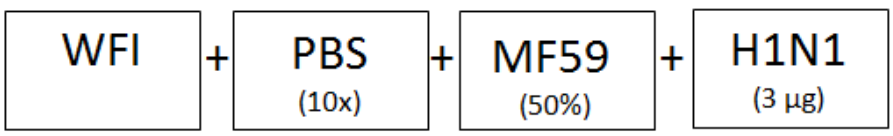

Vaccine formulations were characterized before *in vivo* injection as follows:

1. The pH was measured with a Cyberscan pH 1500 pHmeter (Eutech Instruments Europe BV). The instrument was calibrated in advance with 3 points of standard solution at pH 4, 7, and 10. A volume of 50 µl of each sample formulation was used for pH measurement; the accepted pH range was 7.0 ± 0.5.
2. The osmolality was measured using an Osmomat 030 osmometer (Gonotec GmbH). The instrument was calibrated with MilliQ water and natrium chloride (NaCl) standard solution at 0 and 300 mOsm/Kg. A volume of 50 µl of each formulation was used for the measurements; the accepted osmolality range was 350 ± 60 mOsm/ Kg.
3. The visual inspection was performed by observing the sample for 5 sec after shaking. The formulation should be homogeneous with no presence of any particles.
4. The degree of H1N1 adsorption to oil-in-water was measured by sodium dodecyl sulfate polyacryl amide gel electrophoresis (SDS-PAGE). 250 µl of formulation were ultra-centrifuged 60,000 revolutions per minute (rpm) for 35 min at room temperature (RT) in order to separate the oil and water phases. The supernatant (water phase) was aspirated with 1 ml syringe. 200 µl of supernatant were precipitated using 10% sodium deoxycholat and incubated for 10 min at RT. 9% tri-choroacetic acid was added, and the sample was centrifuged for 10 min at 1,300 rpm at RT. The pellet was suspended in tris 20 mM pH 9 and further diluted with 4x loading sample buffer prepared with the reducing agent DiThioThreitol (Sigma) and heated at 95°C for 10 min. Approximately 0.6 µg standard protein, 0.6 µg formulated protein and the molecular weight marker Seeblue plus (Invitrogen) were loaded onto NuPAGE pre-cast 4–12% bis-tris Gel (Invitrogen). The gels were run with MOPS Running Buffer (50 mM MOPS, 50 mM tris base, 0.1% SDS, 1 mM EDTA, pH 7.7). The proteins were electrophoretically separated at 200 V for 40 min, using the Xcell SureLock Mini-Cell system (Invitrogen), stained with Oriole fluorescent gel stain (Bio Rad) for 90 min and washed with H_2O. Gel images were then digitalized on Gel Doc EZ (BioRad) with UV light.

2.1.1.2. RNA Synthesis and RNA/CNE56 formulation

RNA was prepared as previously reported[65,85]. Briefly, the H1 gene was amplified from the cDNA of the influenza virus A/California/7/2009 (H1N1), and cloned as SalI and NotI fragment into an

optimized replicon construct. DNA plasmid encoding the H1 replicon was amplified in *Escherichia coli*, and purified using Plasmid Maxi kits (Qiagen). DNA was linearized immediately downstream of the 3' end of the SAM sequence by endonuclease restriction digestion with PmeI. The linearized DNA templates were purified by phenol/chloroform extraction and ethanol precipitation before being transcribed into RNA using the MEGAscript T7 kit (Life Technologies) and purified by LiCl precipitation. The RNA was capped using the ScriptCap m7G Capping System (CellScript, Madison, WI), purified by LiCl precipitation, and suspended in nuclease-free water (Life Technologies). SAM(H1) RNA integrity was evaluated on a 1% agarose-LE gel (Ambion). SAM(H1) RNA was formulated with CNE56[86] (containing Tween80 (0.5%), Span85 (0.5%), DoTAP (0.4%) and squalene (4.3%)) prepared as reported in[22,87,86]. The RNA/CNE56 (SAM(H1)) formulation was prepared in RNase free microtubes (Ambion) as followed: the RNA was diluted to a concentration of 300 µg/ml in 560 mM sucrose, 20nM NaCl, and 10mM citrate buffer at pH 6.5. The RNA was added in a drop wise manner to an equal volume of CNE56 to a final concentration of 150 µg/ml. The formulation was complexed for 45 min on ice. The RNA/CNE56 formulations were prepared fresh for each immunization and administered within 2 h following the formulation and checked for pH, osmolality and visual inspection as seen in section 2.1.1.1., and as follows:

1. The particle size was measured after dilution (1:500) of the sample in 0.22 µm filtered phosphate buffered saline (PBS) and measuring the Dynamic Light Scattering (Malvern) using the Zetasizer software (Malvern) version 6.20. The samples were run for 10 times in 3 different experiments. The Z-average mean (intensity averaged particle size diameter nanometer (d.nm)) and polydispersity index (PDI) (calculated number from a 2- parameter fit to the correlation data (z-average)) was measured.
2. The RNA integrity after formulation with CNE56 was measured by electrophoresis. The RNA was extracted from CNE56 by a 1:20 dilution in 2-Propanol (Isopropyl alcohol) (Sigma Aldrich), followed by centrifugation for 25 min at 4°C, and removal of the supernatant. The sample RNA and a standard RNA were mixed with a 2x loading dye (Ambion). RNA samples and standard were denatured for 10 min at 65°C, loaded with a Millenium Marker (Ambion) on a 1% agarose gel (agarose in 1xNorthernMax running buffer), and run at 100V for 40 min. Gel images were then digitalized on GelDoc-It TS imaginge system (UVP) with UV light.

2.1.2. BALB/c immunization and preparation of spleens

A schematic overview of the experimental design can be seen in figure 2.1. Female BALB/c mice, age 6-8 weeks, were immunized on study day 0 and 56 Intramuscular in the quadriceps muscle of each hind leg with 50 µl of vaccine formulation per leg (100 µl total per mouse) with PBS (sigma), MIV, aMIV or SAM(H1). On experimental day 10 post first immunization (d10p1), week 5 post first immunization (w5p1), and day 10 post second immunization (d10p2), week 6 post second immunization (w6p2), 1-6 mice (1-3 experiments) were sacrificed and spleens harvested in 3 ml complete roswell park memorial institute medium (cRPMI) (10% heat inactivated fetal bovine serum (FBS) (low endotoxin (HyClone), 1x Penicillin / Streptomycin (Gibco) and 50 µM β-mercaptoetanol (Sigma)).

Group	Antigen	Adjuvant	Route
PBS	PBS	-	I.M.
#MIV	H1N1 (3 µg)	-	I.M.
*aMIV	H1N1 (3 µg)	MF59 (50 %)	I.M.
**SAM(H1)	H1 (15 µg)	CNE56 (50 %)	I.M.

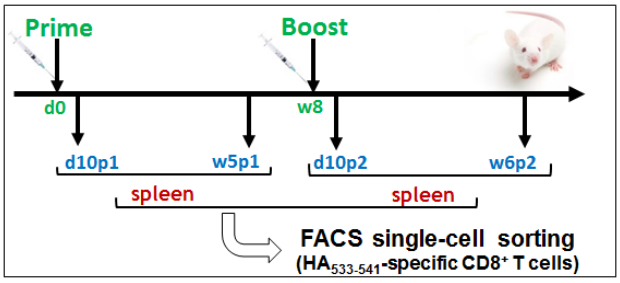

Figure 2.1: Schematic overview of vaccines and immunization scheme. BALB/c mice were vaccinated intramuscular (I.M.) on day 0 (d0, prime) and 56 (w8, boost). Spleens were harvested on the indicated times (day 10 post prime and boost, week 5 post prime and week 6 post boost) and processed. Cell samples were stained and single $CD8^+$ T cells sorted based on their $HA_{533-541}$-specificity. # MIV: pandemic Monovalent Influenza Vaccine, (A/California/07/2009 (H1N1)), * aMIV: $MF59^{TM}$-adjuvanted pandemic Monovalent Influenza Vaccine (A/California/07/2009 (H1N1)), ** SAM(H1) (Self Amplifying mRNA) encoding H1 (A/California/07/2009 (H1N1)).

The spleens were processed to a single-cell suspension by dissociation through a 70 µm mesh filter using the end of a 5 ml syringe on top of a 50 ml tube (Falcon), centrifuged at 1,300 rpm, 15°C for 10 min, and washed twice with wash roswell park memorial institute medium (wRPMI) (2% heat inactivated FBS (low endotoxin (HyClone), 1x Penicillin / Streptomycin (Gibco) and 50 µM β-mercaptoethanol (Sigma)). The cell pellet was suspended in 2 ml of red blood cell lysis buffer (ebioscience) for 2 min at RT, and the reaction was stopped by the addition of 10 ml wRPMI. The sample was filtered on a 70 µm mesh filter and washed twice with wRPMI. An aliquot was taken for

cell counting. 10 µl sample mixed with 190 µl PBS (1:20) and 10 µl was loaded onto a hemocytometer (Hausser Scientific) by gently resting the end of the pipette tip at the edge of the chamber. The hemocytometer was placed in a microscope (Axiovert). The cells were counted using the 10x objective of the microscope. 16 squares in the top left corner square were counted, and the cell concentration was calculated as follows: # cells/ml = #cells in the chamber x dilution factor (1:20) x 10^4. Cell pellet was suspended in cRPMI to a final cell number per well: $6x10^6$ cells per mouse (for the PBS group) or $3x10^7$ cells per mouse (for the vaccinated groups).

2.1.3. *In vivo* cytotoxicity assay and flow cytometry analysis

In order to determine the killing activity of $HA_{533-541}$-specific $CD8^+$ T cells elicited by the different vaccines, target splenocytes from naïve BALB/c mice were prepared and loaded with either 5 µM cognate custom peptide $HA_{533-541}$(IYSTVASSL, JPT), or 10 µM control custom peptide human immuno-deficiency virus (HIV) $gag_{199-207}$ (AMQMLKETI, JPT), for 1 h at 37°C in cRPMI. The cells were then loaded with CarboxyFluorescein Succinimidyl Ester (CFSE) ($HA_{533-541}$ peptide-pulsed cells, Life Technologies) and incubated for 15 min at RT or 5-(and-6)-(((4ChloroMethyl)benzoyl)amino) TetramethylRhodamine (CMTMR) (HIV $gag_{199-207}$ peptide-pulsed cells, Life Technologies) and incubated for 15 min at 37°C. 10^6 cells/CFSE and 10^6 cells/CMTMR ($2x10^6$ cells in total) in 100 µl were adoptively transferred Intravenous in the tail vein of recipient mice, 9 days or 5/6weeks after prime or boost with PBS, MIV, aMIV or SAM(H1). Twenty h after Intravenous injection, mice were sacrificed, spleens harvested and cell suspensions from recipient mice prepared. Cells were stained with live/dead-yellow (Life Technologies) and frequencies of $CFSE^+$ or $CMTMR^+$ target cells were determined by flow cytometry with a LSR-II special order FACS analyzer (BD Biosciences) following the gating strategy shown in figure 2.2.

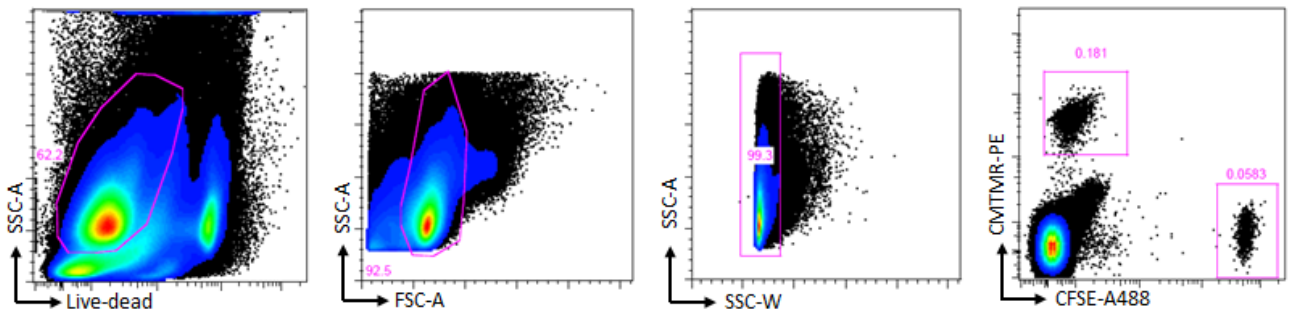

Figure 2.2: Gating strategy for flow cytometry analysis of target cells. Live cells were selected, and lymphocytes were further identified based on morphology (FSC-A) and singlets (SSC-W). $CFSE^+$ or $CMTMR^+$ cells were then identified. Representative dot plots are shown.

The target cell specific lysis was analyzed with FlowJo (software version 9.8.3) and calculated as previously described[88]:

$$\% \text{ specific lysis} = \left(1 - \frac{\left(\frac{\% \text{ CMTMR}^+ \text{ cells}^{\text{CTRL pep}}}{\% \text{ CFSE}^+ \text{ cells}^{\text{FLU pep}}}\right)_{\text{r: naïve mice (average)}}}{\left(\frac{\% \text{ CMTMR}^+ \text{ cells}^{\text{CTRL pep}}}{\% \text{ CFSE}^+ \text{ cells}^{\text{FLU pep}}}\right)_{\text{r: vaccinated mouse}}}\right) \times 100$$

Two experiments were performed for d10p1 and d10p2 timepoints (11-12 mice/timepoint), while one experiment was conducted for w5p1 and w6p2 timepoints (4 mice/timepoint). The data were visualized with GraphPad Prism (software version 6.05), and non-parametric Mann-Whitney U test was used for statistical analysis, p-values less than 0.05 were considered significant.

2.1.4. *Ex vivo* MHC-I $HA_{533-541}$-pentamer staining and sorting of single cells for RT-qPCR

For the detection of $HA_{533-541}$-specific $CD8^+$ T cells, the cells were stained with a recombinant H-2Kd restricted MHC-I pentamer loaded with $HA_{533-541}$ peptide and bound to a phycoerythrin (PE)-labeled streptavidin (0.05 mg/ml in PBS, stabilized with 1% bovine serum albumin (BSA) and 0.01% sodium azide (NaN_3) as preservative) targeting the TCR of $HA_{533-541}$-specific $CD8^+$ T cells[22].

2.1.4.1. MHC-I HA533-541-Pentamer titration: MHC-I $HA_{533-541}$-pentamers were tested at 1 µg, 0.75 µg, 0.5 µg (recommended) and 0.25 µg on splenocytes of naïve and SAM(H1) vaccinated BALB/c mice, at d10p2. Cells were stained in PBS with Live/Dead-Aqua (Life Technologies) in 1/1000 dilution, for 20

min at RT in the dark. Cells were washed twice with 200 µl of cold FACS buffer (PBS, 2% FBS, 0.05% NaN_3), before incubation with 200 µl of H-2K^d restricted MHC-I HA-pentamer ($HA_{533-541}$(IYSTVASSL) (Proimmune)) or the control H-2K^d restricted MHC-I HIV gag-pentamer (HIV gag $_{199-207}$ (AMQMLKETI) (Proimmune)) in FACS buffer. Anti-CD8 allophycocyanin (APC) (BD Biosciences), anti-CD14 fluorescein isothiocyanate (FITC), anti-CD19 FITC, anti-CD335 FITC, and anti-F4/80 FITC (eBioscience) were further added in FACS buffer and incubated for 30 min at 4°C. Cells were washed twice with 200 µl of cold FACS buffer and kept in 200 µl of cold FACS buffer on ice. The samples were run on a LSR-II special order FACS analyzer (BD Biosciences). $HA_{533-541}$-pentamer$^+$ CD8$^+$ T cells were identified by applying the following gating strategy: live cells, morphology, singlets, lineage markers (CD14$^-$, CD19$^-$, CD335$^-$, F4/80$^-$), CD8$^+$, and $HA_{533-541}$-pentamer$^+$ or HIV gag $_{199-207}$-pentamer$^+$ (see gating strategy in figure 2.3). The samples were analyzed using FlowJo (software version 9.8.3) and the working concentration of 0.75 µg (dilution 1/13 based on 30x10^6 cells in 200 µl) was chosen for future experiments. Single-cell sorting was performed using a FACSAria III flow cytometer. Single-cell sorting was performed on $HA_{533-541}$-pentamer$^+$CD8$^+$ T cells in splenocytes from PBS (sigma), MIV, aMIV or SAM(H1)-vaccinated BALB/c mice at different timepoints after immunization.

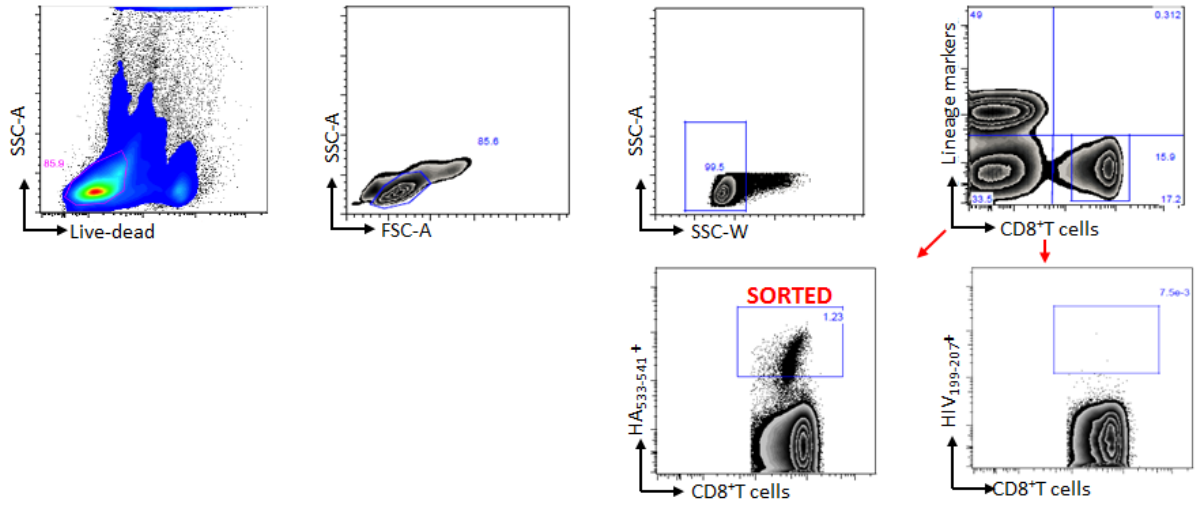

Figure 2.3: Gating strategy for single-cell sorting on a FACS Aria III of $HA_{533-541}$-pentamer$^+$CD8$^+$ T cells. Live cells were selected, and lymphocytes were further identified based on morphology (FSC-A) and singlets (SSC-W). CD8$^+$ T cells were further identified using markers for the discrimination of cell lineages (CD14$^-$ (monocytes), CD19$^-$ (B cells), CD335$^-$ (NK cells), F4/80$^-$ (macrophages)), and $HA_{533-541}$-pentamer$^+$ CD8$^+$ T cells were single-cell sorted. PBS-treated mice were $HA_{533-541}$-pentamer$^-$, and single-cell sorting was based on the CD8$^+$ T-cell gate. Representative dot plots are shown.

2.1.4.2. Single-cell sorting: Cell sorting was performed using a FACSAria III flow cytometer (Becton Dickinson, San Jose, CA) equipped with 405 nm, 488 nm and 633 nm lasers in order to achieve one $HA_{533-541}$ –pentamer^{+}CD8^{+} T-cell per well. Prior to cell sorting, the sorting conditions were set: firstly the cell sorter and fluidics were turned on, then the stream and drop delay were set up. The flow was turned on, and when drop formation was complete, the quality and stability of the stream were checked, by changing the amplitude. The most important step in the machine setup was to determine a correct drop delay. This is of utmost importance since with an incorrect drop delay, there will be no cell present in the drop or wrong cells are detected, meaning that no cell/wrong cell will be sorted. The accurate drop delay was set using Accudrop beads (BD Biosciences), and adjusted until 100% of beads would be sorted. Special settings for the single-cell sorting were done as follows: a technician manually modified the plate reader to fit a specialized single-cell sorting plate, and the direction of the plate was adjusted. The single cells were sorted using a 70 µm ceramic nozzle (BD Biosciences), sheath pressure of 70 Psi (pounds per square inch), and an acquisition rate of 8,000 events per second. The sorting purity and precision was determined; the sample enters the flow cell in a stream and leaves by drops. The FACSAria III considers 3 drops: The leading drop already interrogated by the lasers, the interrogated drop and trailing drop which has to be interrogated next. To analyze the purity, a single-cell mask was set up (the location of the drop was divided into 32 fields, and maximum purity mask (32, indicating how close a contaminating drop was located) and half the maximum phase masks (16, only particles centered within the sorted drop are deflected, so the trajectory is not influenced) was used). To check the centering of the stream into the well, beads were sorted onto the plate, which was placed in the plate reader using a specialized hard shell 96-microplate adaptor (BioRad), and closed with adhesive ELISA film. The resulting beads on the film should not be directly in the middle of the well, but on a right angle, since the trajectory of the drop is not vertical but angular. The sorting plate layout was designed, and which gated population to be sorted into the 96-well plate was specified (the drop which was sorted would be charged via the stream-charging wire in the nozzle). $HA_{533-541}$-pentamer^{+}CD8^{+} T cells from vaccinated mice were single-cell sorted as lineage marker negative (CD14^{-}, CD19^{-}, CD335^{-}, F4/80^{-}), CD8^{+}, and $HA_{533-541}$-pentamer^{+} while CD8^{+} T cells from PBS-treated mice were single-cell sorted as lineage marker negative (CD14^{-}, CD19^{-}, CD335^{-}, F4/80^{-}), CD8^{+}. Cells were deposited into a 96-well sorting plate (1 cell/well) containing 5 µl of nuclease-free

H_2O with 1 mg/ml BSA (Life Technologies) and 1 U/well RNasin (Fermentas) per well. As a negative control, each plate contained one single well with no cell. Two plates for each vaccine group were single-cell sorted at each timepoint and the plates were immediately centrifuged (3,000rpm, 1 min at 4°C), freeze-dried, and stored at -80°C until multiplexing RT-qPCR. Flow cytometry-based experiments were analyzed with FlowJo (software version 9.8.3) and visualized with GraphPad Prism (software version 6.05).

2.2. Multiplexing RT-qPCR of $HA_{533-541}$-pentamer$^{+}CD8^{+}$ T cells

The expression of 96 individual genes in single cells were analyzed by RT-qPCR[89] using the IFC from the Fluidigm system. For detection of specific gene transcripts in single cells, TaqMan primer and a fluorescence probing system were used (FAM-MGB) (Life Technologies). The TaqMan gene expression assay consists of a pair of unlabeled gene specific PCR primers and a TaqMan probe with a FAM dye on the 5' end and MGB-NFQ at the 3' end. When the primers are loose in the solution, the NFQ inhibits the FAM dye, but when the primers attach to a product, the FAM and NFQ is cleaved off and since the NFQ can no longer inhibit the FAM in fluorescence, light is emitted.

2.2.1. cDNA synthesis. The plates were thawed on ice and centrifuged (Eppendorf centrifuge 5430) for 30 sec at 3,800 rpm RT. cDNA from mRNA templates were prepared by adding 2 µl/well of oligo$(dT)_{12-18}$ primers (25 ng/µl final – poly A tail primer site), random hexamers (50 ng/µl final – annealing to random complementary sites on target mRNA), dNTPs (1 mM final – cDNA building blocks) and nuclease-free H_2O (Life Technologies). The plates were gently vortexed, centrifuged for 30 sec at 3,800 rpm RT, and placed in a 65°C preheated heating block (Grant) for 5 min (denaturing), then cooled for 1 min (annealing of primers). 3 µl/well of First Strand buffer (1.8x), DiThioThreitol (0.01 M final – reducing agent), Superscript III (5 U/µl final - reverse transcriptase) and RNAse Out (1 U/µl final – recombinant ribonuclease inhibitor) (Life Technologies) were added. After a short centrifugation (30 sec at 3,800 rpm RT) plates were placed in a PCR machine (Biometra, professional thermocycler) following the program: annealing of random hexamer primers at 25°C for 5 min,

reverse transcription at 50°C for 60 min followed by 15 min at 55°C, inactivation at 70°C for 15 min, then at 12°C until plated were collected.

2.2.2. Quality control. The wells were analyzed for the presence of CD3e mRNA prior to the remaining 95 genes, to control the sorting of 1 T-cell/well, and determine the quality of the cDNA. 9 µl of nuclease-free H_20, TaqMan universal PCR master mix II with uracil-n-glycosylase (UNG – uracil eliminator) (TUMM II) (1x final - DNA polymerase, buffer, dNTP, ROX (Passive reference dye), UNG) and CD3ε TaqMan gene expression assay (1 µM TaqMan primers and 0.3 µM Probe, in tris-EDTA (TE) buffer) (Life Technologies) were mixed, with 1 µl of cDNA. The plates were run on a LC480II qPCR (Roche) with the following program: UNG (eliminate uracil from the sample) at 50°C for 2 min, denaturation at 95°C for 10 min, 50 cycles of amplification at 95°C for 15 sec followed by 60 sec at 60°C, then at 12°C until plated were collected. Only wells positive for the CD3ε cDNA were further analyzed for the remaining biomarkers.

2.2.3. cDNA pre-amplification. cDNAs were pre-amplified, to increase the amount of material per single-cell. Gene-specific primers were used in a multiplex reaction. Nuclease-free H_20, PreAmp Master Mix (1.25x final) and TaqMan gene expression assays (final concentration per assay in PreAmp Master Mix was 57 nM TaqMan primer and 16 nM probe, in TE buffer) (Life Technologies) were added. 5 µl of the cDNA was mixed with 20 µl of the pre-amplification mix and run on a LC480II qPCR (Roche) with the following program: Denature 95°C for 10 min, 20 cycles of amplification at 95°C for 15 sec followed by 4 min at 60°C, then at 12°C until plated were collected. The pre-amplified cDNAs were diluted 4 times in TE buffer (Life Technologies).

2.2.4. Quantification of gene expression. For the analysis of gene-specific expression, the BioMark Real-time PCR system (Fluidigm) was used as reported in McHeyzer-Williams *et al.,* 2015, with BioMark Dynamic Array 96.96 Gene expression IFC chip (Fluidigm). The 96.96 Dynamic Arrays were loaded into the IFC controller Hx for priming. 3.84 µl GE loading reagent (1x final, Fluidigm), nuclease-free H_20 and TUMM II (1.5x final, Life Technologies) were mixed with 2.16 µl pre-amplified cDNA. 5 µl of the sample were loaded on the right side of the 96.96 Dynamic Array. 3 µl of Assay Loading Reagent (1x final, Fluidigm) were mixed with 3 µl of the 96 different TaqMan gene expression assays (final concentration per assay in qPCR was 900 nM TaqMan primer and 250 nM probe) in a 96-well

plate. 5 µl of each assay were loaded into the left side of the 96.96 Dynamic Array. The Fluidigm manufacturer's instructions on the program on "96.96 Real-Time PCR workflow quick reference protocol"[79] were followed. The program on the BioMark was as follows: UNG at 50°C for 2 min, denaturation at 95°C for 10 min, 40 cycles of amplification at 95°C for 15 sec followed by 60 sec at 60°C, then at 12°C until plated were collected. TaqMan assays used for RT-qPCR are displayed in appendix 1.

2.2.5. Transcriptional data analysis

2.2.5.1. Quantification Cycle (Cq) and data exclusion: A positive RT-qPCR reaction is detected by the accumulation of a fluorescent signal. The Cq [89] is defined as the number of cycles required for the fluorescent signal to cross a pre-defined threshold (exceeds background level). Cq levels are inversely proportional to the amount of target cDNA in the sample (the lower the Cq level the greater the amount of target cDNA in the sample see figure 1.6.C.). The individual Cq levels were recorded in the Fluidigm Real-Time PCR Analysis software version 4.1.2, and the Cq values from individual cells were extracted. In total 147'456 data points were generated. A multistep data preparation consisting of supervised pre-processing, data exclusion, and transformation were performed following the approach described in Stålberg *et al*. Exclusion criteria were as follow:

1. wells that failed the quality control given by the software
2. wells where none of the genes were expressed
3. wells negative for $CD3^+$ (lymphocyte marker) and $CD8^+$ ($CD8^+$ T cells sorted)
4. wells positive for $CD4^+$ or $CD19^+$ (B cells)
5. genes not expressed in any well

House-keeping genes were not included in the gene expression panel as burst kinetic of mRNA transcription gives uncorrelated variations between genes at the single-cell level[2,4–7]. Cq_{cutoff} was set at 26 (mean of all max Cq values) and all Cq values above threshold were set to 26 [4]. Cq values were converted in log expression by subtracting the Cq value from a baseline of 26[4–7,21]:

$$Log = Cq_{cutoff} - Cq_{gene}$$

2.2.5.2 Visualization: Most analyses were performed in R, a free software platform (version 3.0.2)[90] for environmental statistical computing and graphing. To globally visualize the data, we used principle component analysis (PCA)[4,21,80,91]. PCA is an unsupervised dimensionality reduction method, which identifies patterns in the dataset and expresses the data in such a way as to highlight their similarities and differences. PCA expresses the direction of the highest variance by its coordinates, which projects the data into two dimensions, PC1 and PC2, of the two vaccines. The confidence eclipse defines the region containing 75% of the data points. To compare across the vaccines or subpopulations of antigen-specific T cells, scatterplots show changes in gene expression level between two conditions tested (timepoints, vaccines, T-cell subpopulations, etc.[8,92]). Genes which fall outside the 15% limit line are determined as differentially expressed genes (DEG) between the conditions tested[92]. After separation of DEG between the vaccines, dot plots were used to visualize both the level of expression and frequency of cells expressing the genes. Further characterization of the DEG was done by clusterization of both genes and cells in a heat map, where the expression of genes in a single-cell could be observed. To confirm clusterization and co-expression of genes, combination maps, in which important genes were shown present/absent together, were applied to the data set.

2.2.5.3. Statistical significance: Fisher's exact test was used to test for significance. DEG analysis was performed using a recently developed method named likelihood ratio test (LRT) published by McDavid *et al.,* 2014. This statistical method measures simultaneous changes in gene mean expression and percentage of cells expressing the given gene. In order to strengthen the statistical significance with LRT, a false discovery rate (FDR) correction was applied. FDR correction is a statistical method where one adjusts the statistical confidence measures based on the number of tests performed.

2.3. Mass cytometry on $HA_{533-541}$-pentamer$^{+}CD8^{+}$ T cells

2.3.1. Metal conjugation to Ab and quality control

2.3.1.1. Metal conjugated Ab. Metal conjugation of Ab was performed using the Maxpar X8 Ab labeling kit (Fluidigm) and used as reported in the protocol from the laboratory of Nolan (Stanford University, Stanford, CA)[93]. Briefly, to pre-load the chelating polymers, the reagent was reconstituted with 95 µl of MaxPar L-Buffer. A sufficient amount of the desired lanthanide metal solution was added to the MaxPar reagent for a final 2.5 mM (5 µl). The samples were vortexed and incubated for 1 h at RT with additional vortexing every 20 min during the incubation period. In a 50 kDa MWCO micro-filter tube 300 µl of R-buffer and 100 µg of the Ab to be conjugated were added. The tubes were centrifuged at 12,000xg for 8 min at RT, and the column flow-through was discarded (in order for Buffer exchanging the Ab). For partial Ab reduction, TCEP stock was diluted to 4 mM with MaxPar R-buffer and 100 µl of diluted TCEP were added to each R-buffer exchanged Ab. The samples were vortexed and incubated for 30 min at 37°C in the dark. After the incubation period, 300 µl of MaxPar C-buffer was added to the partially reduced Ab, centrifuged at 12,000xg for 8 min at RT, and the column flow-through was discarded. This step was repeated with 400 µl of MaxPar C-buffer. During the incubation, the metal loaded polymer tube was cleaned with 200 µl of C-buffer. This mix was transferred to a 3kDa MWCO micro-centrifuge column and centrifuged at 12,000xg for 35 min at RT until the final volume reached < 20 µl and the column flow-through was discarded. The metal-loaded polymer was resuspended in 200 µl of C-buffer and transferred to the corresponding partially reduced Ab in the 50 kDa MWCO tube. The solution was vortexed and incubated for 2 h at 37°C. After the incubation, the 50 kDa MWCO metal-conjugated Ab was washed with 300 µl of MaxPar W-buffer, centrifuged at 12,000xg for 8 min, and the column flow-through was discarded. This step was repeated 3 times with 400 µl of MaxPar W-buffer. For the recovery of metal-conjugated Ab, 50 µl of MaxPar W-buffer were added to the column. The column was flipped over a new collection tube and centrifuged at 1,000x g for 2 min, and the column flow-through was collected. This extraction was repeated with an additional 50 µl of W-buffer. The conjugated Ab was quantified by Qubit 2.0 Fluorometer (Life Technologies) using the highly sensitive and accurate fluorescence-based Qubit quantitation assays (Life Technologies). The expected recovery was above 60%. Once quantified, W-

buffer was exchanged and the Ab was diluted in Ab stabilizer (PBS, 0.1% NaN_3) and stored at a final concentration of 200 µg/ml at 4°C.

2.3.1.2. Quality control and titration. After Ab metal-conjugation, the metal content was determined on CyTOF-1 Mass Cytometer (Fluidigm). The Ab was diluted 1:1000 with digestion buffer (2% Hydrochloric Acid (Fluka) in deionized water). The Ab was serially diluted to achieve a final $1:10^5$ dilution using dilution buffer (2% Nitric Acid (Carlo Erba reagents) in deionized water). 300 µl sample of blank (dilution buffer) and of Tuning Solution containing lanthanum (^{139}La), terbium (^{159}Tb), Thulium (^{169}Tm), iridium ($^{191/193}Ir$) (for normalization calculation) (Fluidigm) were prepared. The CyTOF-1 Mass Cytometer instrument was turned on and the daily performance checked with the Tuning Solution. After the daily performance check, the washing solution was run (Fluidigm) to clean the loop. The samples were then acquired: firstly, 300 µl of the blank (dilution buffer) was injected with a 1 ml syringe (Norm-Ject). Once the signal was stable, 30 sec of data were recorded. 300 µl of each diluted Ab were injected. Once the signal was stable, 30 sec of data were recorded. 1 ml of washing solution (Fluidigm) and 1 ml of H_20 were injected and run for 2 min between each Ab. Finally, the Tuning Solution data was collected. Data analysis was done using the intensity data columns for the analytes of interest. The values for each isotope recorded for the blank, samples and standard were averaged. For the Tuning Solution standard, the average from the data collected before and after the sample acquisition was calculated. The values were filled in the 'Conjugated Ab Metal Content Calculation Spreadsheet,' prepared and standardized by DVS, in order to calculate the number of metal atoms per Ab. A titration of the metal-conjugated Ab was performed using splenocytes from naïve BALB/c mice, unstimulated or stimulated (stimulus as recommended by datasheet of Ab). The metal-conjugated Ab was serially diluted in a range of 0.625-10 µg/ml final concentrations in 50 µl staining reaction and injected into the CyTOF-1 Mass Cytometer. The titration experiments were analyzed with FlowJo (software version 10.0.7).

2.3.2. $CD8^+$ T-cell purification

$CD8^+$ T cells were enriched from total splenocytes using the Dynabeads Untouched™ Mouse CD8 Cells kit (Invitrogen) following the manufacturer's instructions (the volume of reagents used was adapted to the starting number of cells). Briefly, splenocytes were suspended in the isolation buffer (PBS ($Ca2^+$

and $Mg2^+$ free), 0.1% BSA, and 2 mM EDTA). Heat-inactivated FBS (HyClone) and monoclonal Ab Mix (anti-CD4, CD45R (B220), CD11b (Mac1), Ter-119, and CD16/CD32) were added to the cells and incubated for 20 min at 4°C. The cells were washed with isolation buffer and centrifuged at 1,300 rpm for 8 min at 4°C. The cells were suspended in the isolation buffer and pre-washed Mouse Depletion Dynabeads were added and incubated for 15 min at RT with gentle tilting and rotation. Additional isolation buffer was added and the sample was gently suspended. The tubes were placed on magnets (Invitrogen) for 2 min and the supernatants containing the untouched $CD8^+$ T cells were transferred to new tubes.

2.3.3. Cell staining with $HA_{533-541}$-pentamer and a panel of 32 metal-labeled Ab

Purified $CD8^+$ T cells were incubated at $5x10^6$/well for 1 h at RT in low barium PBS, 2% FBS, 0.05% NaN_3 with a 1:4 dilution of PE-conjugated $HA_{533-541}$-pentamer or HIV gag $_{199-207}$-pentamer in a single well. Pentamer-loaded cells were pooled, then plated at 10^6/well and stained for 30 min at RT with metal-labeled Ab "extracellular 1" staining (in house conjugated (section 2.3.1.1) or pre-conjugated, appendix 2). Cells were stained with a cell-ID Intercalator Rhodium (^{103}Rh) (Fluidigm) diluted 1:2000 (a cationic nucleic acid intercalator that contains natural abundance ^{103}Rh and is used for the discrimination of dead cells from live cells), and CD16/CD32 Fcblock (Pharmingen) in cell staining medium (CSM) buffer (low-barium PBS, 0.5% BSA, protease-free (Sigma) filtered through a 22 µm Nalgene polypropylene bottle (Millipore)). The cells were washed twice with CSM buffer before staining for 30 min at 4°C with metal-labeled Ab "extracellular 2" staining (in house conjugated (section 2.3.1.1) or pre-conjugated metal-labeled Ab, appendix 2) in CSM buffer. The cells were washed twice with CSM buffer and fixed for 15 min at 4°C with Cytofix (Becton Dickinson). The cells were washed with CSM buffer and with Cell Staining Medium-saponin (CSM-S) (CSM, 0.3% Saponin (Sigma) filtered with Nalgene polypropylene bottle) and suspended in CSM-S buffer for permabilization 30 min at RT. The cells were washed once with CSM-S and stained with metal-labeled Ab "intracellular" (in house conjugated (section 2.3.1.1) or pre-conjugated, appendix 2) diluted in CSM-S for 30 min at RT. The cells were washed twice with CSM-S buffer and stained with DNA intercalator-$^{191/193}Ir$ (500X) diluted with CSM-S 1:1000 for 20 min RT. The sample were washed once with CSM-S and pooled to avoid variability. Finally, cells were washed once with CSM and pellet left

dry until acquisition. Immediately before the injection, the samples were suspended in ultrapure water (Millipore) with 0.2x CyTOF Calibration EQ Four Element Calibration Beads (Cerium ($^{140/142}$Ce), europium ($^{151/153}$Eu), holmium (^{165}Ho), and lutetium ($^{175/176Lu}$) (Fluidigm) and filtered through a 30 µm filter (Becton Dickinson). The samples were acquired on a CyTOF-1 Mass Cytometer, as explained in section 2.3.1.2.

2.3.4. Mass cytometry data analysis

For normalization of samples using the 4 beads, the program Matlab normalizer (version 0.1) was used. The concatenation of the samples was done in FlowJo (version 10.0.7).

The gating strategy and number analysis was done using Cytobank[83] on normalized and concatenated samples and single cells were identified by DNA (^{191}Ir) vs. DNA (^{193}Ir) (singlets), cells length vs DNA (^{191}Ir (singlets), ^{191}Ir vs ^{103}Rho (live), CD45^{+} vs. CD3^{+} / CD4^{-} /CD8^{+} and finally of the protein marker of interest (gating strategy is shown in figure 2.4).

Hereafter, t-distributed stochastic neighbor embedding (t-SNE) was applied, which is a machine learning algorithm. This algorithm is dimensionally reducing high-dimensionally data. After application, the data can be visualized in a scatter plot into a space of 2 or more dimensions, where high or low expression of the certain biomarker can be observed in clusters[94].

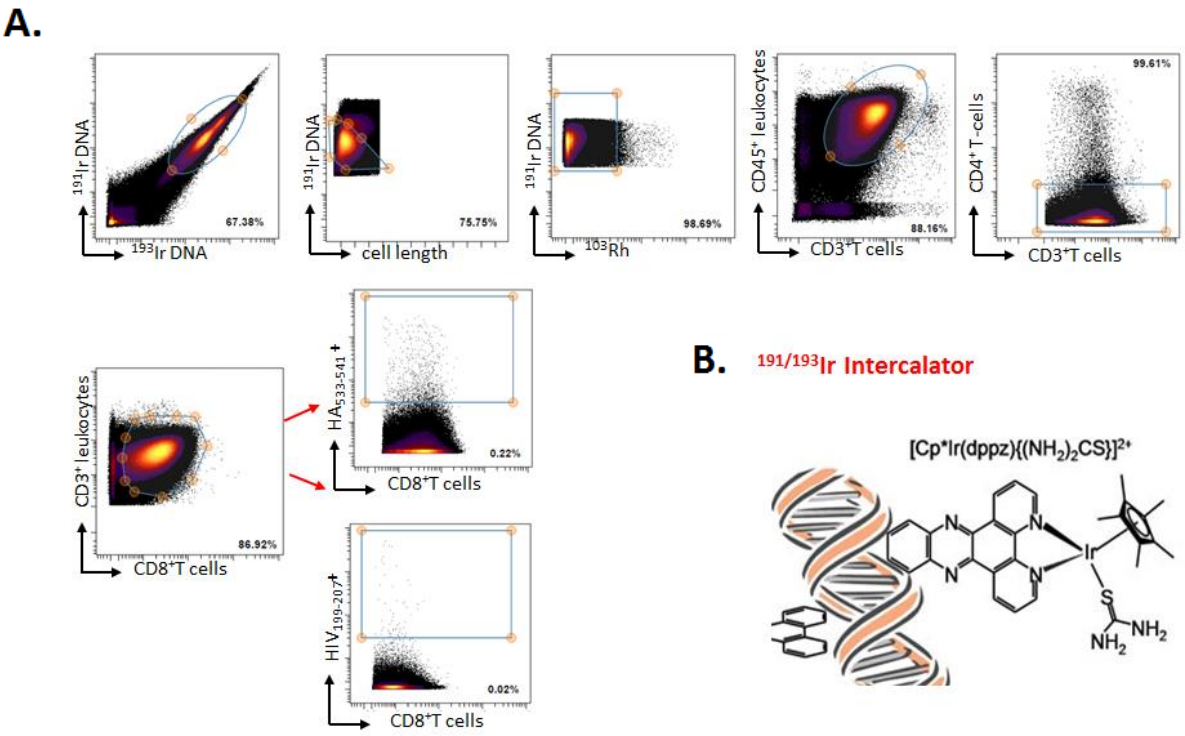

Figure 2.4: Gating strategy for CyTOF (Fluidigm) analysis of $HA_{533-541}$-pentamer^{+}$CD8^{+}$ T cells. A. Cells were selected based on singlets (Iridium (^{191}Ir) DNA vs ^{193}Ir DNA), cell length (^{191}Ir DNA vs cell length) and live cells (^{191}Ir DNA vs. Rhodium (^{103}Rh)). Lymphocytes were further identified based on $CD45^{+}CD3^{+}$ T cells and $CD3^{+}CD4^{-}$ T cells. $CD3^{+}CD8^{+}$ T cells were selected, and $HA_{533-541}$-pentamer^{+} / HIV gag $_{199-207}$-pentamer^{+} were visualized. **B.** The chemical structure of $^{191/193}$Ir DNA-intercalator. Representative dot plots are shown.

2.4. Ethical statement

All mouse studies were performed at the Novartis Vaccines and Diagnostics S.r.l. (now GSK Vaccines S.r.l.) Animal Research Center in compliance with all the current Italian laws on the care and use of animals in experimentation (Legislative Decree 116/92), and with the Company Animal Welfare Policy and Standards. Protocols were approved by the Italian Ministry of Health (authorizations 249/2011-B and 22/2015-PR).

Chapter 3: Formulation, single-cell sorting and *in vivo* cytotoxicity of $HA_{533-541}$-pentamer$^{+}CD8^{+}$ T cells

$CD8^{+}$ T cells are induced during viral infections, and are considered the killer cells of the immune system, with fewer known subpopulations and functions during the immune response. Current knowledge postulates that no antigen-specific $CD8^{+}$ T cells are induced by subunit-based seasonal influenza vaccination, however, in this study, we characterized $CD8^{+}$ T cells induced by either MF59-adjuvanted subunit protein vaccine aMIV or RNA-based SAM(H1) vaccines and their potential cytotoxic nature *in vivo*. The antigen-specific $CD8^{+}$ T cells were single-cell sorted based on positive staining by antigen-specific $HA_{533-541}$-pentamer for further characterization.

3.1. Characterization of vaccine formulations: H1N1+MF59 (aMIV) and CNE56-formulated SAM(H1)

MIV, aMIV and SAM(H1) formulations were checked for various parameters before *in vivo* use. All samples were within a pH range of 7.0 ± 0.5. The aMIV formulation always had an osmolality of 300±60 mOsm/Kg. The SAM(H1) formulation was slightly hypertonic (300 – 450 mOsm/Kg), which was expected due to the composition of the buffer. No visual particulate contamination or precipitation was observed in any formulations. The integrity of the H1N1 antigen (aMIV) after formulation with MF59 was measured by SDS-page. The H1N1 antigen was segmented as HA trimer: HA0 51 kDa, HA1 28 kDa and HA2 14 kDa[95] (figure 3.1.A). The integrity of H1N1 antigen was maintained throughout the formulations. The RNA vaccine was created as a monocistronic vector (figure 3.1.B). SAM(H1) was formulated with CNE56, and the integrity of the replicons was confirmed on an agarose gel both before and after formulation (figure 3.1.C). Moreover, to examine if the RNA was correctly complexed to CNE56 during the formulation, particle size light-scattering was measured (figure 3.1.D). The particle size of CNE56 before formulation was 114.5 d.nm (0.53 SD) with a PDI of 0.13 (0.01 SD), and increased as expected to 132.3 d.nm (0.30 SD), PDI of 0.14 (0.01 SD), after the complexation with RNA. The purity was still maintained.

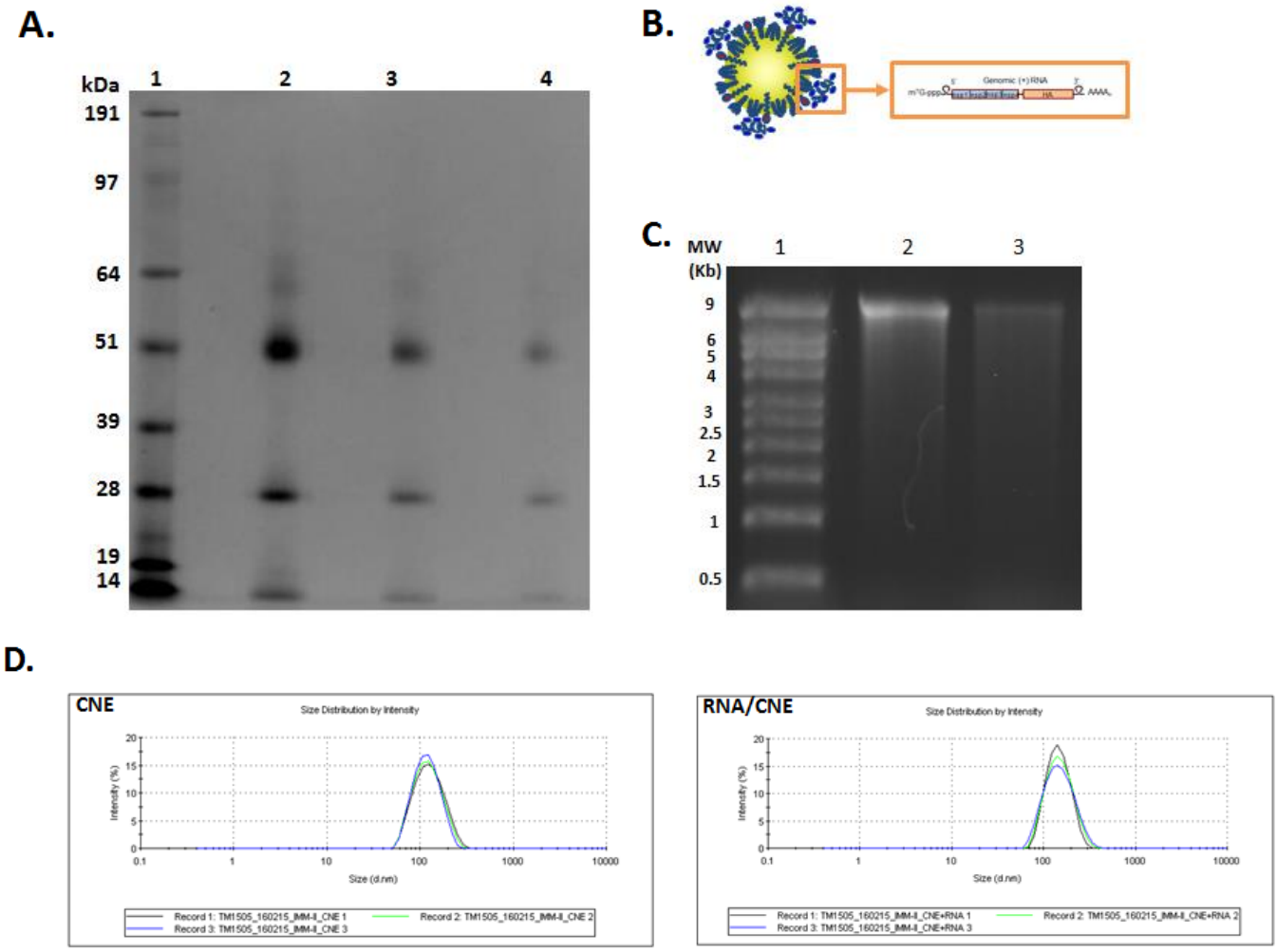

Figure 3.1: H1N1 protein formulated with MF59™ or Self-amplifying mRNA (SAM) vectors formulated with CNE. Before the immunization of BALB/c mice, vaccine formulations were prepared as sterile PBS, 3 µg of H1N1 (A/California/07/2009) antigen alone (MIV) or with 50% MF59 (aMIV), or 15 µg SAM(H1). **A.** SDS page of aMIV formulation (lane 1 (molecular weight ladder in kilodalton (KDa)), lane 2 (standard 24.8 µg), lane 3 (12.4 µg), lane 4 (6.2 µg)). **B.** SAM(H1) construct (orange box) derived from an alphavirus genome, contain a 5' cap, four nonstructural genes (nsp1-4), a 26S subgenomic promoter, the vaccine antigen (HA), and a 3' polyadenylated tail and is formulated with CNE. **C.** The integrity of SAM(H1) after formulation of the *in vitro* synthesized RNAs was confirmed by electrophoresis on an agarose gel (lane 1 (RNA molecular weight (W) ladder in kilobasepair (Kb)), lane 2 (RNA before formulation, 500 ng) and lane 3 (RNA after formulation, 500 ng)). **D.** Particle size of the formulation was measured by DLS before (CNE alone) and after (RNA/CNE) the formulation.

3.2. SAM(H1) induced $HA_{533-541}$-specific cytotoxic $CD8^+$ T cells

It has been shown in a previous study that SAM(H1) vaccine induces a higher frequency of cytokine$^+$CD8$^+$ T cells, with a T_H1 phenotype, compared to aMIV, where only a few cells express cytokine$^+$CD8$^+$ T cells[22]. Cytotoxic activity was determined *in vivo* by measuring the lysis of CFSE-labeled splenocytes, pulsed with H-2K^d-restricted $HA_{533-541}$ peptide or CMTMR-labeled splenocytes, pulsed with unrelated control HIV gag $_{199-207}$ peptide. The pulsed cells were adoptively transferred into mice previously immunized with PBS, MIV, aMIV or SAM(H1). The percentage of CFSE$^+$ and CMTMR$^+$ cells present in the spleens was measured by flow cytometry 20 h after adoptive transfer (figure 3.2.A-B). The specific lysis was calculated as described previously[88]: ratio = R = (% CMTMR+ cells / % CFSE+ cells); % specific lysis = [1- (R PBS control mice / R immunized mice)] x 100. At all timepoints after vaccination, mice immunized with SAM(H1) showed significantly fewer CFSE$^+$ target cells compared to MIV and aMIV, especially at d10p1. No specific lysis was detected in the PBS-treated control group, and $HA_{533-541}$-specific CD8$^+$ T cells were mostly active at d10p1 and d10p2 after vaccination. SAM(H1)-vaccinated mice showed a significantly increased specific lysis compared to PBS at all timepoints, and was only not statistically different from MIV on d10p2, and from aMIV on w6p2. These data confirm previous studies which has demonstrated that SAM(H1) induces specific CD8$^+$ T cells (figure 3.2.C)[22].

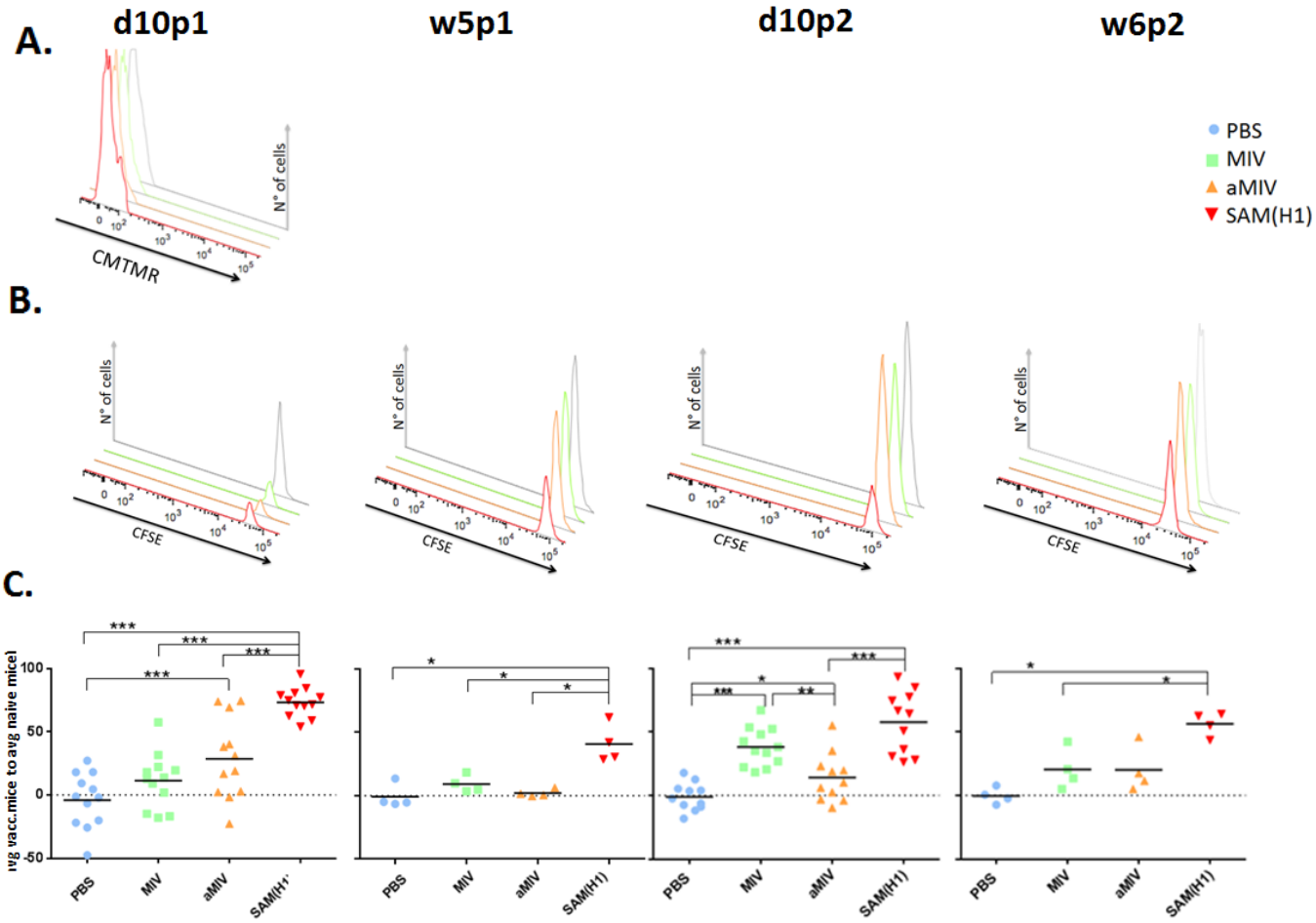

Figure 3.2: SAM(H1) elicit strong cytotoxic activity of $HA_{533-541}$-specific $CD8^+$ T cells *in vivo*. BALB/c mice were immunized intramuscular twice, 8 weeks apart, with PBS, 3 µg of H1N1 antigen (A/California/07/2009) alone (MIV) or with 50% MF59™ or 15 µg SAM(H1) (A/California/07/2009) formulated with CNE. One day before the sacrifice of mice, they were adoptively transferred with naive BALB/c splenocytes loaded with either 5 µM cognate CFSE-peptide $HA_{533-541}$(IYSTVASSL), or 5 µM CMTMR-control peptide HIV gag $_{199-207}$ (AMQMLKETI). Splenocytes of vaccinated mice were processed, stained for CFSE and CMTMR, and gated as: live cells, morphology, singlets, $CMTMR^+$ or $CFSE^+$. Representative histograms indicating the frequency of recovered **A.** a representative histogram of $CMTMR^+$ at d10p1 and **B.** $CFSE^+$ cells at all timepoints, on concatenated samples (n=1-2 experiments, 4-12 mice). **C.** *In vivo* cytotoxicity assay was conducted in mice immunized with SAM(HA) or protein with or without MF59 formulations, at 4 different timepoints. The graphs show the $HA_{533-541}$-specific lysis calculated of the single mice. Statistical significance was determined comparing all the groups. D10 n=2 experiments, w5+w6 n=1 experiment; non-parametric two tailed Mann-Whitney ***p<0.0001, ** p<0.001 *p<0.05.

3.3. Single-cell sorting of $HA_{533-541}$-pentamer$^{+}CD8^{+}$ T cells

The two vaccines were shown to induce cytotoxic $CD8^{+}$ T cells, SAM(H1) more so than aMIV. To understand which cells are activated, and what function they might have, a single-cell characterization was performed. To obtain single $HA_{533-541}$-pentamer$^{+}CD8^{+}$ T cells for transcriptome analysis, splenocytes were stained with H-2K_d-restricted $HA_{533-541}$-pentamer or with control HIV gag $_{199-207}$-pentamer, and visualized as 10^6 singlets (5 different experiments) (figure 3.3.A). MIV, aMIV and SAM(H1) induced higher frequencies of $HA_{533-541}$-pentamer$^{+}CD8^{+}$ T cells compared to PBS-treated mice at all timepoints (figure 3.3.B-C). Only background frequencies of HIV gag $_{199-207}$-pentamer$^{+}CD8^{+}$ T cells were observed (figure 3.3.B). Only SAM(H1) immunization induced increased $HA_{533-541}$-pentamer$^{+}CD8^{+}$ T cells (figure 3.3.C), with a higher number after the second immunization, although there was pronounced variance in responder mice. One mouse from the PBS-treated group and 2 mice from aMIV and SAM(H1) immunization groups (figure 3.3.D) were chosen for future single-cell high throughput multiplexed RT-qPCR characterization. Two 96-well plate/mouse for PBS (very low frequency of $HA_{533-541}$-pentamer$^{+}CD8^{+}$ T cells was found, so the single-cell sorting was done based on the expression of $CD8^{+}$ T cells, and only at d10p2), aMIV and SAM(H1) were chosen for single-cell sorting.

A.

	PBS	MIV	aMIV	SAM(H1)
D10p1	I*II		I*II	I*I*II
W5-6p1	I*II		I*II	I*I*II
D9-10p2	I*I*II	I*	I*I*II	I*I*IIII
w6p2	I*I*II	I*	I*I*II	I*I*IIII

*pool of 2 mice

D.

X10^6 cells	PBS	aMIV	SAM(H1)
D10p1	52.30	129.58	169.93
	-	171.13	187.86
W5p1	22.96	100.56	207.55
	-	157.66	282.51
D10p2	35-66	107.43	159.18
	-	188.9.	906.14
W6p2	24.46	361.84	995.16
	-	669.01	8679.04

B.

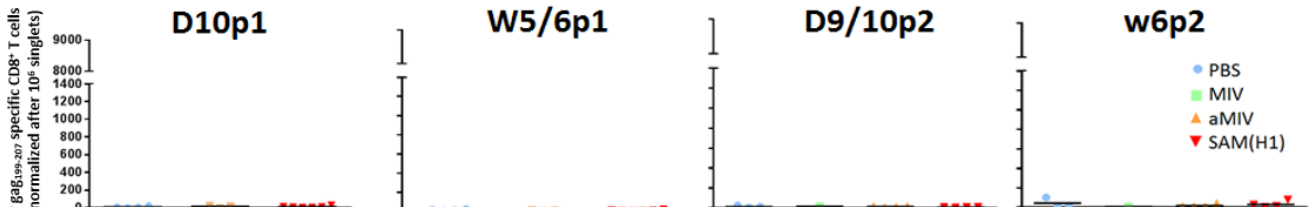

C.

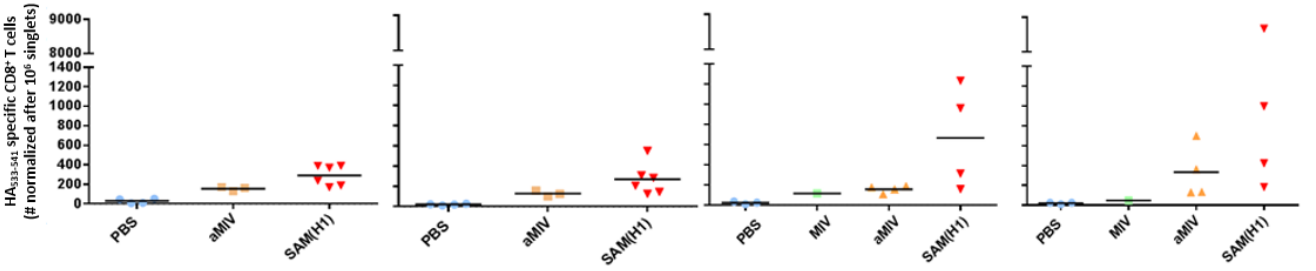

Figure 3.3: Numbers of Flu HA$_{533-541}$-pentamer$^+$CD8$^+$ T cells increase after SAM(H1) vaccination. In different experiments **A.** in pool/single experiments, BALB/c mice were immunized intramuscularly twice, 8 weeks apart, with PBS, 3 µg of H1N1 antigen (A/California/07/2009) alone (MIV) or with 50% MF59^{TM} or 15 µg of SAM(H1) (A/California/07/2009) formulated with CNE. On experimental days d10p1, w5p1/w6p1, d9p2/d10p2 or w6p2, mice were sacrificed, splenocytes processed, stained, and gated as: live cells, morphology, singlets, CD3$^+$, CD8$^+$, HA$_{533-541}$-pentamer$^+$. **B.** The distribution of HIV gag $_{199-207}$–pentamer$^+$ CD8$^+$ T cells after vaccination at all timepoints, showed as individual/pool of mice. **C.** The distribution of HA$_{533-541}$-pentamer$^+$CD8$^+$ T cells after vaccination at all timepoints, showed as individual/pool of mice. **D.** Two plates per mice for PBS (CD8$^+$ T-cell sorted, d10p2 only), aMIV and SAM(H1) were chosen for single-cell sorting for high throughput multiplex RT-qPCR.

Chapter 4: Single-cell transcript analysis of $HA_{533-541}$-pentamer^{+}CD8^{+} T cells

To determine the transcriptional state of $HA_{533-541}$-pentamer^{+}CD8^{+} T cells after single-cell sorting, RT-qPCR was applied as described in section 2.2, by preparation of cDNA, quality control of the single cells, pre-amplification of material and finally the RT-qPCR. After this, a thorough data pre-processing step was done, decreasing the 96 biomarkers to 86 (ignoring; *il-1r*, *ccr6*, *cd70*, *il-4*, *il-5, il-9*, *il-10*, *il-13*, *il-22, mmp2* due to the absence of cells expressing these genes, appendix 1, marked #). The biomarkers considered in this panel are seen in appendix 1 and were selected from literature. These markers indicate the state of the cell, whether it is activated, homed, exhausted or apoptotic. Also markers that can subdivide the cells into effector, effector memory or central memory response are present, together with functions such as cytotoxicity and regulation. The panel consists also of markers associated with CD4^{+} T cells that either overlap with CD8^{+} T-cell functions, or are used as negative markers.

4.1. Characterization of single-cell gene expression by $HA_{533-541}$-pentamer^{+}CD8^{+} T cells

After completion of the RT-qPCR and the pre-processing, the total number of cells analyzed for each timepoint is shown in figure 4.1.A. In general, 100-175 cells were analyzed, except aMIV at w5p1 (75), due to a low quality of the sample. Then, data corresponding to each cell was loaded into the R program and two-component, unsupervised PCA was applied to group cells on variance of expression of the 86 genes measured. PCA compared (i) early vs. late timepoint (d10p1/w5p1 and d10p2/w6p2) (figure 4.1.B), (ii) after first and second doses d10p1 vs. d10p2 or w5p1 vs. w6p2 (figure 4.1.C), and (iii) between SAM(H1) and aMIV at all timepoints (figure 4.1.D). The PCA revealed a pronounced heterogeneity at the single-cell level for all measured timepoints. Early vs. late timepoint had on the principal component 1 between 12-16% variance and on the principal component 2 between 7-11% variance, indicating that the samples measured are transcriptionally similar. This was true for the two vaccines both after prime and boost (figure 4.1.B). The variance between first and second dose did

not further increase the transcriptional difference significantly. The principal component 1 had a variance between 10-21%, and the principal component 2 had a variance between 8-10% for both early timepoint d10p1/d10p2 and the late timepoint w5p1/w6p2 (figure 4.1.C). When the two vaccines were compared, transcriptional overlap was also observed. At d10p1, w5p1 and w6p2, differences were not observable, however, the best separation was seen after boost (d10p2). At d10p2, a slight difference between SAM(H1) and the aMIV/PBS-induced cells was seen (figure 4.1.D).

A.

	d10p1	w5p1	d10p2	w6p2
PBS	-	-	147	-
aMIV	166	75	172	164
SAM(H1)	106	137	175	157

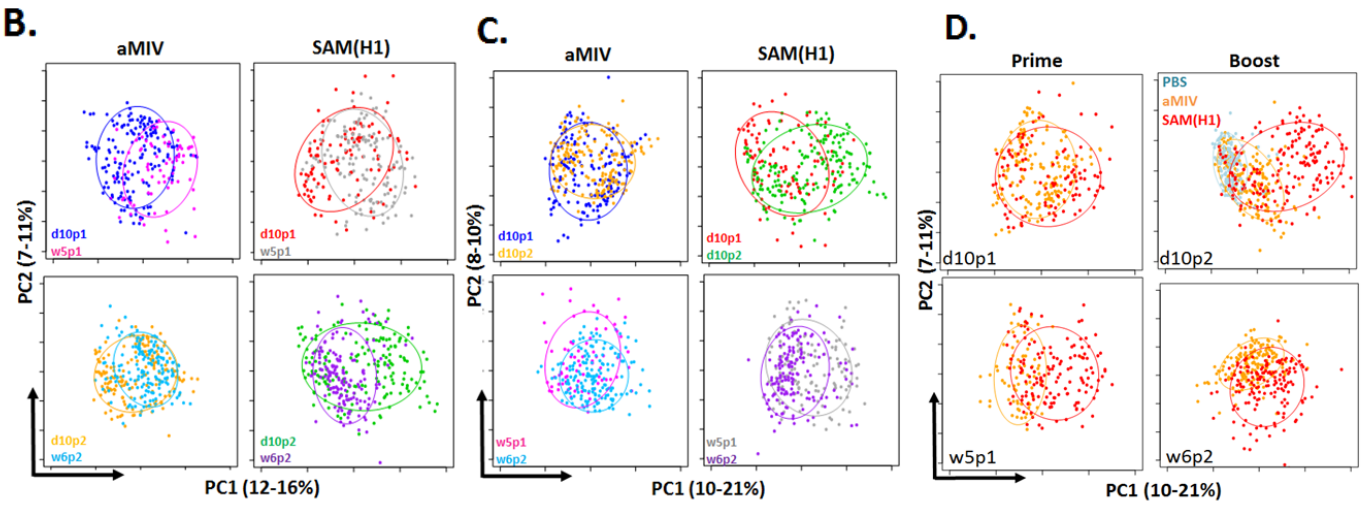

Figure 4.1: Unsupervised PCA reveals a pronounced heterogeneity at the single-cell level. After single-cell sorting and RT-qPCR, transcript expression data were pre-processed and by using the program R, a principal component analysis (PCA) was performed **A.** Number of cells considered. **B.** early (d10) vs. late (w5/6) response, **C.** prime versus boost (d10p1/d10p2) or (w5p1/w6p2) or **D.** SAM(H1) (red) versus aMIV (yellow) at all timepoints. The PBS (light blue) represents total $CD8^+$ T cells and RT-qPCR at d10p2.

To increase the homogeneity of the dataset analyzed by PCA, the $HA_{533-541}$-pentamer$^{+}CD8^{+}$ T cells were subdivided in four populations based on the expression of standard naïve/memory markers[19,96]: T_{EFF} (*il-7rα*$^{-}$cd62l^{-}), T_{EM} (*il-7rα*$^{+}$cd62l^{-}), T_{CM} (*il-7rα*$^{+}$cd62l^{+}) or a phenotype associated with naïve/non-T_{EFF} population T_{NAIVE} (*il-7rα*$^{-}$cd62l^{+}) (figure 4.2.A). Due to the low frequency of $HA_{533-541}$-pentamer$^{+}CD8^{+}$ T cells in PBS and T_{NAIVE} groups, these were excluded from subsequent analysis. The total number of cells analyzed by subpopulation is shown as pie charts (figure 4.2.B). aMIV expressed approximately 45-50% of T_{CM} at all timepoints, and >40% of T_{EM} at w5p1 and w6p2. SAM(H1) had increased T_{EM} frequencies with >60% at w5p1 and beyond. T_{EFF} was only highly increased in SAM(H1) at d10p1. The naïve subpopulation was <10.5% at all timepoints and was left out during analysis due to the low cell number. T_{EFF}, T_{EM} and T_{CM} subpopulations for each vaccine group were analyzed using the 86 total genes in PCA. Both aMIV (figure 4.3.A) and SAM(H1) (figure 4.3.B) clearly induced $HA_{533-541}$-pentamer$^{+}CD8^{+}$ T cells belonging to one of the three subpopulations, with a slight overlap, seen at all timepoints.

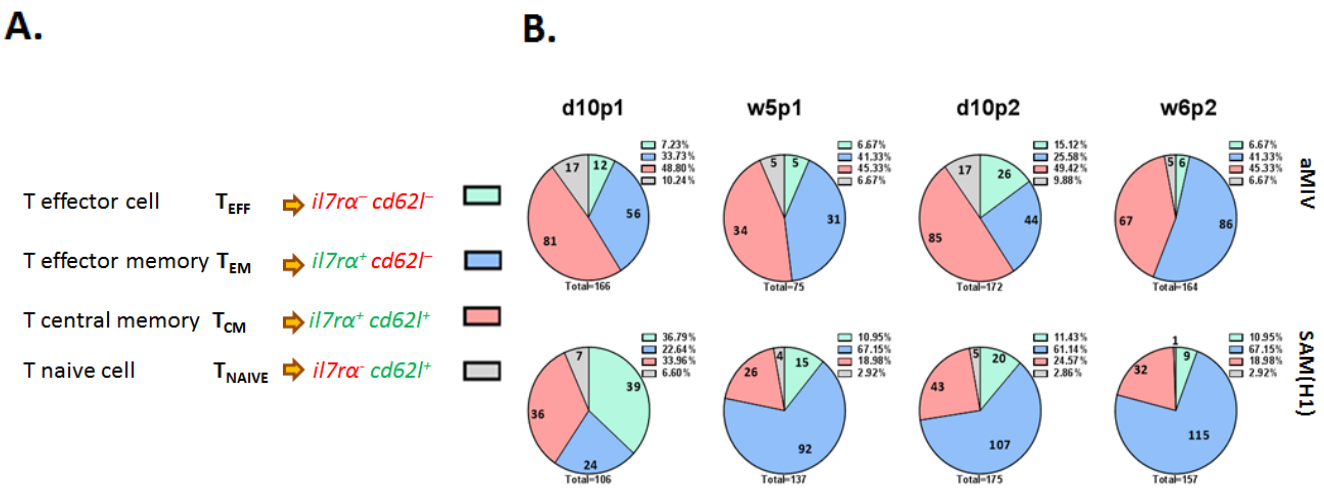

Figure 4.2: Separation based of known effector/memory markers decreases the heterogeneity of the dataset. To decrease the heterogeneity of the dataset, the cells were divided in **A.** four different categories based on known differentiation markers, T_{EFF} (*il-7rα*$^{-}$ *cd62l*$^{-}$), T_{EM} (*il-7rα*$^{+}$ *cd62l*$^{-}$), T_{CM} (*il-7rα*$^{+}$ *cd62l*$^{+}$) and T_{NAIVE} (*il-7rα*$^{-}$ *cd62l*$^{+}$) population. **B.** The total number of cells in the transcriptional single-cell analysis is visualized by pie chart. The individual numbers of cells in the subpopulation are within, the total number is located below and percentages of the 4 subpopulations are in the right upper corner of the pie chart. Green=T_{EFF}, blue=T_{EM}, red=T_{CM}, grey=T_{NAIVE}. T_{NAIVE} cell populations have been excluded due to low cell number.

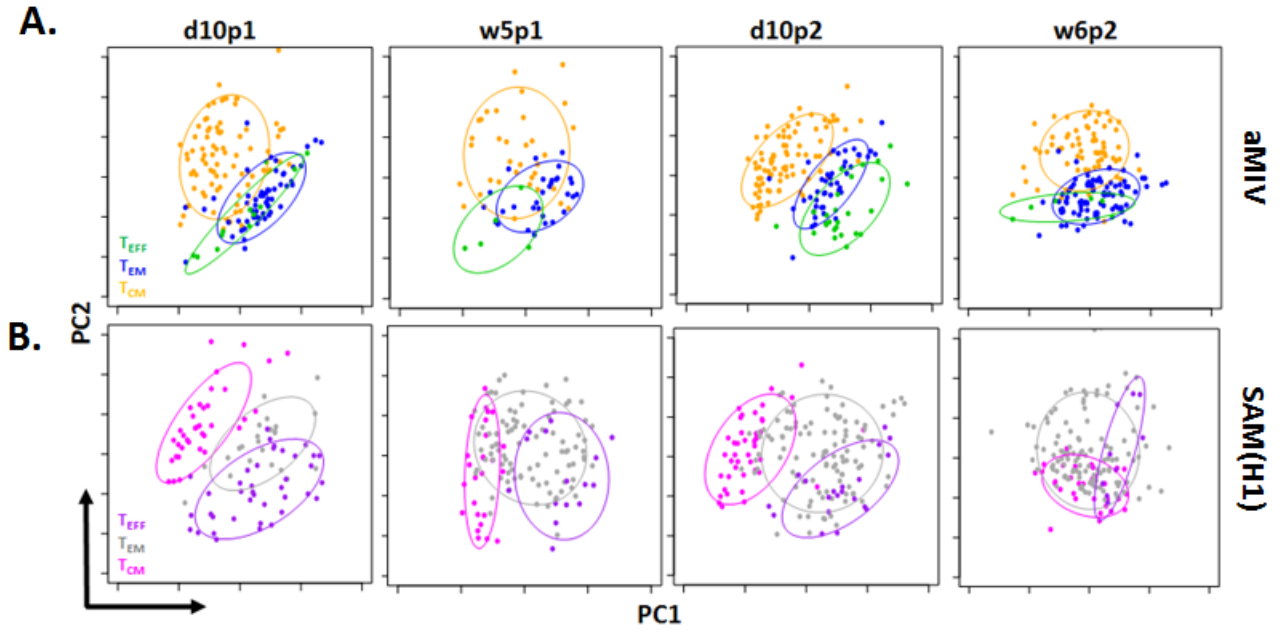

Figure 4.3: T_{EFF}, T_{EM} and T_{CM} subpopulations were observable for each vaccine. Different gene expression profiles in the three subpopulations can be observed within the two vaccines: **A.** aMIV at all timepoints, effector T-cell (T_{EFF}) (green), effector memory T-cell (T_{EM}) (blue) and central memory T-cell (T_{CM}) (orange) and **B.** SAM(H1) at all timepoints, T_{EFF} (purple), T_{EM} (grey) and T_{CM} (pink).

Given this data, a deeper characterization of genes important for the separation was the next analysis. By 86 gene scatterplot, the frequency of cells expressing the genes are shown (genes that fall outside of the limit line are over-expressed in cells: left side SAM(H1) and right side aMIV). It was observed that T_{EFF} (figure 4.4) and T_{EM} (figure 4.5) cells in aMIV and SAM(H1) groups demonstrated different gene expression profiles, while T_{CM} (figure 4.6) cells in aMIV and SAM(H1) showed similar gene expression profiles. Further characterization of the genes of interest (genes that fell out of the limit line) was done with bar plotting and Fisher's test (appendix 3.A-C). The three subpopulations are individually explained below and significance appointed with *$p \leq 0.05$, **$p \leq 0.001$.

4.1.1. T_{EFF} subpopulation: This subpopulation was expressed in only few cells at all timepoints (figure 4.2.B). Nonetheless, a transcriptional difference could be appreciated between T_{EFF} cells induced by the two vaccines, especially for d10p1 (PC1 19% variance, PC2 9% variance) and d10p2 (PC1 22% variance, PC2 11% variance) (figure 4.4.A).

aMIV primed T_{EFF} cells showed significantly higher frequency of cells expressing *bcl3* ($p \leq 0.05$, priming), *41bb* ($p \leq 0.05$, survival) and *cd160* ($p \leq 0.05$, inhibition) at d10p1 (figure 4.4.B, appendix 3.A). At d10p2, this profile had shifted to a significantly higher frequency of cells expressing genes of the TNFR superfamily, *cd27* and *girt* ($p \leq 0.05$, positively regulate the survival, proliferation and function of $CD8^+$ T cells during immune activation), *tgf-β*, *camklv* ($p \leq 0.05$, regulation), *cxcr3* ($p \leq 0.001$, inflammatory homing) and *pd1* ($p \leq 0.05$, exhaustion/terminal differentiation). *eomes* ($p \leq 0.05$) which is considered a gene for priming future T_{CM} phenotype was also present, confirming that mostly T_{CM} cell subpopulation are found within aMIV (pie chart figure 4.2.B). On the contrary, SAM(H1) induced cells at d10p1 with significant frequencies of *gzma* ($p \leq 0.05$), *gzmb* ($p \leq 0.05$) and *gzmk* ($p \leq 0.001$) (cytotoxic profiling), *cx3cr1* ($p \leq 0.05$, inflammatory recruitment) and *icos* ($p \leq 0.05$, activation) transcripts. At d10p2, the cytotoxic profile of *gzma* ($p \leq 0.001$), *gzmb* ($p \leq 0.001$), *gzmk* (ns) and *perforin* (ns) and inflammatory recruitment *ccr5* (ns), *cx3cr1* ($p \leq 0.001$) and *cxcr6* ($p \leq 0.001$) remained. However, also *klrd* ($p \leq 0.001$), *klrk* ($p \leq 0.001$) and *klrc* ($p \leq 0.001$) (regulation, activation and preservation respectively), *spi6* ($p \leq 0.05$, inhibition of cytotoxic cell apoptosis) and terminally differentiated SLEC population (*blimp*$^+$(ns), *tbet*$^+$(*ns*), *klrg1*$^+$($p \leq 0.05$) and *eomes*$^-$ ($p \leq 0.05$)) genes were upregulated (figure 4.4.B, appendix 3.A). In summary, two different T_{EFF} populations were distinguished between aMIV- and

SAM(H1)-induced $CD8^+$ T cells. To summarize, aMIV driven T_{EFF} cells were mainly characterized by a cell-maintenance and TNFS pathways with cxcr3 inflammatory homing, while SAM(H) driven T_{EFF} cells were mainly associated with perforin/granzyme (lytic granule) pathways, and a SLEC population was found within this subpopulation. Clustering and characterization of gene transcripts could not be reliably performed at W5p1 and w6p2 due to low numbers of T_{EFF} cells at these timepoints (figure 4.4, appendix 3.A).

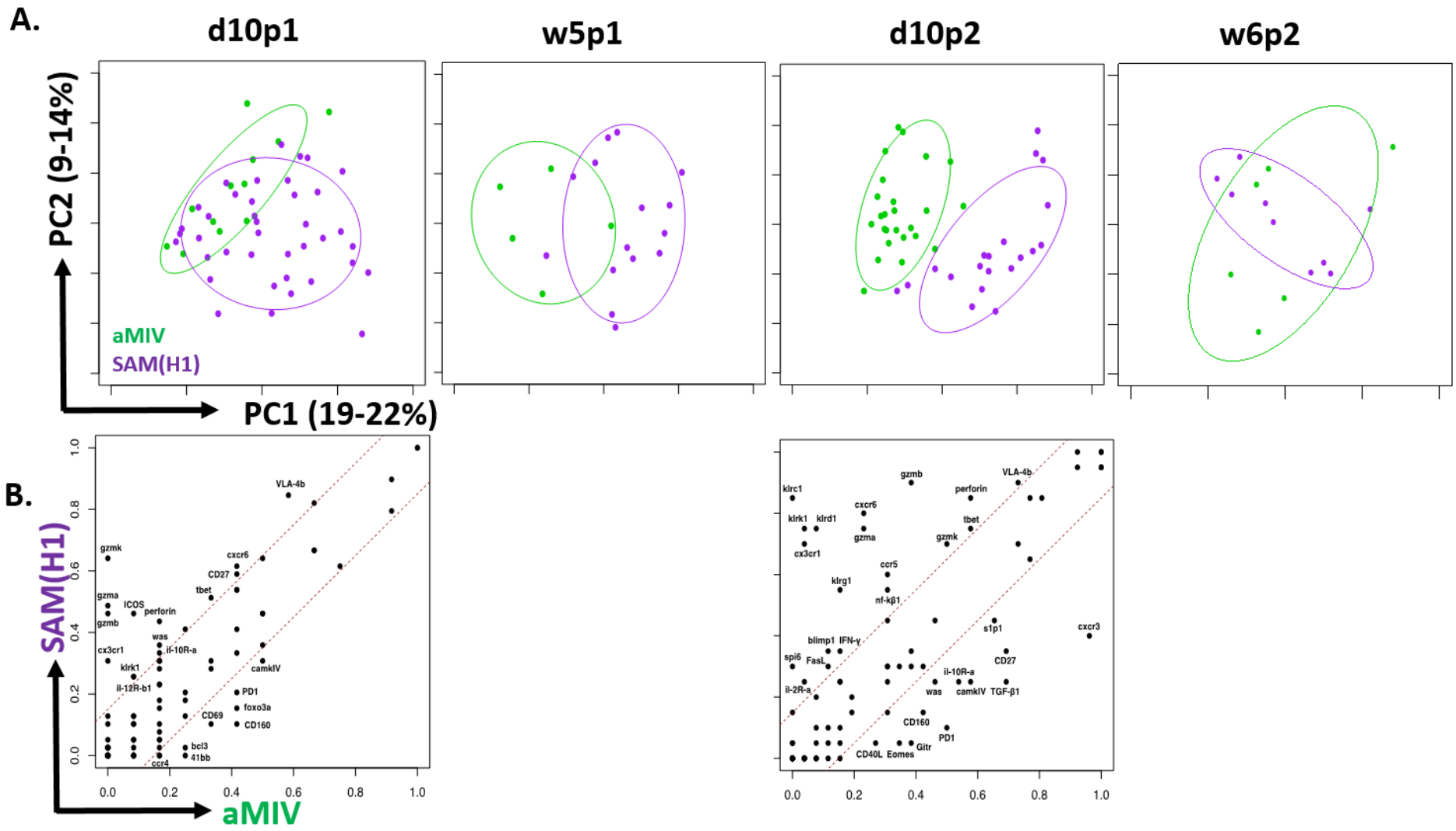

Figure 4.4: T_{EFF} cells in aMIV and SAM(H1) vaccine groups show different DEG profiles. Cells classified as T_{EFF} (*il7ra*, *cd62l*) are visualized. **A.** Principal component analysis (PCA) reveals increased difference in gene expression between aMIV (green) and SAM(H1) (purple) at d10p2. **B.** Scatterplot show the frequency of cells expressing the genes. The limit line (·····) indicates genes which are expressed in ≤15% of the cells in the two vaccines. Named genes in the upper left corner of the plot are increasingly frequent in cells stimulated by SAM(H1), and named genes in the lower right corner are increasingly frequent in cells stimulated by aMIV. The timepoints w5p1 and w6p2 are left out due to low number of cells. DEG = differentially expressed genes.

4.1.2. T_{EM} subpopulation: T_{EM} cells were slightly more numerous than T_{EFF} (figure 4.2.B). The variance measured was highest in the first component at the d10 timepoint both after prime d10p1 (PC1 17% variance, PC2 6% variance) and boost d10p2 (PC1 21% variance, PC2 8% variance) compared with the late timepoints after prime w5p1 (PC1 15% variance, PC2 8% variance), and boost w6p2 (PC1 10% variance, PC2 8% variance) (figure 4.5.A). Cells within the T_{EM} subpopulation conserved transcriptional differences between the two vaccines (figure 4.5, appendix 3) as seen in the T_{EFF} subpopulation.

No genes were significantly upregulated in the aMIV group at d10p1, but 2 genes from the TNF superfamily *cd40l* and *gitr* ($p \leq 0.05$-0.001, proliferation and survival) were upregulated for the rest of the timepoints. At w5p1, a significant upregulation of *gata3* ($p \leq 0.05$, homeostasis), *tgfb1* ($p \leq 0.05$, regulation), *icos* ($p \leq 0.05$, co-stimulatory), *cd44* ($p \leq 0.05$, antigen maturation), *cd27* ($p \leq 0.05$, maintenance and survival) and *CXCR3* ($p \leq 0.05$, inflammatory homing) was detected. At w6p2, the upregulation of *gata3* ($p \leq 0.05$, homeostasis) and *ox40* ($p \leq 0.001$, "recall of memory") would indicate a memory response. However, the exhaustion profile and T_{CM} priming phenotype was no longer observed within the T_{EM} as expected (figure 4.5.B, appendix 3.B). SAM(H1) vaccine group showed significant increases in the frequency of cells expressing genes at all timepoints when compared with cells from aMIV vaccine group, however the transcript profile was similar to the one seen in the T_{EFF} subpopulation. A significant upregulation of cytotoxic markers like *gzma*, *gzmb*, *gzmk*, *perforin* and *ifn*-γ, inflammatory recruitment markers like *ccr5*, *cxcr3*, *cxcr6*, *cx3cr1,* and regulation, activation and preservation markers like *klrk*, *klrd* and *klrc* was seen at most timepoints. At d10p2, the T_{EM} subpopulation no longer had terminally differentiated SLEC subtypes (solitary $tbet^+$). A cluster of cells significantly upregulating transcripts linked with cytotoxic and inflammatory recruitment ($gzma^+$, $gzmb^+$, $gzmk^+$, $cx3cr1^+$, $ccr5^+$) and KLR ($klrk^+$, $klrd^+$, $klrc^+$) was interestingly observed at d10p2, while it remained below 20% within aMIV driven cells (figure 4.5.B, appendix 3.B). To summarize, aMIV driven T_{EM} cells were mainly characterized like the T_{EFF} subpopulation, by a cell-maintenance and TNFS pathways, however with an induced memory profile at w6p2. SAM(H1) driven T_{EM} cells were still showing a cytotoxic nature, whereas the SLEC population found in T_{EFF} subpopulation had disappeared (figure 4.5, appendix 3.B).

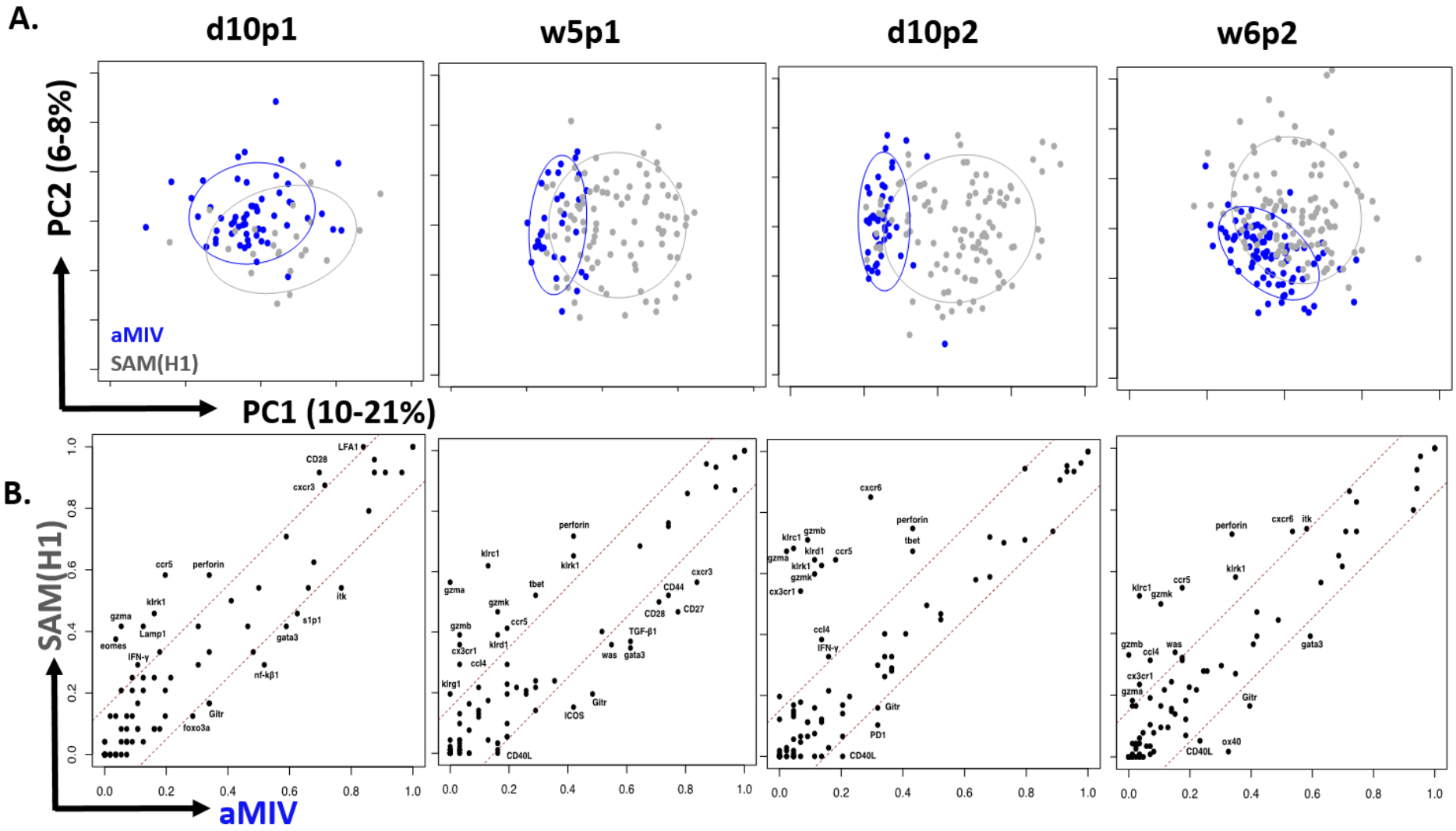

Figure 4.5: T_{EM} cells in aMIV and SAM(H1) vaccine groups show different DEG profiles. Cells classified as T_{EM} (*il7ra*$^{+}$, *cd62l*$^{-}$) are visualized. **A.** Principal component analysis (PCA) reveals increased difference in gene expression between aMIV (blue) and SAM(H1) (grey) at all timepoints but d10p1 **B.** Scatterplot show the frequency of cells expressing the genes. The limit line (·····) indicates genes which are expressed in ≤15% of the cells in the two vaccines. Named genes in the upper left corner of the plot are increasingly frequent in cells stimulated by SAM(H1), and named genes in the lower right corner are increasingly frequent in cells stimulated by aMIV. DEG = differentially expressed genes.

4.1.3. T_{CM} subpopulation: T_{CM} cells had pronounced transcriptional overlap between the two vaccines at most timepoints, with very low variance <15% at all timepoints (figure 4.6.A); d10p1 (PC1 15% variance, PC2 10% variance), w5p1 (PC1 13% variance, PC2 9% variance), d10p2 (PC1 14% variance, PC2 6% variance), and w6p2 (PC1 11% variance, PC2 7% variance).

aMIV driven T_{CM} cells expressed more memory markers than T_{EFF} at most timepoints. At 10p1, cells stimulated by aMIV had increased expression of *cd44* ($p \leq 0.05$, antigen maturation), *gata3* ($p \leq 0.05$, homeostasis and activation), *cxcr4* and *cd69* ($p \leq 0.05$, memory homing to bone marrow). At w5p2, *stat5* ($p \leq 0.05$, memory homeostasis) was expressed in more aMIV-induced cells, with also *il-2rγ* ($p \leq 0.05$, stimulation), *tgfb1* ($p \leq 0.05$, regulation) and TNF marker *cd40l* ($p \leq 0.05$, proliferation). At d10p2, only *ccr7* ($p \leq 0.05$, lymphatic organ homing) was observed, and w6p2 only TNF *ox40* ($p \leq 0.001$, co-stimulatory recall memory responses).

SAM(H1) driven T_{CM} cells still expressed cytotoxic markers. At 10p1, cells induced by SAM(H1) had increased expression of *tgfb1* ($p \leq 0.05$, regulation) and il-21r ($p \leq 0.05$, long-term maintenance and functionality). At w5p2, *gzmk* ($p \leq 0.05$, cytotoxic marker) and *klrk1* ($p \leq 0.05$, activation of cytotoxic $CD8^+$ T cells). At d10p2, *klrk1* ($p \leq 0.05$, activation of cytotoxic $CD8^+$ T cells)) and *gzmk* ($p \leq 0.001$, cytotoxic marker) were still observed, along with *ccr5* ($p \leq 0.001$, memory marker for lung homing during viral infection) and *tbet* ($p \leq 0.05$, SLEC, but only in 35% of the cells). At w6p2, cytotoxic markers (*ifn-γ, gzmk, il-10rα*), memory markers (*ccr5, stat5a, il-21r, eomes*), klr (*klrc, klrk*) and activation (*lfa1*) was observed.

Of the genes with significantly different expressions, aMIV driven T_{CM} cells showed memory responses at most timepoints, while SAM(H1) driven T_{CM} cells showed cytotoxic and memory responses (figure 4.6, appendix 3.C). Despite a slightly significant difference in frequencies of cells expressing genes, they were mostly located close to the 15% line (with slightly significant difference in frequency of cells expressing the gene) and not analyzed further (figure 4.6.B, appendix 3.C).

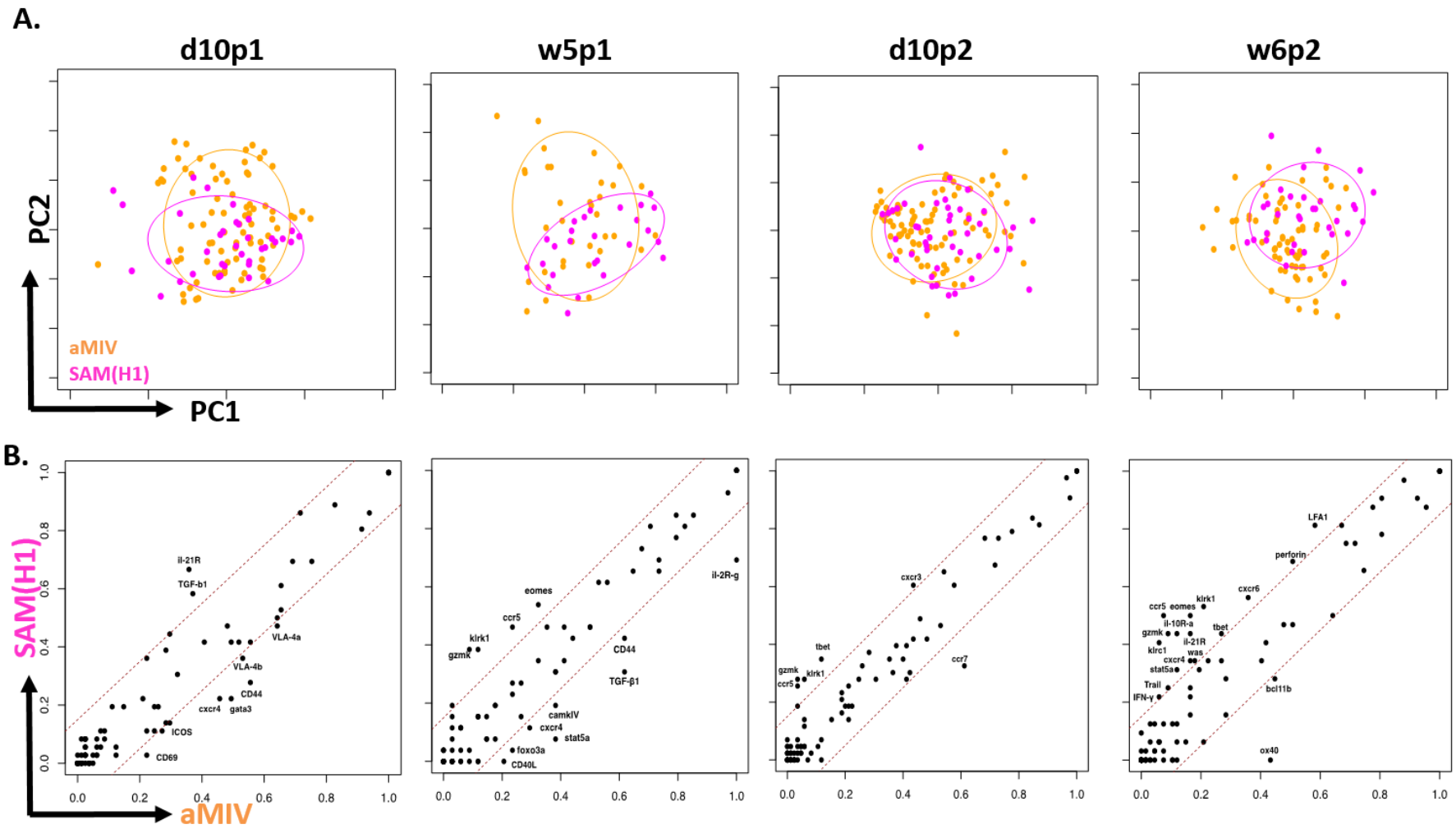

Figure 4.6: T_{CM} cells in aMIV and SAM(H1) vaccine groups show similar DEG profiles. Cells classified as T_{CM} (*il7ra*$^{+}$, *cd62l*$^{+}$) are visualized. **A.** Principal component analysis (PCA) reveals similar gene expression between aMIV (orange) and SAM(H1) (pink) at all timepoints. **B.** Scatterplot show the frequency of cells expressing the genes. The limit line (·····) indicates genes which are expressed in ≤15% of the cells in the two vaccines. Named genes in the upper left corner of the plot are increasingly frequent in cells stimulated by SAM(H1), and named genes in the lower right corner are increasingly frequent in cells stimulated by aMIV. DEG = differentially expressed genes.

4.2. Differentially expressed genes (DEG) between vaccines

Transcriptional difference could be seen in T_{EFF} and T_{EM} subpopulation between the vaccines. The next question was to identify the genes accounting for this difference. Most differences were seen at d10p2, and this timepoint will be the focus of the rest of this thesis. By applying two statistical significance tests, LRT^3 (measurement of level of expression and frequency of cells expressing the gene) and FDR correction (hypothesizing the rate of type I errors in null hypothesis testing when conducting multiple comparisons), a list with DEG between the two vaccines for the 3 subpopulations was established (figure 4.7.A). Twelve genes were differentially expressed between T_{EFF} subpopulations, 36 genes between T_{EM} subpopulations and 7 genes between T_{CM} subpopulations. Some genes appeared on all three lists, and a total of 39 genes were identified. Of the 12 genes from the T_{EFF} cells, mainly effector biomarkers such as inflammatory recruitment (*cx3cr1*, *cxcr3*, *cxcr6*), cytotoxic profile (*gzma*, *gzmb*, *perforin*), regulate, activate, prevent and inhibit apoptosis (*klrd*, *klrc*, *klrk, spi6*), SLEC (*klrg*), exhaustion and terminally differentiated (*pd1*) were identified. T_{EM} cells showed both effector and memory markers, with multipurpose function (homing, homeostasis, cytotoxicity and regulation). Interestingly, 10 of the DEG found in the T_{EFF} gene list were also found in T_{EM} cells, all except *cxcr3* and *spi6*. The 7 differentially expressed genes within the T_{CM} cells included memory (*ccr5*, *klrc*, *il-21r*, *il-2rγ*), cytotoxicity preparedness (*gzmk*, *klrk*) and stimulation (*was*).

Heat maps performed using all 39 genes show that T_{EFF}/T_{EM} cells induced by SAM(H1) vaccine had a great overlap (figure 4.7.B), while T_{CM} cells were clustered individually. Cells in the aMIV vaccinated group remained highly heterogeneous between the three subpopulations (figure 4.7.C).

A.

T_{EFF} (12)	
Gene	LRT/FDR
klrc1	2.80E-08
gzma	1.59E-06
klrd1	8.15E-06
klrk1	1.41E-05
cxcr6	3.11E-05
cx3cr1	3.11E-05
klrg1	0.0003
cxcr3	0.0004
gzmb	0.0061
spi6	0.0320
perforin	0.0400
pd1	0.0472

T_{CM} (7)	
Gene	LRT/FDR
ccr5	0.0103
gzmk	0.0104
klrc1	0.0104
was	0.0230
il-2rγ	0.0378
klrk1	0.0378
il-21r	0.0378

T_{EM} (36)			
Gene	LRT/FDR	Gene	LRT/FDR
cxcr6	8.30E-14	*klrg1*	0.00364
gzma	4.09E-13	*btla*	0.00402
klrc1	1.62E-12	*blimp1*	0.00547
gzmb	4.93E-12	*tlr4*	0.00664
klrd1	2.50E-11	*lfa1*	0.00715
klrk1	3.40E-08	*traf2*	0.00735
cx3cr1	1.49E-07	*trail*	0.01059
ccr5	1.92E-07	*tgf-B1*	0.01251
gzmk	6.97E-07	*il-10rα*	0.01558
perforin	1.89E-05	*ccl4*	0.01558
cd40l	5.78E-05	*pd1*	0.01722
was	0.0004	*cd69*	0.01783
il-2rγ	0.00081	*mki67*	0.02063
il-2rα	0.00225	*ifn-γ*	0.02063
cd44	0.00233	*notch2*	0.02077
cd8	0.00240	*tim3*	0.02179
ccr4	0.00240	*selplg*	0.02179
ccr7	0.00336	*bcl6*	0.04289

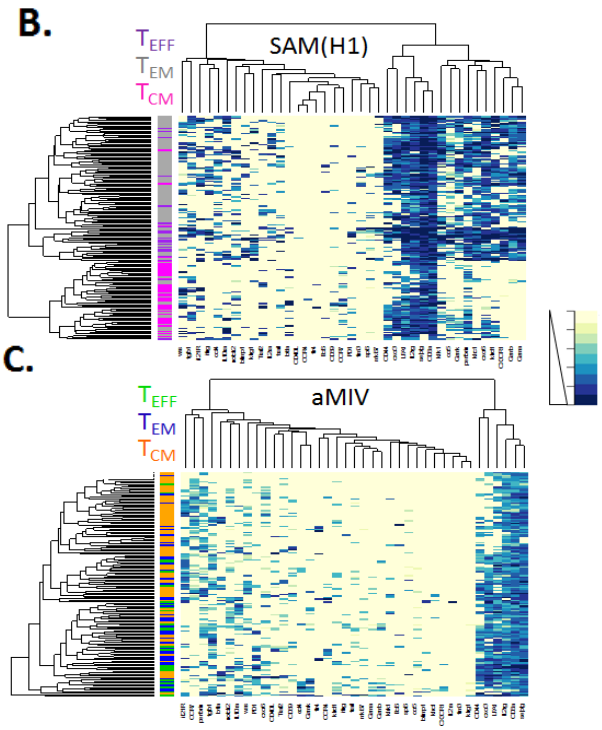

Figure 4.7: DEG between CD8^{+}T-cell subpopulations induced by the two vaccines at d10p2. By applying two statistical significance tests (likelihood ratio test (LRT) & false discovery rate (FDR) correction test) a list of genes that were differentially expressed between the two vaccines could be found in each subpopulation. **A.** Twelve DEG in T_{EFF} cells, 36 DEG in T_{EM} cells, and 7 DEG in T_{CM} cells. Certain genes overlap between the three subpopulations and give a total of 39 genes in the DEG list. Heat maps performed using all 39 genes show a defined clusterization of cells from the three subpopulations in **B.** SAM(H1) and **C.** aMIV vaccine group. DEG = differentially expressed genes

PCA analyses were performed on the genes listed in figure 4.7.A for each T-cell subpopulation (figure 4.8, 4.9, 4.10).

Twenty-six and twenty T_{EFF} cells were analyzed from aMIV and SAM(H1) vaccine groups, respectively. PCA performed on the total 39 DEG genes increased (PC1 = 32% variance, PC2=12% variance) (figure 4.8.A) compared to the PCA completed with 86 genes (figures 4.4). In addition, if the PCA was restricted to the 12 T_{EFF} DEG, this variance increased further (PC1 = 54% variance, PC2=13% variance) (figure 4.8.B). The 12 genes were presented as dot plots, where both transcript expression and quantity were measured. Most of the effector genes were expressed in more cells and at a higher level within SAM(H1) induced cells, compared to aMIV induced cells, especially the KLRs. The only exception was *cxcr3* and *pd1*, which were more expressed in aMIV driven T_{EFF} cells (figure 4.8.C).

Forty-four and 107 T_{EM} cells were analyzed in aMIV and SAM(H1) vaccine groups, respectively. As with T_{EFF} cells, PCA completed on the 39 DEG increased the variance (figure 4.9.A) (PC1 = 31% variance, PC2=9% variance) compared with the total 86 genes (figures 4.5). If the PCA was applied to the T_{EM} associated 36 DEG, the variance did not increase further (PC1 = 34% variance, PC2=7% variance) (figure 4.9.B). However, if the PCA was applied to the 12 T_{EFF} DEG, an increased variance was seen (PC1 = 51% variance, PC2=11% variance) (figure 4.9.C). This indicated that the effector genes were responsible for the differences. To confirm this hypothesis, the 10 DEG found in both T_{EFF} and T_{EM} cells were subtracted from the 36 genes in the T_{EM} subpopulation, and these 26 DEG were applied to a PCA. The 26 genes abolished the variance (PC1 = 17% variance, PC2=11% variance) (figure 4.9.D), indicating that the separator genes are found in the effector list. The 12 effector DEG were shown as dot plots, and most of the effector genes were expressed in more cells and at a higher level within SAM(H1) driven T_{EM} cells, compared to aMIV driven T_{EM} cells. As seen with the T_{EFF} subpopulation, more aMIV induced T_{EM} cells were positive for *pd1*. The *cxcr3* transcript, however, was increased in SAM(H1) induced T_{EM} cells, compared to T_{EFF} cells (figure 4.9.E).

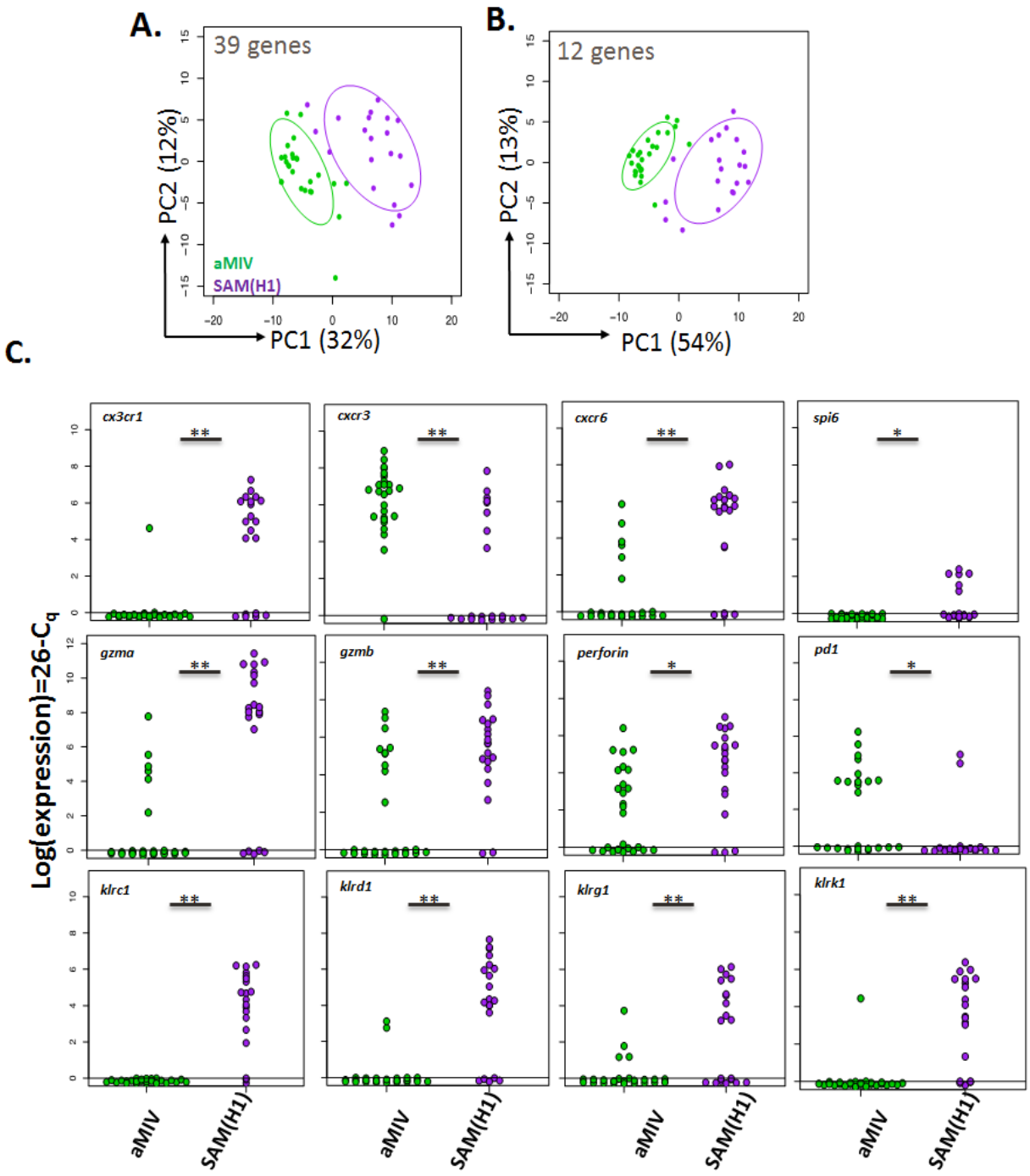

Figure 4.8: T_{TEFF} signature with T_{EFF} DEG at d10p2. Twenty-six cells in the aMIV (purple) vaccine group and twenty cells in the SAM(H1) (green) vaccine group were analyzed. **A.** principal component analysis (PCA) was completed using the 39 differentially expressed genes (DEG). **B.** PCA was completed using the 12 T_{EFF} DEG. **C.** To observe the expression level of the genes, a dot plot for each of the 12 effector genes was performed. Likelihood ratio test: **p<0.001, *p<0.05.

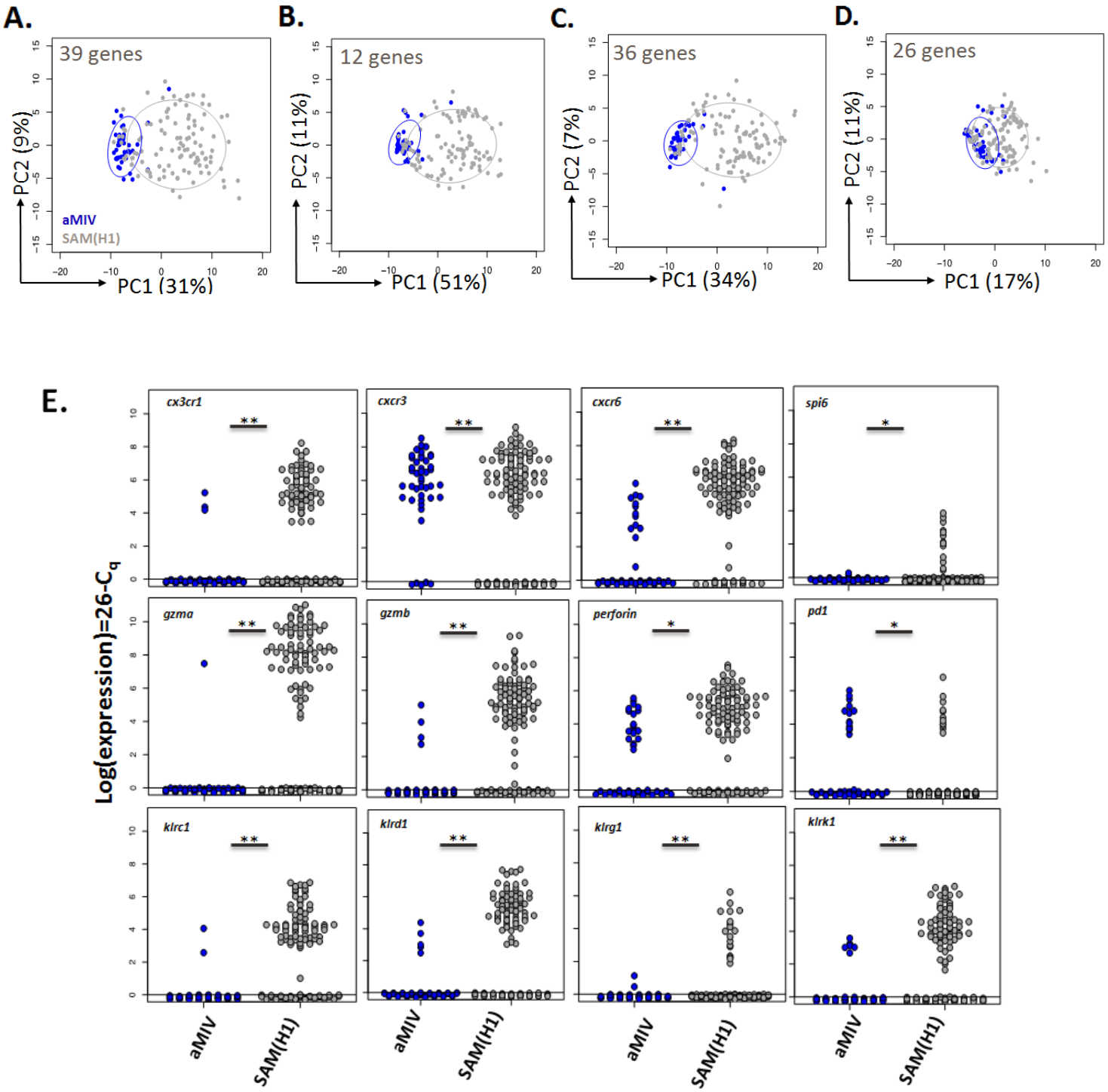

Figure 4.9: T_{EM} signature with T_{EFF} DEG at d10p2. Fourty-four cells in the aMIV (blue) vaccine group and 107 cells in the SAM(H1) (grey) vaccine group were analyzed. **A.** = principal component analysis (PCA) was completed using the 39 differentially expressed genes (DEG). **B.** PCA was completed using the 36 T_{EM} DEG. **C.** PCA was completed using the 12 T_{EFF} DEG. **D.** PCA was completed using 26 T_{EM} genes (10 T_{EFF} genes (*–spi6* and *cxcr3*) - 36 T_{EM} genes). **E.** To observe the expression level of the genes, a dot plot for each of the 12 effector genes was performed. Likelihood ratio test: **p<0.001, *p<0.05.

In the T_{CM} cell subpopulation, eighty-five cells from aMIV group and forty-three cells from SAM(H1) vaccine group were analyzed. PCA on the 39 DEG did not increase the variance compared to the total 86 genes (figures 4.6) (PC1 = 18% variance, PC2=9% variance) (figure 4.10.A), however, the 7 DEG did increase the variance (PC1 = 35% variance, PC2=25% variance) (figure 4.10.B). The overlap between the two vaccines is still present, however, T_{CM} cells induced by SAM(H1) seem to contain other two subpopulations. This interesting profile warrants further analyses that are beyond the scope of this thesis.

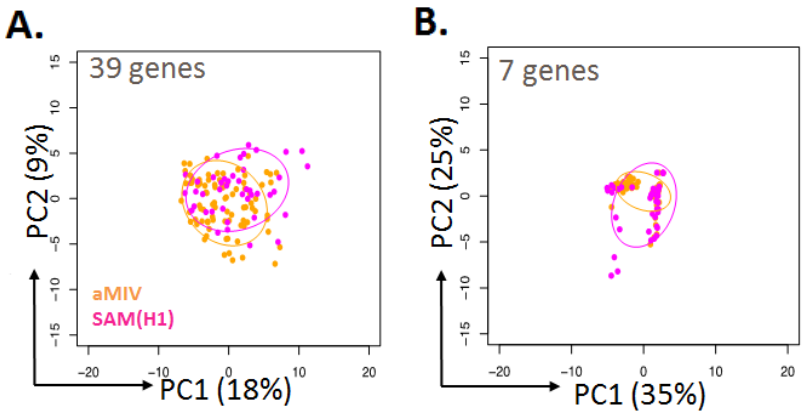

Figure 4.10: T_{CM} signature with T_{CM} DEG at d10p2. Eighty-five cells in the aMIV (orange) vaccine group and forty-three cells in the SAM(H1) (pink) vaccine group were analyzed. **A.** Principal component analysis (PCA) was completed using the 39 differentially expressed genes (DEG). **B.** PCA was completed using the 7 T_{CM} DEG.

4.3. Single-cell characterization

A list of DEG was made, and this showed that out of 12 effector genes, most were upregulated in the SAM(H1) vaccine group, and most were of cytotoxic nature. The PCA showed a transcriptional difference in the T_{EFF} and T_{EM} subpopulations, and these will be further dissected. Of the 26 T_{EFF} cells in aMIV and 20 T_{EFF} cells in SAM(H1), a percentage of T_{EFF} cells expressing a given gene was calculated. In the T_{EFF} subpopulation, most aMIV-induced cells were positive for *cxcr3* (96%), and half of the cells were positive for *pd1*. A high number of T_{EFF} cells were expressing *perforin* (42%) and *gzmb* (38%), but the rest of the 12 genes were expressed in 23% or less of the cells (table 4.1). SAM(H1) driven T_{EFF} cells were positive for most of the 12 effector genes, with only *pd1* (10%) and *spi6* (30%) expressed in

fewer cells. In the T_{EM} cell subpopulation, aMIV induced cells were upregulating the *cxcr3* transcript (88%) and *perforin* (43%), but the percent of cells expressing *pd1* had decreased from 50% to 31%. C*xcr6* was still expressed in approximately 1/3 of T_{EM} cells, while most other effector genes were expressed in 13% or less of the cells. SAM(H1) stimulated cells still highly expressed most of the 12 effector genes, but compared with T_{EFF} cells, had a higher frequency of cells expressing *cxcr3* and a lower frequency of cells expressing *klrg1*.

aMIV

T_{EFF}	%	T_{EM}	%
klrc1	0	*gzma*	2
spi6	0	*klrc1*	4
klrk1	3	*spi6*	4
cx3cr1	3	*klrg1*	4
klrd1	7	*cx3cr1*	6
klrg1	15	*gzmb*	9
gzma	23	*klrd1*	11
cxcr6	23	*klrk1*	13
gzmb	38	*cxcr6*	29
perforin	42	*pd1*	31
pd1	50	*perforin*	43
cxcr3	96	*cxcr3*	88

SAM(H1)

T_{EFF}	%	T_{EM}	%
pd1	10	*pd1*	10
spi6	30	*spi6*	13
cxcr3	40	*klrg1*	17
klrg1	55	*cx3cr1*	53
cx3cr1	70	*klrd1*	65
gzma	75	*klrk1*	63
klrd1	75	*gzma*	66
klrk1	75	*klrc1*	70
cxcr6	80	*gzmb*	71
klrc1	85	*cxcr3*	73
perforin	85	*perforin*	75
gzmb	90	*cxcr6*	85

Table 4.1: Percentage of cells expressing 12 effector DEG in T_{EFF} and T_{EM} cell subpopulations at d10p2. By using likelihood ratio test (LRT) and False Discovery Rate (FDR) correction, 12 effector differentially expressed genes (DEG) were found to differentiate the two vaccines. Percentage of cells expressing a given gene is seen for the two T_{EFF} and T_{EM} cell subpopulations induced by aMIV and SAM(H1) vaccines.

To put the 12 DEG into perspective, a hierarchical clustering of single cells was performed for the T_{EFF} (figure 4.11) and T_{EM} (figure 4.12) cells.

$CD8^+$ T_{EFF} cells driven by aMIV mainly expressed *cxcr3*. Most of the cells were also *perforin* positive; however, of the single cells expressing *pd1*, none did express any of the cytotoxic markers, except a few cells which were positive for *gzmb* and *cxcr6* (figure 4.11.A). No cell expressed *klrc* or *spi6*, and only one cell expressed *klrk* and *cx3rcr1*. If this is visualized with a combination map, this confirmed the signature seen in the hierarchical clustering. Cells were mainly *cxcr3*$^+$*pd1*$^-$*perforin*$^+$ (19,2 % of cells) or *cxcr3*$^+$*pd1*$^+$*perforin*$^-$*(15,4% of cells)* (figure 4.11.B). T_{EFF} cells in the aMIV vaccinated group were more homogeneous than cells in the SAM(H1) vaccinated group. Cells induced by SAM(H1) showed a

cytotoxic phenotype, with most of the cytotoxic biomarkers from the 12 DEG present in the single cells (figure 4.11.C). Most cells did not express *pd1*, *spi6* or *cxcr3*. This is a reverse phenotype to what is seen in the aMIV group. The combination map of SAM(H1) induced T_{EFF} cells was not as homogeneous as for aMIV induced cells. Most cells were unique in their features, with a higher number of cells expressing multiple cytotoxic transcripts (figure 4.11.D).

In the T_{EM} subpopulation, $CD8^+$ T cells induced by aMIV still highly expressed *cxcr3* in all cells, and *perforin* in almost half of the cells. Interestingly, when *pd1* was present, *cxcr6* was absent. Four signatures were observed: $cxcr3^+pd^-cxcr6^-perforin^-$(22,7% of the cells), $cxcr3^+pd^+cxcr6^-perforin^-$ (13,6% of the cells), $cxcr3^+pd^+cxcr6^-perfori^+$ (9% of the cells) and $cxcr3^+pd^-cxcr6^+perforin^-$ (6,8% of the cells). Cytotoxic markers were absent in all except one single cells (figure 4.12.A). As with T_{EFF} cells, most aMIV induced T_{EM} cells were homogeneous. Many transcripts were single, double or triple-upregulated (figure 4.12.B). Again, unlike aMIV, $CD8^+$ T_{EM} cells induced by the SAM(H1) vaccine upregulated cytotoxic genes, and showed a more complex and heterogeneous signature (figure 4.12.C). Most cells were negative for *spi6*, *pd1* and *klrg* transcript. 73% of T_{EM} cells expressed *cxcr3* compared to 40% of the T_{EFF} cells. The combination map clearly indicated a highly heterogeneous population of T_{EM} cells induced by SAM/H1) vaccine with an enrichment in multi transcript positive cells (figure 4.12.D).

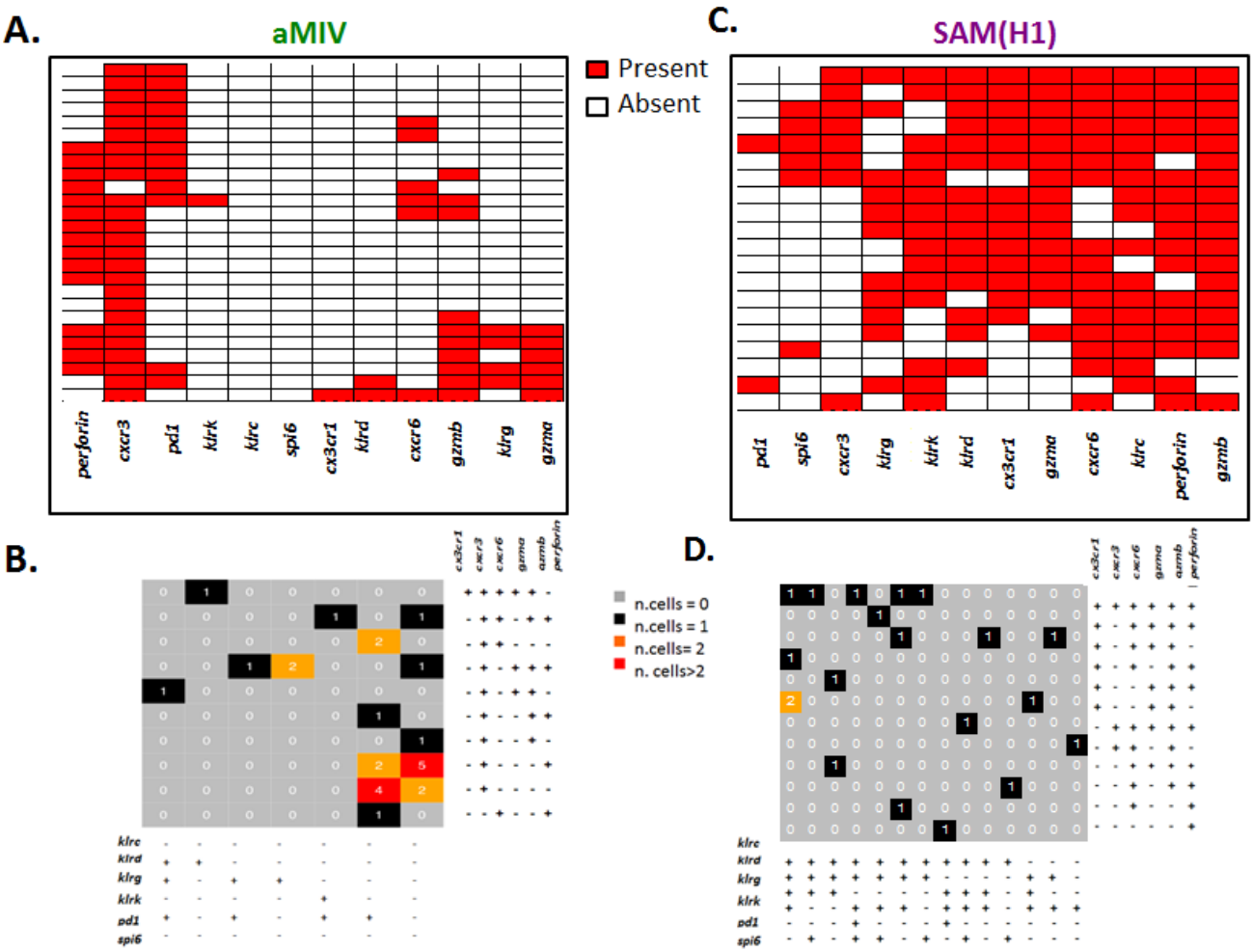

Figure 4.11: Hierarchical clustering of T_{EFF} cells based on presence-absence of 12 effector DEG d10p2. Twenty-six cells in the aMIV vaccine group and twenty cells in the SAM(H1) vaccine group were analyzed. **A.** Hierarchical map and **B.** combination map indicating enrichment of cells positive for multiple transcripts in the aMIV vaccine group. **C.** Hierarchical map and **D.** combination map indicating enrichment of cells positive for multiple transcripts in the SAM(H1) vaccine group. Hierarchical clustering heat map: red = transcript present, white = transcript absent. Combination map: grey = 0 cells positive, black = 1 cell positive, orange = 2 cells positive, red = >2 cell positive. DEG = differentially expressed genes

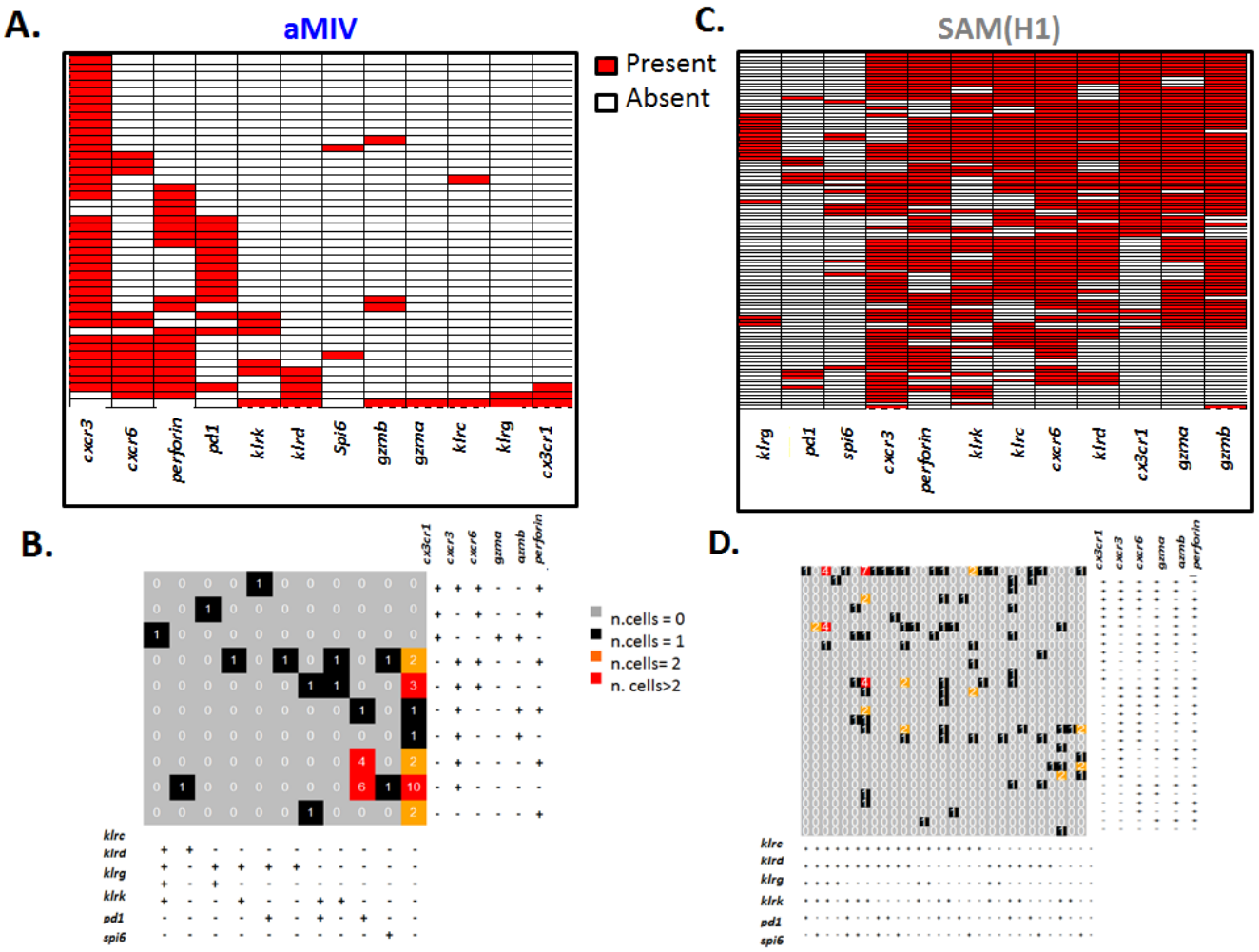

Figure 4.12: Hierarchical clustering of T_{EM} cells based on presence-absence of 12 effector DEG d10p2. Forty-four cells in the aMIV vaccine group and 107 cells in the SAM(H1) vaccine group were analyzed. **A.** Hierarchical map and **B.** combination map indicating enrichment of cells positive for multiple transcripts in the aMIV vaccine group. **C.** Hierarchical map and **D.** combination map indicating enrichment of cells positive for multiple transcripts in the SAM(H1) vaccine group. Hierarchical clustering heat map: red = transcript present, white = transcript absent. Combination map: grey = 0 cells positive, black = 1 cell positive, orange = 2 cells positive, red = >2 cell positive. DEG = differentially expressed genes

Chapter 5: Mass cytometry

Flow cytometry is a highly performing technology platform for the analysis of protein expression on single cells. However, there is a need for increasing the numbers of fluorophores for the detection of multiple markers on a single cell. Mass cytometry is a novel technique that allows increasing the numbers of parameters by using metal-labeled Ab without the issue of spectral overlap. Currently there is 40+ metals available, with a possibility and promise of >100 markers over time. To determine if the transcripts identified in the previous section (chapter 4) were translated into proteins, we applied mass cytometry to the study of aMIV and SAM(H1)-induced $CD8^+$ T cells $HA_{533-541}$-pentamer$^+CD8^+$ T-cells subsets were identified and the molecular signature found in the transcript analysis was validated at the protein level.

5.1. Evaluation of $HA_{533-541}$-pentamer$^+CD8^+$ T cells

Due to the complexity of the CyTOF-1 machine, this pilot study on protein characterization was set up at different days. Splenocytes from PBS-treated mice were processed on day 3 post second immunization (d3p2), splenocytes from aMIV vaccinated mice were analyzed on day 9 post second immunization (d9p2) and w6p2, while splenocytes from SAM(H1) vaccinated mice were taken at d10p2 and w6p2. In one pilot experiment, splenocytes from 3 individual BALB/c mice were enriched for $CD8^+$ T cells by negative selection, pooled, and stained with H-$2K^d$-restricted $HA_{533-541}$-pentamer and the 32 metal-labeled Ab (appendix 2). The gating was completed in Cytobank[83] (figure 2.4.A) and the number of $HA_{533-541}$-pentamer$^+CD8^+$ T-cells was normalized based on 10^6 singlets (figure 5.1). As previously observed with flow cytometry, $HA_{533-541}$-pentmer$^+CD8^+$ T cells could also be distinguished by mass cytometry for both vaccine delivery systems after boost. aMIV (776 $HA_{533-541}$- pentmer$^+CD8^+$ T cells per 10^6 singlets at d9p2) and SAM(H1) (1030 $HA_{533-541}$- pentmer$^+CD8^+$ T cells per 10^6 singlets at d10p2) vaccines induced higher number of $HA_{533-541}$- pentmer$^+CD8^+$ T-cells compared to PBS-treated mice (151 $HA_{533-541}$- pentmer$^+CD8^+$ T cells per 10^6 singlets at d3p2) (figure 5.1.A). Individual plots indicated the frequency of $HA_{533-541}$- pentmer$^+CD8^+$ T cells (not normalized), and here 0.02% of cells from PBS d3p2, 0.15% of cells from aMIV at d10p2 and 0.10% of cells from SAM(H1) d10p2 were

$HA_{533-541}$-pentmer^{+}CD8^{+} T cells (figure 5.1.B). The background of pentamer staining observed in PBS-treated mice might represent a pool of naïve cells with a TCR cross-reactive with $HA_{533-541}$ or alternatively, non-specific binding of the pentamer; in any case, the number of $HA_{533-541}$-pentamer^{+}CD8^{+} T cells was much lower in PBS-treated mice compared to aMIV and SAM(H1)-vaccinated mice after normalization (figure 5.1.A)

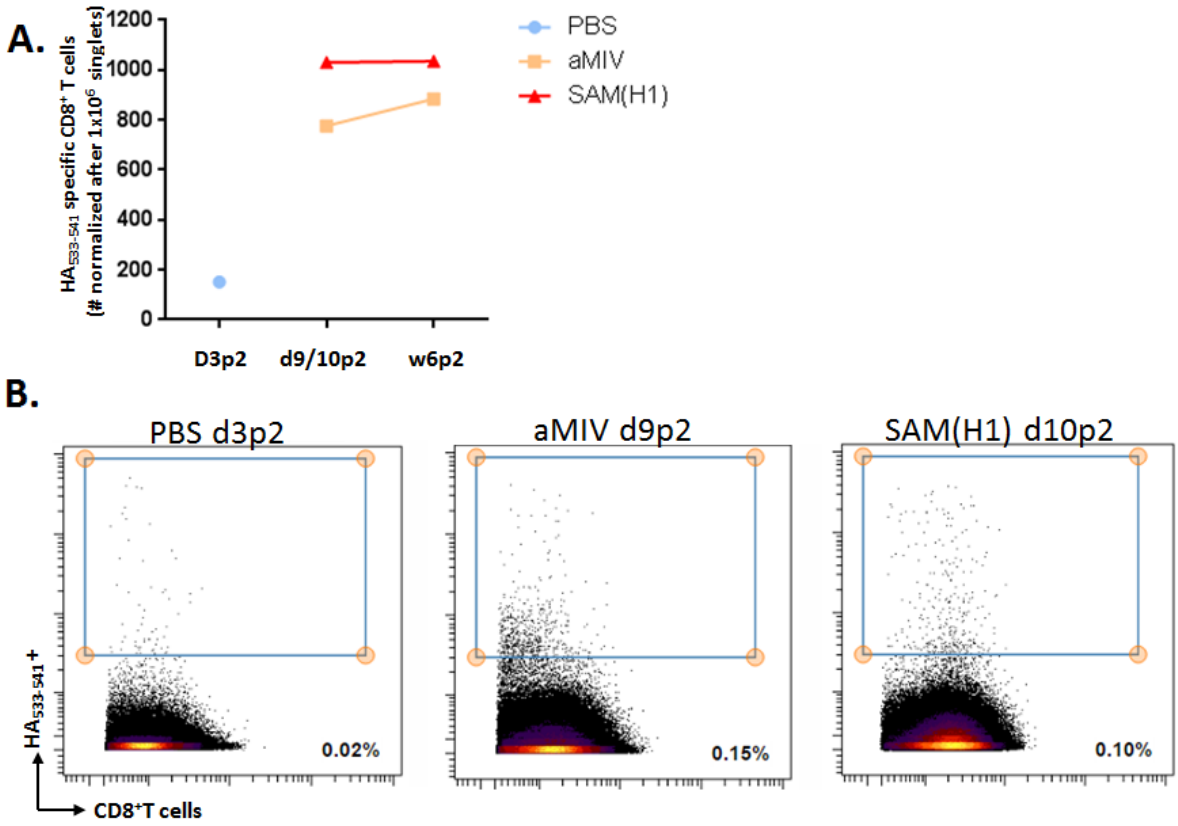

Figure 5.1: Mass cytometry preliminary data suggests that the number of $HA_{533-541}$-pentamer^{+} CD8^{+} T cells increases after two doses of aMIV and SAM(H1) vaccines. In one experiment, 3 BALB/c mice were immunized intramuscular twice, 8 weeks apart, with PBS, 3 µg of H1N1 antigen (A/California/07/2009) with 50% MF59^{TM} (aMIV) or 15 µg SAM(H1) (A/California/07/2009) formulated with CNE. At d3p2 for PBS, d9p2/w6p2 for aMIV and d10p2/w6p2 for SAM(H1), mice were sacrificed and splenocytes were processed. CD8^{+} T cells were enriched and stained. Samples were concatenated and gated in Cytobank[83] as: singlets, cell length and live cells, lymphocytes were further identified based on CD45^{+}CD3^{+} T cells and CD3^{+}CD4^{-} T cells. CD3^{+}CD8^{+} T cells were selected, and $HA_{533-541}$-pentamer^{+} cells were visualized (see figure 2.4.A for the complete gating strategy). **A.** Numbers of $HA_{533-541}$-pentamer^{+} CD8^{+} T cells after vaccination at all timepoints showed as concatenated samples and normalized to 10^{6} CD8^{+} T cells. **B.** Individual raw plots (not normalized) of $HA_{533-541}$-pentamer^{+} CD8^{+} T cells are shown for PBS (d3p2), aMIV (d9p2) and SAM(H1) (d10p2).

To compare transcriptional data with protein expression, known memory markers CD62L and IL-7Rα used previously, were applied to the gating strategy. A schematic plot is shown in figure 5.2.A with T_{NAIVE} cells in the upper left corner, T_{EFF} in the lower left corner, T_{EM} in the lower right corner and T_{CM} in the upper right corner. A representative plot is also shown for total $CD8^+$ T cells after SAM(H1) vaccination (figure 5.2.B). When applying this gating strategy to $HA_{533\text{-}541}$-pentamer$^+CD8^+$ T cells (not normalized), few cells were observed in the PBS vaccinated group (69 per 10^6 cells), with no T_{EM} and T_{CM} cells observed at d3p2. aMIV had an increased number of $HA_{533\text{-}541}$-pentmer$^+CD8^+$ T cells (397 per 10^6 cells) at d9p2 with clear T_{EFF} and T_{CM} cell populations. SAM(H1) at d10p2 did not show the same memory marker profile despite having similar numbers of $HA_{533\text{-}541}$-pentmer$^+CD8^+$ T cells (398 per 10^6 cells). The reason behind this different memory profile is unclear, and needs to be tested further, however, many other memory markers are being used for memory characterization in mass cytometry[81] and other analyses will be performed, but are out of the scope of this thesis. The memory markers as used in the transcriptional analysis could not be applied here, and an analysis on the total $HA_{533\text{-}541}$-pentmer$^+CD8^+$ T-cell subpopulation was done.

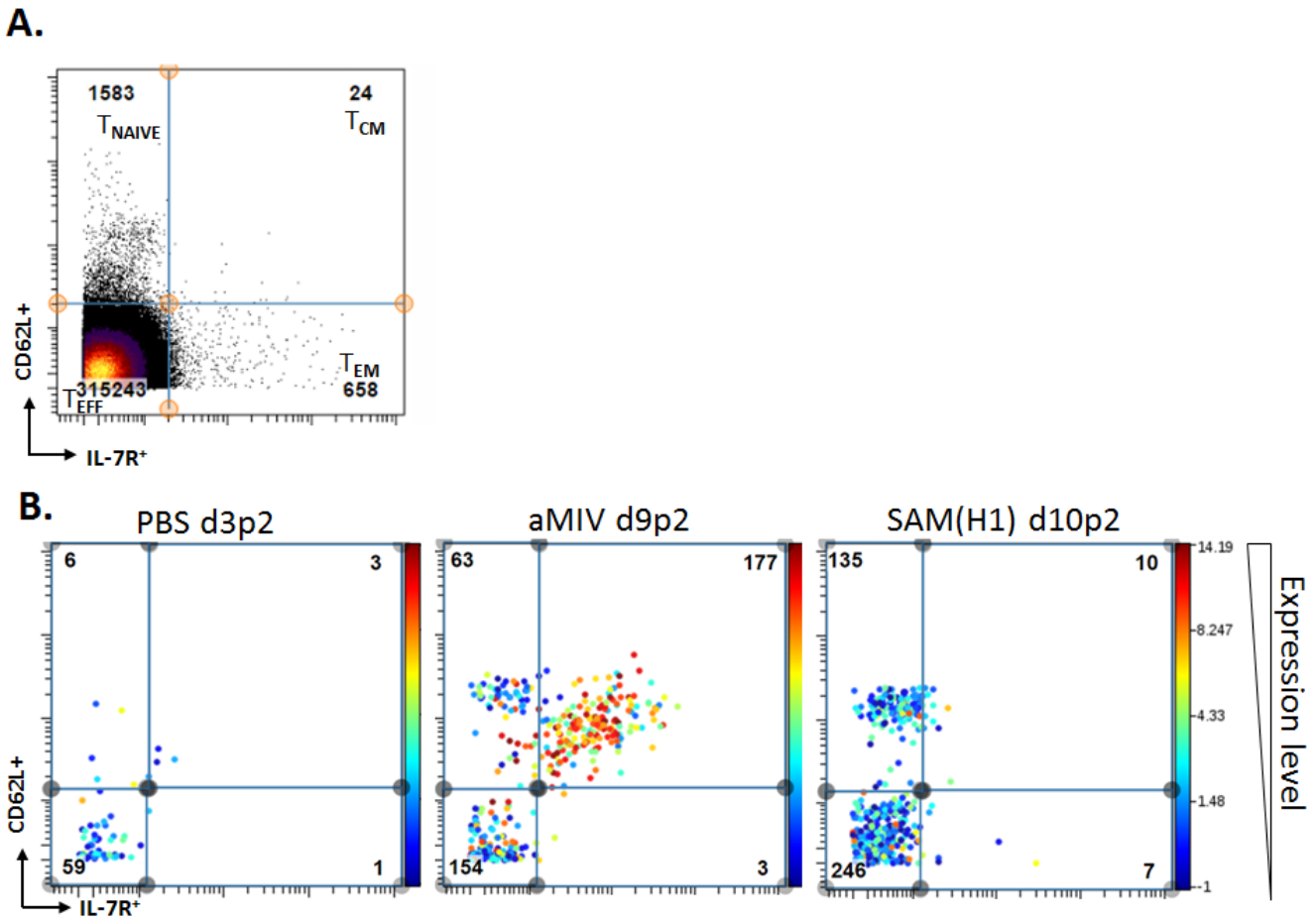

Figure 5.2: Identification of $HA_{533-541}$-pentmer$^{+}CD8^{+}$ T_{NAIVE} , T_{EFF} , T_{EM} and T_{CM} cell subpopulations by mass cytometry. A. The four different phenotypes based on known memory markers T_{NAIVE} (IL-7Rα^{-} CD62L^{+}), T_{EFF} (IL-7Rα^{-} CD62L^{-}), T_{EM} (IL-7Rα^{+} CD62L^{-}) and T_{CM} (IL-7Rα^{+}CD62L^{+}) are plotted. Representative dot plot showing total CD8^{+} T cells from SAM(H1) vaccinated mice. **B.** $HA_{533-541}$-pentmer^{+}CD8^{+}T cells at d3p2 for PBS, d9p2 for aMIV and d10p2 for SAM(H1) vaccines in t-SNE. The Y-channel illustrates DC62L (^{164}Dy), X-channel illustrates IL-7Rα (^{174}Lu). The color scale goes from low (blue), through medium (green/yellow) to highly expressed (red) of $HA_{533-541}$-pentamer^{+} cells.

After samples' acquisition, expression of the different markers was evaluated on the $HA_{533-541}$-pentamer$^{+}CD8^{+}$ T cells. The number of cells positive is shown in table 5.1. The number of cells positive for a given protein marker is indicated for aMIV at d9p2 and SAM(H1) at d10p2, and normalized to 10^{6} singlets. Some of the markers upregulated in the transcript analysis were also upregulated at the protein level. aMIV driven cells showed increased frequencies of CXCR3 (8.2-fold) and PD1 (1.2-fold),

while more SAM(H1) driven cells expressed cytotoxic markers (KLRK1 (1.6-fold), perforin (27.1-fold) and GzmB (39.3-fold)). Surprisingly, CXCR6 was expressed in more aMIV driven cells (6.3-fold), and perforin was highly upregulated in SAM(H1) driven cells, while in the transcript analysis, perforin was highly present in response to both vaccines within the T_{EFF} and T_{EM} subpopulations. However, the protein analysis was based on total $HA_{533-541}$- pentmer$^{+}CD8^{+}$ T cells and not on memory subpopulations, so variations between transcript and protein analyses might be expected.

	aMIV D9p2	SAM(H1) D10p2
CCR5	388	13
IL-7Rα (CD127)	432	23
CCR6	419	33
*CXCR3	352	43
*CXCR6	165	26
CD25 (IL-2Rα)	607	85
CD69	427	72
FasL (CD178)	6306	62
CD11a (LFA1)	357	118
CD62L	612	475
*PD1 (CD279)	632	531
TRAIL (CD253)	8	0
IFN-γ	0	0
TNF-α	0	3
*KLRG1	0	3
*KLRK1 (CD314)	306	495
TGF-β1	5	20
CCR4	10	30
CCR7(CD197)	3	26
*Perforin	7	190
IL-2	23	349
*GzmB	23	904

Table 5.1: Transcript data confirmed by protein expression on $HA_{533-541}$-pentmer$^{+}CD8^{+}$ T cells. At d10p2 after vaccination, 22 of the protein markers in $HA_{533-541}$- pentmer$^{+}CD8^{+}$ T cells were estimated based on 10^{6} singlets. Numbers of cells positive for the indicated protein are indicated for cells induced by aMIV and SAM(H1), where proteins higher expressed are indicated in red in one of the vaccines. The 6 biomarkers indicated with a * are also present in the 12 T_{EFF} differentially expressed genes (DEG), found within the 96 gene expression biomarker list from the transcriptional analysis.

Data analysis was performed on 151, 776 and 1030 $HA_{533-541}$- pentmer$^{+}CD8^{+}$ T-cell from PBS, aMIV and SAM(H1) treatment groups, respectively, using t-SNE, an algorithm to reduce high-dimensionally data into 2 or more dimensions, which then can be observed in a scatterplot[94,97]. Markers used in the gating strategy (anti-PE (anti-pentamer), CD3, CD4, CD8, CD44, CD45) and biomarkers that were not taken into account in the transcript analysis (IL-17a, IL-17f, LY6) were removed from the t-SNE analysis. The individual t-SNE plots of the 6 biomarkers found in the T_{EFF} DEG list from the transcript analysis are shown in figure 5.3 (aMIV group) and figure 5.4 (SAM(H1) group) – KLRG1 was cut from further analysis due to low number of positive cells (3 and 0 for SAM(H1) and aMIV, respectively). $HA_{533-541}$- pentmer$^{+}CD8^{+}$ T cells from PBS-treated mice were mainly negative for all 6 biomarkers (figure 5.3 and figure 5.4).

CXCR3 (352 cells (aMIV) vs. 43 cells (SAM(H1))), CXCR6 (165 cells (aMIV) vs. 26 cells (SAM(H1))) and PD1 (632 cells (aMIV) vs. 531 cells (SAM(H1))) were frequently expressed in aMIV induced cells (figure 5.3). The 776 $HA_{533-541}$- pentmer^{+}CD8^{+} T cells induced by aMIV were divided up in 1 large population and 2 smaller subpopulations. One of the small subpopulations was highly positive for CXCR3, CXCR6 and PD1. PD1 was furthermore highly upregulated individually in the second small subpopulation, while the larger population was negative for all 3 markers (figure 5.3). Out of the 1030 $HA_{533-541}$-pentmer^{+}CD8^{+} T cells induced by SAM(H1), 1 large population, one small population and 2 smaller subpopulations were observed. SAM(H1) induced cells were negative for both CXCR3 and CXCR6, but highly positive for PD1 in the small population, and present in one of the smaller subpopulations (figure 5.3).

KLRK1 (495 cells (SAM(H1)) vs. 306 cells (aMIV)), perforin (190 cells (SAM(H1)) vs. 7 cells (aMIV)) and GzmB (904 cells (SAM(H1)) vs. 23 cells (aMIV)) were upregulated in SAM(H1) induced cells (figure 5.4). The 1030 $HA_{533-541}$-pentmer^{+}CD8^{+} T cells induced by SAM(H1) were divided as previously: 1 large population, one small population and 2 small subpopulations were observed. The small population was medium expressing KLRK1, while perforin expression was scattered over the 4 populations. GzmB was highly expressed in most of the cells (figure 5.4). 776 $HA_{533-541}$-pentmer^{+}CD8^{+} T cells induced by aMIV were divided into 1 large population and 2 smaller subpopulations, and only expressed KLRK1 in one of the smaller subpopulations (figure 5.4).

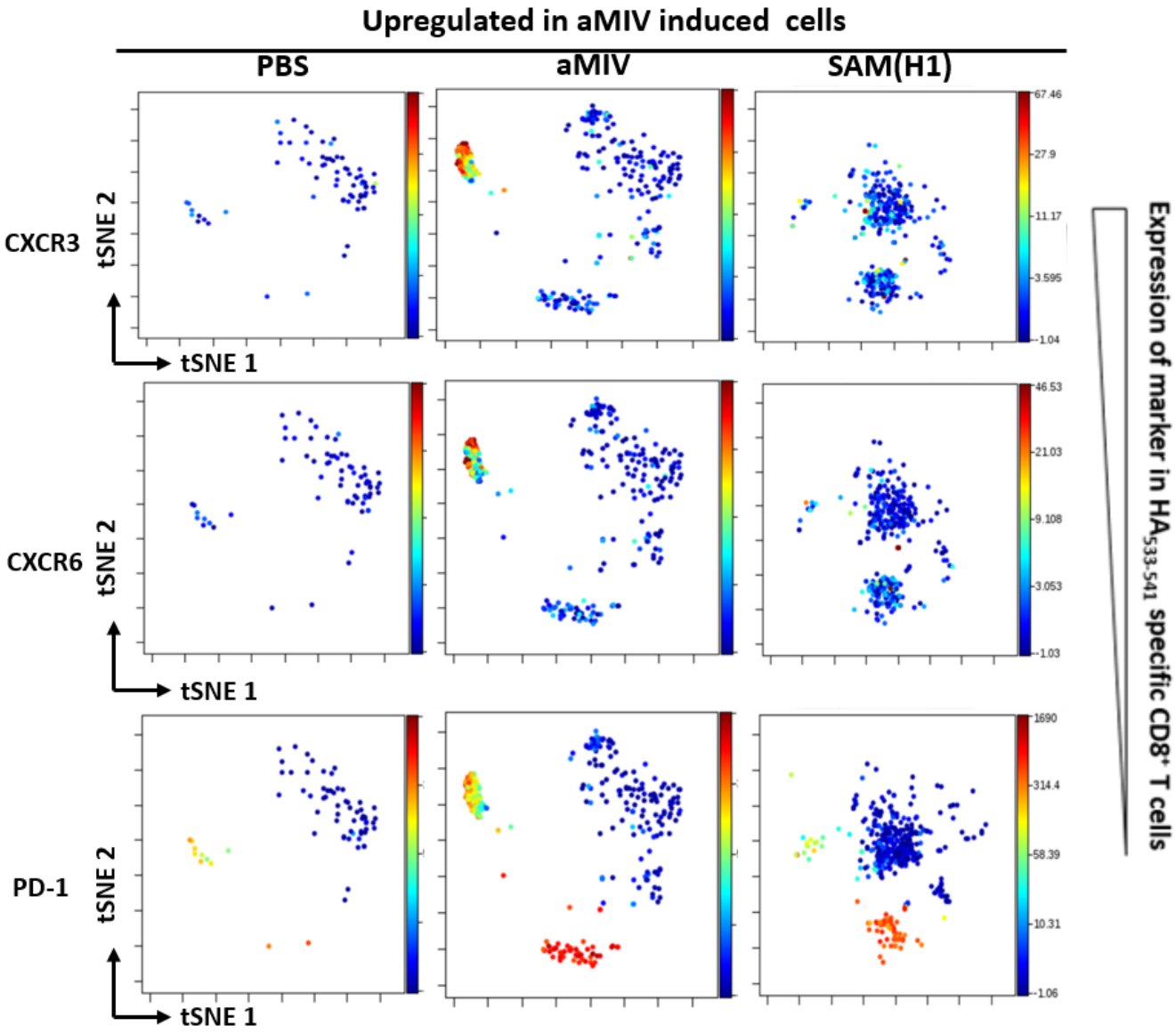

Figure 5.3: Protein expression in aMIV induced $HA_{533-541}$-pentamer$^{+}CD8^{+}$ T cells confirms transcriptional data. 151, 776, and 1030 $HA_{533-541}$-pentamer$^{+}CD8^{+}$ T cells induced by PBS, aMIV and SAM(H1), respectively were analysed by t-SNE, including 22 of the CyTOF markers not used in the gating and/or not found in the transcriptome analysis. Of the 12 T_{EFF} DEG found in the transcriptome gene expression analysis, 3 markers were also upregulated in cells induced by aMIV at the protein level: CXCR3, CXCR6 and PD1. The color scale goes from low (blue), through medium (green/yellow) to highly expressed (red).

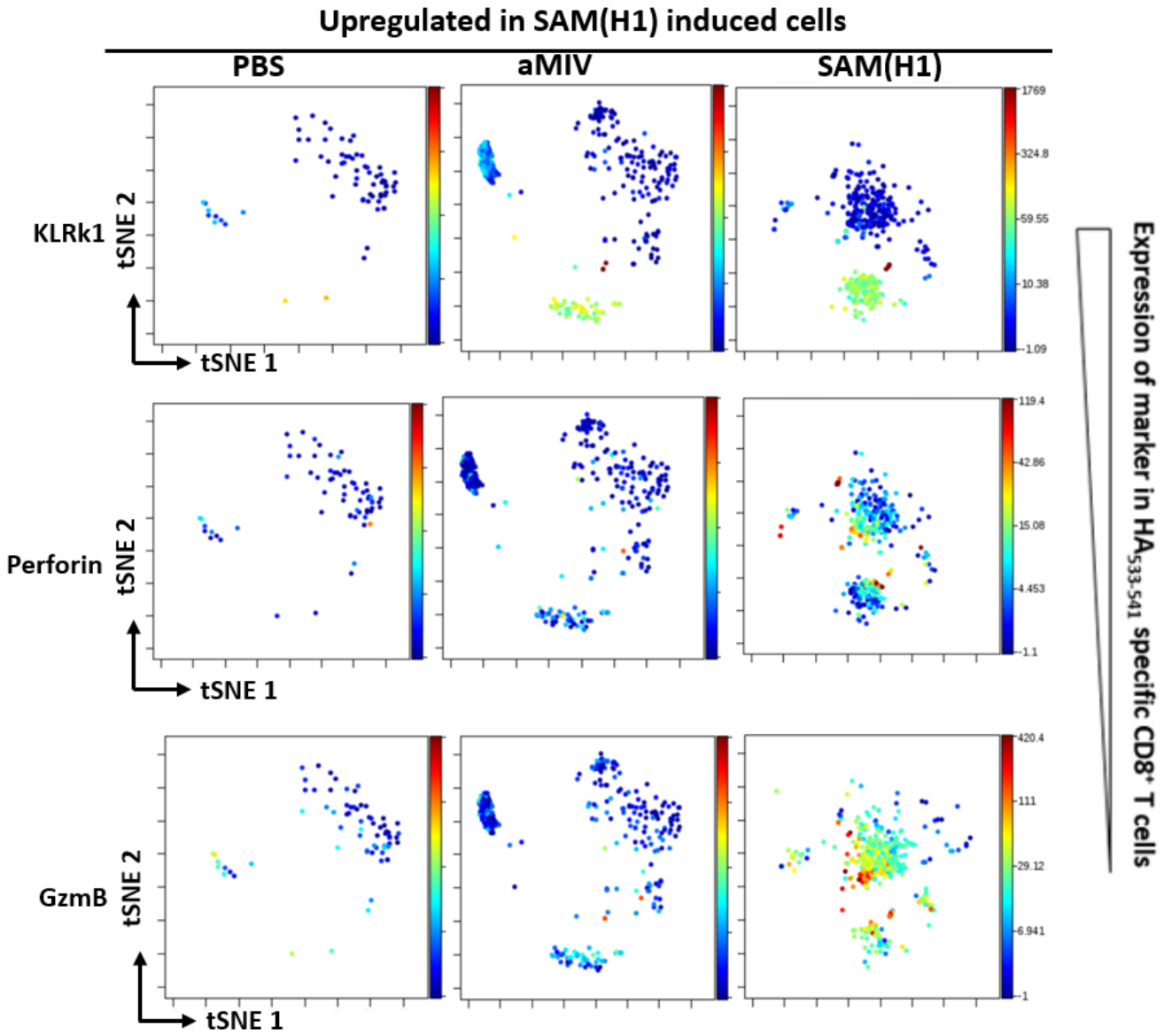

Figure 5.4: Protein expression in SAM(H1) induced $HA_{533-541}$-pentamer$^{+}CD8^{+}$ T cells confirms transcriptional data. 151, 776, and 1030 $HA_{533-541}$-pentamer$^{+}CD8^{+}$ T cells from PBS, aMIV, and SAM(H1) treatment groups were analysed with t-SNE, including 22 of the CyTOF markers not used in the gating and/or not found in the transcriptome analysis. Of the 12 T_{EFF} DEG found in the transcriptome gene expression analysis, 3 markers were upregulated in cells induced by SAM(H1) at the protein level: KLRK1, perforin and GzmB. The color scale goes from low (blue), through medium (green/yellow) to highly expressed (red).

Chapter 6: Discussion and Conclusions

Analyses of single cells are necessary to understand in depth the heterogeneous nature in which cells respond and behave to biological stimuli[1–4,6,21,69–72,74,91,92,98–101]. These new single-cell approaches can refine our cellular classification schemes and enable the direct assessment of molecular mechanisms that have conventionally been obscured in bulk samples, where cells of a particular type, based on only a few biomarkers, were deemed identical. Understanding cellular mechanisms of action following vaccination and revealing new and functionally distinct subsets of immune cells would give the opportunity to improve and develop better cross-protective vaccines.

Influenza protein-based vaccines have been commercially available for a long time, and continue to be the most successful strategy to reduce disease burden and economical costs associated with the infection. Currently, the efficacy of licensed vaccines depends on the match between the annual vaccines and circulating strains, and better cross-protective vaccines need to be developed. In order to do this, the nature of the immune response needs to be investigated and exactly understood to direct the vaccine to target both humoral and cellular immunity. In this thesis, we focused on the characterization of $HA_{533\text{-}541}$-pentmer^{+}CD8^{+}T cells at the single-cell level. For this purpose, a mouse model of influenza was used and mice were vaccinated with either RNA-based SAM(H1)[22,65,66,85,87,86,102] or MF59-adjuvanted subunit H1N1 aMIV[54–57,59,84,103,104]. The two vaccines were previously shown to induce similar protection rates in mice after infection[22]. Moreover, both vaccines stimulated antigen-specific CD4^{+} T cells, but only SAM(H1) induced a robust CD4^{+} T_H1 cell response, detected in splenocytes after *in vitro* stimulation with HA peptides[22]. This antigen-specific response was characterized by using a combination of five cytokines (IL-2, IL-4/IL-13, TNF-α, IFN-γ). In addition, SAM(H1) but not aMIV, induced cytokine^{+}CD8^{+} T_H1 cells[22]. *In vitro* stimulation is currently the preferred way for the estimation of antigen-specific T cells. While this type of analysis is fit for the identification of already known cellular populations, it cannot properly describe the complex and heterogeneous immune response occurring after vaccination and better methods for the characterization of CD8^{+} T cells need to be developed.

For a deeper characterization of antigen-specific $CD8^+$ T cells after vaccination, BALB/c-restricted MHC-I $HA_{533\text{-}541}$-pentamers were used *ex vivo* to identify the population of interest[105–108]. Both SAM(H1) and aMIV vaccines did induce $HA_{533\text{-}541}$-pentamer$^+CD8^+$ T cells compared to the PBS-treated group or the HIV gag $_{199\text{-}207}$-pentamer$^+$ controls. Only SAM(H1) immunization induced a high number of $HA_{533\text{-}541}$-pentamer$^+CD8^+$ T cells after boost. Despite the common belief that protein vaccines, like aMIV, only induce humoral and cellular $CD4^+$ T cell responses, and not HA-specific $CD8^+$ T cells[22,109,110], the latter population was found in our experimental settings using HA-specific pentamers. It is likely that the use of pentamers rather than standard T cell assay such as intracellular cytokine detection allowed us to detect these antigen-specific $CD8^+$ T cells. For pre-clinical studies like ours, there are major availability of different MHC-I pentamers restricted to different mouse species. Clinical studies are, however, hindered by the lack of pentamers against different human leukocyte antigen (HLA) subtypes that humans possess[18]. There are 3 major MHC-I genes in HLA (HLA-A, HLA-B, HLA-C) and 3 minor genes (HLA-E, HLA-F, HLA-G), all possessing different alleles, making the HLA extremely variable[18,82,111–115]. A few influenza-restricted pentamers are commercially available, but most HLA pentamers are directed towards other epitopes of the influenza virus than HA, due to the fact that T cells after infections are directed to internal proteins and not the surface protein HA. One study used commercially available pentamers to distinguish peptide-stimulated influenza-specific $CD8^+$ T cells, directed to internal proteins, in peripheral blood after seasonal immunization. The study found an increase of antigen-specific $CD8^+$ T cells after vaccination using the pentamers[116]. However for studies where one does not want to stimulate the cells before pentamer staining, a large amount of blood needs to be extracted from vaccinated subjects in order to detect and isolate low frequency cells, which is difficult. Also, clinical trials have to take the ethical aspect into account, as a genetic screening of the HLA subtypes needs to take place before the start of the study, which requires permission of the donors. A possibility to overcome this issue, is to develop general race HLA-pentamers, such as HLA-A2 which is found in >50% of Caucasians and Asians[117,118].

To characterize single cells, one needs a correct system. The BioMark platform from Fluidigm is a novel, interesting and already used technology platform for single-cell studies[1,21,92]. It is a quick way of identifying biomarkers up/down-regulated e.g. after vaccination, in search of molecules of interest, which induce a wanted immune response for protection, or in other research fields[2,4,6,21,73,80,91,99,119–

[121]. We used this particular RT-qPCR platform to set up a high-throughput screening for biomarker identification, and to find a certain signature after two immunizations. After vaccination with SAM and aMIV, transcripts from single $HA_{533-541}$-pentamer$^{+}CD8^{+}$ T cells were analyzed and data suggested that these cells induced by the different vaccines were highly heterogeneous. The cells were therefore, clusterized into three known subpopulations during data analysis; T_{EFF} (*il-7rα*$^{-}$*cd62l*$^{-}$), T_{EM} (*il-7rα*$^{+}$*cd62l*$^{-}$) and T_{CM} (*il-7rα*$^{+}$ *cd62l*$^{+}$) as seen in previous studies[40–44]. Flatz *et al*. directly sorted single cells from the three subpopulations, which in retrospect could have been more optimal, as a more even number of T_{EFF}, T_{EM} and T_{CM} cells would have been analyzed[1]. Nevertheless, $HA_{533-541}$-pentamer$^{+}CD8^{+}$ T cells within the T_{EFF} and T_{EM} subpopulations showed great transcriptional differences between the two vaccines, whereas T_{CM} cells were more similar. T_{EFF} cells provided a signature between the two different vaccines based on 12 DEG. 10 of the 12 DEG were also expressed in T_{EM} cells. Specific cell subtypes were found; aMIV driven T_{EFF} cells were much more homogeneous than those from the SAM(H1) group. T_{EFF} cells driven by aMIV were mostly characterized by two following subsets: ~20% of cells were *cxcr3*$^{+}$*pd1*$^{-}$*perforin*$^{+}$ and ~15% of cells were *cxcr3*$^{+}$*pd1*$^{+}$*perforin*$^{-}$. The remaining ~65% of cells were either positive for *gzma*, *gzmb* and *klrg* or did not express any of the 12 DEG genes. T_{EFF} cells from SAM(H1) were more heterogeneous, highly expressing cytotoxic markers like *klr*, *gzm* and *cxcr* genes, but expressed little *pd1* and *cxcr3*. The two vaccines induced *perforin* expression in T_{EFF} cells. In the T_{EM} cell subpopulation, the same trend was observed; $HA_{533-541}$-pentamer$^{+}CD8^{+}$ T cells induced by aMIV were highly homogeneous, whereas SAM(H1) induced cells were more heterogeneous. Cells induced by aMIV were mainly divided into four subsets: ~23% of cells were *cxcr3*$^{+}$*pd*$^{-}$*cxcr6*$^{-}$*perforin*$^{-}$, ~14% of cells were *cxcr3*$^{+}$*pd1*$^{+}$*cxcr6*$^{-}$*perforin*$^{-}$, 9% of cells were *cxcr3*$^{+}$*pd1*$^{+}$*cxcr6*$^{-}$*perforin*$^{+}$ and ~7% of cells were *cxcr3*$^{+}$*pd1*$^{-}$*cxcr6*$^{+}$*perforin*$^{-}$. The remaining 47% of cells did not express any of the 12 DEG genes. $HA_{533-541}$-pentamer$^{+}CD8^{+}$ T cells induced by SAM(H1) shared similarities with T_{EFF} cells, they were multi-transcript positive, but not many cells did express *pd1*, *spi6* and *klrg*. These observations in aMIV driven cells are novel, as $HA_{533-541}$-pentamer$^{+}CD8^{+}$ T cells have never been reported after aMIV vaccination. This molecular signature is the first to be identified in antigen-specific $CD8^{+}$ T cells after vaccination with MF59 adjuvanted subunit protein in a mouse model. Despite the lack of some cytotoxic markers, the biological relevance of these cells indicate a possible inflammatory entry to the peripheral tissues like lungs[18,28]. The high presence of *pd1* gene

could indicate exhausted cells, but recent data suggest that this marker is not necessarily a marker of exhausted cells, as when absent, an increase of exhausted T cells are observed[37]. The function of *pd1* after vaccination needs further investigation. Previous studies showed that SAM(H1) induced cytotoxic $CD8^+$ T cells[22,85]. This thesis expanded on these results and highlighted the expression of specific biomarkers, thus, deepening our knowledge of the cytotoxic $CD8^+$ T cells induced by SAM RNA vaccines. Our data confirms similar observations reported with other vaccines like RNA(β-galactosidase)-, plasmid-DNA- or recombinant replication delivery in mouse and human studies[1,122,123]. Hoerr *et al.* used an RNA vaccine, encoding for a model antigen (β-galactosidase), and reported the induction of antigen-specific cytotoxic T cells in mice after stimulation with peptide[122]. In a different study, plasmid DNA vaccines encoding a malaria antigen elicited a cytotoxic T cell response, characterized and measured by multiple HLA-restricted alleles[124] [123]. Antigen-specific $CD8^+$ T cells have also been studied with DNA vaccines encoding HIV antigens in mice. This particular study used single-cell transcripts for signature identification following different prime-boost combinations of plasmid-DNA, recombinant replication-defective adenovirus or recombinant lymphocytic choriomeningitis virus. Six genes were identified; *Eomes*, *ccr7*, *cxcr3* within a T_{CM} subpopulation, and *klrk*, *klrg*, and *ccr5* within the T_{EM} subpopulation. The percentages of cells expressing these markers changed depending on the vaccine delivery combination[1]. Systems vaccinology[125] is currently being applied to a few clinical trial studies, such as the study reported by Pulendran's group on trivalent inactivated influenza vaccines and MF59-adjuvanted trivalent inactivated influenza vaccine. They investigated serum Ab titers and multi-cytokine producing $CD4^+$ T cells and found that magnitude of the adaptive immune response increased after MF59 vaccination in infants[126]. If HLA-pentamers were available, our study could be applied in clinical trials for the molecular signature identification of single $CD8^+$ T cells also, provided enough T cells are stimulated. Currently, these molecular signatures are estimated in peripheral blood mononuclear cells using bulk sample microarray data, which has been seen in a study of influenza trivalent vaccine[127] and yellow fever YF-17D vaccine[128] in humans. A single-cell approach will further increase our knowledge of adaptive immune responses after vaccination and identify their molecular signatures. Within vaccinology, computational methods such as systems vaccinology and platforms, as our single-cell study, would help to understand the

molecular mechanisms and refine the signatures, and develop potential correlate of immunity for better and more cross-protective vaccines.

The signature identified at the transcript level was also evaluated at the protein level *ex vivo*. This analysis was completed with cutting edge single-cell mass cytometry phenotype profiling by the CyTOF technology platform. Also here, $HA_{533-541}$-pentamer$^{+}CD8^{+}$ T cells were identified after vaccination with aMIV and SAM(H1). The memory markers IL-7rα and CD62L could not be used to distinguish T_{EFF}, T_{EM} and T_{CM}, as performed with the transcript analysis because cells in the SAM(H1) vaccinated group did not show IL-7Rα expression after the second immunization, for unknown reasons. Other markers are used as alternatives to distinguish memory subtypes in literature. One study determined different subpopulation clusters as T_{NAIVE} ($CD45RA^{+}CD27^{+}CD62L^{+}CCR7^{+}$), T_{CM} ($CD45RA^{-}CD27^{+}CD62L^{+}CCR7^{-}$), T_{EM} ($CD45RA^{-}CD27^{-}CD62L^{-}CCR7^{-}$), and short-lived T_{EFF} ($CD45RA^{+}CD27^{-}$ $CD62L^{-}CD28^{-}$ $KLRG1^{+}CD57^{+}$)[129], and this approach will be further investigated for our study. Six biomarkers of the T_{EFF} cell DEG list were shared with the mass cytometry biomarker list; CXCR3, CXCR6 and PD1 for cells induced by aMIV, and KLRK1, Perforin and GzmB for cells induced by SAM(H1). A small subset of cells in the aMIV vaccination group expressed CXCR3 and CXCR6, as seen with the transcript analysis. Two small cell subsets were highly up regulating PD1, which confirmed the transcript analysis. Interestingly, cells from SAM(H1) did not express CXCR6, despite the transcript being present, but did express PD1, also in two small subsets, one highly and one medium expressed. A subset of cells from the SAM(H1) vaccinated group expressed KLRK1, while a spread of cells expressed perforin across different subsets. GzmB was highly expressed in most cells, confirming the transcript analysis. Cells from aMIV vaccinated group did not express GzmB like the transcript, but did not appear to be perforin^{+} either. One subset of aMIV induced cells did express KLRK1, which was not seen with the transcript analysis. In summary, part of the signature found in the transcript analysis was also expressed at the protein level. The lack of complete overlap between transcripts and proteins might be explained by different kinetics for these molecules or by the different clusterization of cell subpopulations we had to apply, working on total $HA_{533-541}$-pentamer$^{+}CD8^{+}$ T cells rather than memory T cell subtypes. This study will be further expanded on the whole $CD8^{+}$ T cell population in addition to $HA_{533-541}$-pentamer$^{+}CD8^{+}$ T cells.

By applying an *in vivo* cytotoxicity assay, our data confirmed that $CD8^+$ T cells elicited by the protein subunit vaccines, both with or without adjuvants, indeed did have some cytotoxic properties compared to cells from the PBS control group. This indicated that cytotoxic cells are present after MIV and aMIV vaccination, nevertheless, the two vaccines probably did not induce any of the standard cytokines measured as antigen-specific $CD8^+$ T-cell markers, and therefore could not be found by standard *in vitro* stimulation assays. Cells from SAM(H1) immunization group were highly cytotoxic, validating the signature found in both transcript and protein analyses. This demonstrated that RNA-based SAM(H1) and aMIV vaccine signatures identified in our study were functionally relevant *in vivo*. Supplementary investigation which confirmed this cytotoxicity has been completed in $CD8^+$ T-cell depleted mice, where the protective role of the HA-specific T cells induced after vaccination was observed[22].

In summary, our study describes the setup and application of single-cell analysis in a high dimensional cell profiling. Different cell signatures were distinguished between the two vaccine platforms at the RNA and protein level, and functional assay confirmed this signature. This type of study might help in understanding which cells are implicated in protection, hence, which cells should be targeted by vaccination. The present thesis was implemented in the field of vaccinology, but could also be applied to other medical fields with a potential for single-cell biomarker identification in pre-clinical research.

Reference list

1. Flatz, L. *et al.* Single-cell gene-expression profiling reveals qualitatively distinct CD8 T cells elicited by different gene-based vaccines. *PNAS* **108,** 8–13 (2011).

2. Bengtsson, M., Hemberg, M., Rorsman, P. & Ståhlberg, A. Quantification of mRNA in single cells and modelling of RT-qPCR induced noise. *BMC Mol. Biol.* **9,** 63 (2008).

3. McDavid, A. *et al.* Data exploration, quality control and testing in single-cell qPCR-based gene expression experiments. *Bioinformatics* **29,** 461–7 (2013).

4. Ståhlberg, A., Rusnakova, V., Forootan, A., Anderova, M. & Kubista, M. RT-qPCR work-flow for single-cell data analysis. *Methods* **59,** 80–8 (2013).

5. Ståhlberg, A., Kubista, M. & Åman, P. Single-cell gene-expression profiling and its potential diagnostic applications. *Expert Rev Mol Diagn.* **11,** 735–740 (2011).

6. Ståhlberg, A. & Kubista, M. The workflow of single-cell expression profiling using quantitative real-time PCR. *Expert Rev. Mol. Diagn.* **14,** 323–31 (2014).

7. Ståhlberg, A. & Bengtsson, M. Single-cell gene expression profiling using reverse transcription quantitative real-time PCR. *Methods* **50,** 282–8 (2010).

8. Esumi, S. *et al.* Method for single-cell microarray analysis and application to gene-expression profiling of GABAergic neuron progenitors. *Neurosci. Res.* **60,** 439–51 (2008).

9. Fei, Y. *et al.* Characterization of Receptor Binding Profiles of Influenza. *Biomolecules* **5,** 1480–1498 (2015).

10. Spensieri, F. *et al.* T cells expand after vaccination , exert helper function , and predict antibody responses. *PNAS* **110,** 2–7 (2013).

11. Wilkinson, T. M. *et al.* Preexisting influenza-specific CD4+ T cells correlate with disease protection against influenza challenge in humans. *Nat. Med.* **18,** 274–80 (2012).

12. Perez-Shibayama, C. *et al.* IFN-γ-producing CD4+ T cells promote generation of protective germinal center-derived IgM+ B cell memory against Salmonella Typhi. *J. Immunol.* **192,** 5192–200 (2014).

13. Kuby, J. *et al*. Owen Kuby Immunology. *Book* **7th editio,** (2009).

14. Zhou, L., Chong, M. M. W. & Littman, D. R. Review Plasticity of CD4 + T Cell Lineage Differentiation. *Immunity* **30,** 646–655 (2009).

15. O'Gorman, W. E. *et al.* The Split Virus Influenza Vaccine rapidly activates immune cells through Fcγ receptors. *Vaccine* **32,** 5989–97 (2014).

16. Becher, B. *et al.* resource High-dimensional analysis of the murine myeloid cell system. *Nat. Immunol.* **15,** 1181–1191 (2014).

17. Bendall, S. C., Nolan, G. P., Roederer, M. & Chattopadhyay, P. K. A deep profiler ' s guide to cytometry. *TREIMM* **33,** 1–10 (2012).

18. Murphy KM, P Travers, M. W. Janeway's Immunobiology. *Book* **8th editio,** (2012).

19. Chua, B. Y. *et al.* The use of a TLR2 agonist-based adjuvant for enhancing effector and memory CD8 T-cell responses. *Immunol. Cell Biol.* **92,** 377–83 (2014).

20. McLane, L. M. *et al.* Differential localization of T-bet and Eomes in CD8 T cell memory populations. *J. Immunol.* **190,** 3207–15 (2013).

21. Arsenio, J. *et al.* Early specification of CD8+ T lymphocyte fates during adaptive immunity revealed by single-cell gene-expression analyses. *Nat. Immunol.* **15,** 365–72 (2014).

22. Brazzoli, M. *et al.* Induction of broad-based immunity and protective efficacy by self-amplifying mRNA vaccines encoding influenza virus hemagglutinin. *PLoS One* **11,** 1–25 (2016).

23. Salti, S. M. *et al.* Granzyme B Regulates Antiviral CD8 + T Cell Responses. *J. Immunol.* **187,** 6301–6309 (2016).

24. Bratke, K., Kuepper, M., Bade, B. & Jr, J. C. V. Immunity to infection Differential expression of human granzymes A , B , and K in natural killer cells and during CD8 + T cell differentiation in peripheral blood. *Eur J Immunol* **35,** 2608–2616 (2005).

25. Suzuki, I. *et al.* Fas Ligand Costimulates the In Vivo Proliferation of CD8 + T Cells. *J Immunol* **165,** 5537–43 (2016).

26. Whitmire, J. K., Tan, J. T. & Whitton, J. L. Interferon- □ acts directly on CD8 ƨ T cells to increase their abundance during virus infection. *J Exp Med* **201,** 1053–1059 (2005).

27. Suresh, M., Singh, A. & Fischer, C. Role of Tumor Necrosis Factor Receptors in Regulating CD8 T-Cell Responses during Acute Lymphocytic Choriomeningitis Virus Infection. *J. Virol.* **79,** 202–213 (2005).

28. Hickman, H. D. *et al.* CXCR3 Chemokine Receptor Enables Local CD8 + T Cell Migration for the Destruction of Virus-Infected Article CXCR3 Chemokine Receptor Enables Local CD8 + T Cell Migration for the Destruction of Virus-Infected Cells. *Immunity* **42,** 524–537 (2015).

29. Faure, S., Autran, B., Debre, P. & Combadie, C. The chemokine receptor CX3CR1 controls homing and anti-viral potencies of CD8 effector-memory T lymphocytes in HIV-infected patients. *AIDS* **17,** 1279–90 (2003).

30. Zhang, M. *et al.* Serine Protease Inhibitor 6 Protects Cytotoxic T Cells from Self-Inflicted Injury by Ensuring the Integrity of Cytotoxic Granules. *Immunity* **24,** 451–461 (2006).

31. Rapaport, A. S. *et al.* The Inhibitory Receptor NKG2A Sustains Virus- Specific CD8 + T Cells in Response to a Lethal Poxvirus Infection Article The Inhibitory Receptor NKG2A Sustains Virus-Specific CD8 + T Cells in Response to a Lethal Poxvirus Infection. *Immunity* **43,** 1112–1124 (2015).

32. Moser, J. M., Gibbs, J., Jensen, P. E. & Lukacher, A. E. CD94-NKG2A receptors regulate antiviral CD8 + T cell responses. *Nat. Immunol.* **3,** 189–195 (2002).

33. Yuzefpolskiy, Y., Baumann, F. M., Kalia, V. & Sarkar, S. Early CD8 T-cell memory precursors and terminal effectors exhibit equipotent in vivo degranulation. *Cell. Mol. Immunol. (* **12,** 400–408 (2015).

34. Wiemann, K. *et al.* Systemic NKG2D Down-Regulation Impairs NK and CD8 T Cell Responses In Vivo. *J Immunol* **175,** 720–9 (2016).

35. Park, H. J. *et al.* PD-1 Upregulated on Regulatory T Cells during Chronic Virus Infection Enhances the Suppression of CD8 + T Cell Immune Response via the Interaction with PD-L1 Expressed on CD8 + T Cells. *J Immunol* **194,** 21–23 (2016).

36. Urbani, S. *et al.* PD-1 Expression in Acute Hepatitis C Virus (HCV) Infection Is Associated with HCV-Specific CD8 Exhaustion . *J Virol* **80,** 11398–11403 (2006).

37. Odorizzi, P. M., Pauken, K. E., Paley, M. A., Sharpe, A. & Wherry, E. J. Genetic absence of PD-1 promotes accumulation of terminally differentiated exhausted CD8 + T cells. *J Exp Med* **212,** 1125–1137 (2015).

38. Palendira, U. *et al.* Selective accumulation of virus-specific CD8+ T cells with unique homing phenotype within the human bone marrow. *Blood* **112,** 3293–302 (2008).

39. Duffy, D. *et al.* Neutrophils transport antigen from the dermis to the bone marrow, initiating a source of memory CD8+ T cells. *Immunity* **37,** 917–29 (2012).

40. Masopust, D., Kaech, S. M., Wherry, E. J. & Ahmed, R. The role of programming in memory T-cell development. *Curr. Opin. Immunol.* **16,** 217–225 (2004).

41. Sallusto, F., Lenig, D., Förster, R., Lipp, M. & Lanzavecchia, a. Two subsets of memory T lymphocytes with distinct homing potentials and effector functions. *Nature* **401,** 708–712 (1999).

42. Seder, R. A., Darrah, P. A. & Roederer, M. T-cell quality in memory and protection: implications for vaccine design. *Nat. Rev. Immunol.* **8,** 247–258 (2008).

43. Rutishauser, R. L. *et al.* Transcriptional repressor Blimp-1 promotes CD8(+) T cell terminal differentiation and represses the acquisition of central memory T cell properties. *Immunity* **31,** 296–308 (2009).

44. Kaech, S. M. & Cui, W. Transcriptional control of effector and memory CD8+ T cell differentiation. *Nat. Rev. Immunol.* **12,** 749–761 (2012).

45. Medina, R. A. & García-sastre, A. Influenza A viruses : new research developments. *Nat. Rev.* **9,** 590–603 (2011).

46. Chu, C. M., Andrews, C. H. & Gledhill, A. W. Influenza in 1948-1949. *World Health Organ.* **3,** 187–214 (1950).

47. Tong, S. *et al.* New World Bats Harbor Diverse Influenza A Viruses. *PLoS Pathog.* **9,** 1–12 (2013).

48. Fouchier, R. A. M. *et al.* Characterization of a novel influenza A virus hemagglutinin subtype (H16) obtained from black-headed gulls. *J. Virol.* **79,** 2814–2822 (2005).

49. A, K., T, M. & S, B. Universal Influenza Vaccines. *In Prep.*

50. WHO. WHO influenza fact sheet. (2016). at <http://www.who.int/mediacentre/factsheets/fs211/en/>

51. FDA. U.S. Food and Drug Administration. (2016). at <www.fda.gov/>

52. Wong, S. & Webby, R. J. Traditional and New Influenza Vaccines. *Tradit. New Influ. Vaccines* **26,** 476–492 (2013).

53. Van Buynder, P. G. *et al.* The comparative effectiveness of adjuvanted and unadjuvanted trivalent inactivated influenza vaccine (TIV) in the elderly. *Vaccine* **31,** 6122–6128 (2013).

54. Della Cioppa, G., Vesikari, T., Sokal, E., Lindert, K. & Nicolay, U. Trivalent and quadrivalent MF59 - adjuvanted influenza vaccine in young children: A dose- and schedule-finding study. *Vaccine* **29,** 8696–8704 (2011).

55. Vesikari, T. *et al.* Enhanced immunogenicity of seasonal influenza vaccines in young children using MF59 adjuvant. *Pediatr. Infect. Dis. J.* **28,** 563–71 (2009).

56. O'Hagan, D. T., Ott, G. S., Nest, G. Van, Rappuoli, R. & Del Giudice, G. The history of MF59(®) adjuvant: a phoenix that arose from the ashes. *Expert Rev. Vaccines* **12,** 13–30 (2013).

57. Milanetti, F. *et al.* Safety and immunogenicity of co-administered MF59-adjuvanted 2009 pandemic and plain 2009-10 seasonal influenza vaccines in rheumatoid arthritis patients on biologicals. *Clin. Exp. Immunol.* **177,** 287–94 (2014).

58. O'Hagan, D. T., Ott, G. S., De Gregorio, E. & Seubert, a. The mechanism of action of MF59 - an innately attractive adjuvant formulation. *Vaccine* **30,** 4341–8 (2012).

59. Calabro, S. *et al.* Vaccine adjuvants alum and MF59 induce rapid recruitment of neutrophils and monocytes that participate in antigen transport to draining lymph nodes. *Vaccine* **29,** 1812–23 (2011).

60. Olson, M. R. & Varga, S. M. CD8 T Cells Inhibit Respiratory Syncytial Virus (RSV) Vaccine-Enhanced Disease. *J Immunol* **179,** 5415–24 (2014).

61. Zhao, G. *et al.* Development of a heat-stable and orally delivered recombinant M2e-expressing B. subtilis spore-based influenza vaccine. *Hum. Vaccines Immunother.* **10,** 3649–3658 (2014).

62. Wahlgren, J. Mallard or chicken? Comparing the isolation of avian influenza A viruses in embryonated Mallard and chicken eggs. *Infect Ecol Epidemiol* **1,** 1–6 (2015).

63. Zeiger, R. Current issues with influenza vaccination in egg allergy. *J. Allergy Clin. Immunol.* **10,** 834–840 (2002).

64. Schotsaert, M., Saelens, X. & Leroux-Roels, G. Influenza vaccines: T-cell responses deserve more attention. *Expert Rev. Vaccines* **11,** 949–62 (2012).

65. Geall, A. J. *et al.* Nonviral delivery of self-amplifying RNA vaccines. *PNAS* **109,** 1–6 (2012).

66. Hekele, A. *et al.* Rapidly produced SAM(®) vaccine against H7N9 influenza is immunogenic in mice. *Emerg. Microbes Infect.* **2,** e52 (2013).

67. Brito, L. A. *et al. Self-Amplifying mRNA Vaccines*. *Book* **Chaptr 7,** (Elsevier Ltd, 2015).

68. Calabro, S. *et al.* The adjuvant effect of MF59 is due to the oil-in-water emulsion formulation, none of the individual components induce a comparable adjuvant effect. *Vaccine* **31,** 3363–9 (2013).

69. Stegle, O., Teichmann, S. A. & Marioni, J. C. Computational and analytical challenges in single-cell transcriptomics. *Nat. Rev. Genet.* **16,** 133–145 (2015).

70. Kanter, I. & Kalisky, T. Single cell transcriptomics: methods and applications. *Front. Oncol.* **5,** 53 (2015).

71. Proserpio, V. & Mahata, B. Single-cell technologies to study the immune system. *Immunology* **147,** 133–140 (2015).

72. Tang, F., Lao, K. & Surani, M. A. Development and applications of single cell transcriptome analysis. *Nat. Methods* **8,** 6–11 (2011).

73. Devonshire, A. S., Elaswarapu, R. & Foy, C. a. Applicability of RNA standards for evaluating RT-qPCR assays and platforms. *BMC Genomics* **12,** 118–128 (2011).

74. Bengtsson, M., Ståhlberg, A., Rorsman, P. & Kubista, M. Gene expression profiling in single cells from the pancreatic islets of Langerhans reveals lognormal distribution of mRNA levels. *Genome Res* **10,** 1388–1392 (2005).

75. Papin, J. F., Vahrson, W. & Dittmer, D. P. SYBR Green-Based Real-Time Quantitative PCR Assay for Detection of West Nile Virus Circumvents False-Negative Results Due to Strain Variability SYBR Green-Based Real-Time Quantitative PCR Assay for Detection of West Nile Virus Circumvents False-Negative R. *J. Clin. Microbiol.* **42,** 1511–1518 (2004).

76. Bishop, R. Applications of fluorescence in situ hybridization (FISH) in detecting genetic aberrations of medical significance. *Biosci. Horizons* **3,** 85–95 (2010).

77. Kurimoto, K. *et al.* An improved single-cell cDNA amplification method for efficient high-density oligonucleotide microarray analysis. *Nucleic Acids Res.* **34,** 1–17 (2006).

78. Spear, A. & Faaberg, K. S. Development of a genome copy specific RT-qPCR assay for divergent strains of type 2 porcine reproductive and respiratory syndrome virus. *J. Virol. Methods* **218,** 1–6 (2015).

79. Team, C. Fluidigm. (2016). at <https://www.fluidigm.com/>

80. Newell, E. W., Sigal, N., Nair, N., Kidd, B. A. & Greenberg, H. B. *NIH Public Access*. **31,** 623–629 (2013).

81. Newell, E. W., Sigal, N., Bendall, S. C., Nolan, G. P. & Mark, M. Cytometry by Time-of-Flight Shows Combinatorial Cytokine Expression and Virus-Specific Cell Niches within a Continuum of CD8+ T Cell Phenotypes. *Immunity* **36,** 142–152 (2013).

82. Horowitz, A. *et al.* Regulation of Adaptive NK Cells and CD8 T Cells by HLA-C Correlates with Allogeneic Hematopoietic Cell Transplantation and with Cytomegalovirus Reactivation. *J. Immunol.* **195,** 4524–4536 (2015).

83. Cytobank. Cytobank. (2016). at <http://www.cytobank.org/>

84. Vono, M. *et al.* The adjuvant MF59 induces ATP release from muscle that potentiates response to vaccination. *Proc. Natl. Acad. Sci. U. S. A.* **110,** 21095–100 (2013).

85. Lazzaro, S. *et al.* CD8 T-cell priming upon mRNA vaccination is restricted to bone-marrow-derived antigen-presenting cells and may involve antigen transfer from myocytes. *Immunology* **146,** 312–326 (2015).

86. Brito, L. A. *et al.* A cationic nanoemulsion for the delivery of next-generation RNA vaccines. *Mol. Ther.* **22,** 2118–29 (2014).

87. Bogers, W. M. *et al.* Potent immune responses in rhesus macaques induced by nonviral delivery of a self-amplifying RNA vaccine expressing HIV type 1 envelope with a cationic nanoemulsion. *J. Infect. Dis.* **211,** 947–955 (2015).

88. Jin, H. *et al.* Induction of Th1 type response by DNA vaccinations with N, M, and E genes against SARS-CoV in mice. *Biochem Biophys Res Commun* **328,** 979–986 (2005).

89. Bustin, S. A. *et al.* The MIQE Guidelines : Minimum Information for Publication of Quantitative Real-Time PCR Experiments. *Clin Chem* **622,** 611–622 (2009).

90. Team, R. C. R: A Language and Environment for Statistical Computing. *R Found. Stat. Comput.* (2011). at <http://www.r-project.org/>

91. Buganim, Y. *et al.* Single-cell gene expression analyses of cellular reprogramming reveal a stochastic early and hierarchic late phase. *Cell* **150,** 1209–1222 (2013).

92. McHeyzer-Williams, L. J., Milpied, P. J., Okitsu, S. L. & McHeyzer-Williams, M. G. Class-switched memory B cells remodel BCRs within secondary germinal centers. *Nat. Immunol.* **16,** 296–305 (2015).

93. Noland, G. Protocol. (2016). at <http://web.stanford.edu/group/nolan/>

94. Maaten, L. Van Der. Accelerating t-SNE using Tree-Based Algorithms. *J. Mach. Learn. Res.* **15,** 3221–3245 (2014).

95. Athmaram, T. *et al.* Yeast expressed recombinant Hemagglutinin protein of Novel H1N1 elicits neutralising antibodies in rabbits and mice. *Virol. J.* **8,** 524 (2011).

96. Kallies, A. Distinct regulation of effector and memory T-cell differentiation. *Immunol. Cell Biol.* **86,** 325–332 (2008).

97. Mair, F., Hartmann, F. J., Mrdjen, D. & Tosevski, V. The end of gating ? An introduction to automated analysis of high dimensional cytometry data. *Eur J Immunol* **46,** 34–43 (2016).

98. Trapnell, C. *et al.* The dynamics and regulators of cell fate decisions are revealed by pseudotemporal ordering of single cells. *Nat. Biotechnol.* **32,** 381–6 (2014).

99. Kippner, L. E., Kim, J., Gibson, G. & Kemp, M. L. Single cell transcriptional analysis reveals novel innate immune cell types. *PeerJ* **2,** 1–17 (2014).

100. Gaublomme, J. T. *et al.* Single-Cell Genomics Unveils Critical Regulators of Th17 Cell Pathogenicity. *Cell* **163,** 1400–1412 (2015).

101. Rohr, J. C., Gerlach, C., Kok, L. & Schumacher, T. N. Single cell behavior in T cell differentiation. *Trends Immunol.* **35,** 170–7 (2014).

102. Ulmer, J. B., Mason, P. W., Geall, A. & Mandl, C. W. RNA-based vaccines. *Vaccine* **30,** 4414–8 (2012).

103. Baudner, B. C. *et al.* MF59 emulsion is an effective delivery system for a synthetic TLR4 agonist (E6020). *Pharm. Res.* **26,** 1477–85 (2009).

104. Rubinstein, F. *et al.* Influenza A / H1N1 MF59 adjuvanted vaccine in pregnant women and adverse perinatal outcomes : multicentre. *BMJ* **393,** 1–12 (2013).

105. Toapanta, F. R. & Ross, T. M. Impaired immune responses in the lungs of aged mice following influenza infection. *Respir Res* **19,** 1–19 (2009).

106. Singh, N., Pandey, A., Jayashankar, L. & Mittal, S. K. Bovine Adenoviral Vector – based H5N1 Influenza Vaccine Overcomes Exceptionally High Levels of Pre-existing Immunity Against Human Adenovirus. *Mol Ther* **16,** 965–971 (2008).

107. Vemula, S. V *et al.* Broadly Protective Adenovirus-Based Multivalent Vaccines against Highly Pathogenic Avian Influenza Viruses for Pandemic Preparedness. *PLoS One* **8,** 1–12 (2013).

108. Zhang, X. *et al.* Treatment of pulmonary metastatic tumors in mice using lentiviral vector-engineered stem cells. *Cancer Gene Ther.* **15,** 73–84 (2008).

109. Cox, R. J., Brokstad, K. A. & Ogra, P. Influenza Virus : Immunity and Vaccination Strategies . Comparison of the Immune Response to Inactivated and Live , Attenuated Influenza Vaccines. *Scand J Immunol* **59,** 1–15 (2004).

110. R. Brighta, D. Carterb, S. Daniluka, F. Toapantab, A. Ahmada, V. Gavrilova, M. Massarea, P. Pushkoa, N. Mytled, T. Rowed, G. Smitha, T. R. Influenza virus-like particles elicit broader immune responses than whole virion inactivated influenza virus or recombinant hemagglutinin. *Vaccine* **25,** 3871–3878 (2007).

111. P. Kiepiela, A. Leslie, I. Honeyborne, D. Ramduth, C. Thobakgale, S. Chetty, P. Rathnavalu, C. Moore, K. Pfafferott, L. Hilton, P. Zimbwa, S. Moore, T. Allen, C. B. Dominant influence of HLA-B in mediating the potential co-evolution of HIV and HLA. *Nature* **432,** 769–775 (2004).

112. C. Moore, M. John, I. James, F. Christiansen, C. Witt, S. M. Evidence of HIV-1 Adaptation to HLA-Restricted Immune Responses at a Population Level. *Science* **296,** 1439–1443 (2002).

113. V. Braud, D. Allan, C. O'Callaghan, K. Söderström, A. D'Andrea, G. Ogg, S. Lazetic, N. Young, J. Bell1, J. Phillips, L. L. & A. M. HLA-E binds to natural killer cell receptors CD94/NKG2A, B and C. *Nature* **391,** 795–799 (1998).

114. S. Peng, A. Mattox, Si. Best, A. Barbu, J. Burns, B. Akpeng, J. Jeang, B. Yang, E. Ishida, C. Hung, T. Wu, S. P. Identification of the murine H-2Db and human HLA-A*0201 MHC class I-restricted HPV6 E7-specific cytotoxic T lymphocyte epitopes. *Cancer Immunol.* **65,** 261–271 (2016).

115. I. Zidia, N. Kharratb, R. Abdelhedib, A. Hassinea, A. Laaribia, H. Yahiaa, N. Abdelmoulac, L. Abidd, A. Rebaib, R. R. Nonclassical human leukocyte antigen (HLA-G, HLA-E, and HLA-F) in coronary artery disease. *Hum. Immunol.* **77,** 325–329 (2015).

116. Avetisyan G, Aschan J, Hassan M, L. P. No TEvaluation of immune responses to seasonal influenza vaccination in healthy volunteers and in patients after stem cell transplantation.itle. *Transplantation* **86,** 257–63 (2008).

117. Chaux, P., Lurquin, C. & Cornelis, G. A MAGE-A4 peptide presented by HLA-A2 is recognized by cytolytic T lymphocytes. *Eur J Immunol* **29,** 3329–3337 (1999).

118. Michael Browning a, P. K. b. Genetic diversity of HLA-A2: evolutionary and functional significance. *Immunol. Today* **17,** 165–170 (1996).

119. Fischer, B. M. *et al.* Use of high-throughput RT-qPCR to assess modulations of gene expression profiles related to genomic stability and interactions by cadmium. *Arch. Toxicol.* **Online,** (2015).

120. Trivedi, S. & Ranasinghe, C. The influence of immunization route, tissue microenvironment, and cytokine cell milieu on HIV-specific $CD8^+$ T cells measured using Fluidigm Dynamic arrays. *PLoS One* **10,** 1–21 (2015).

121. Wang, Y. & Bhattacharya, D. Adjuvant-specific regulation of long-term antibody responses by ZBTB20. *J. Exp. Med.* **211,** 841–56 (2014).

122. H. Obst, R. & Rammensee, H. G. In vivo application of RNA leads to induction of specific cytotoxic T lymphocytes and antibodies. *Eur J Immunol* **30,** 1–7 (2000).

123. R. Wang, D. Doolan, T. Le, R. Hedstrom, K. Coonan, Y. Charoenvit, T. Jones, P. Hobart, M. Margalith, J. Ng, W. Weiss, M. Sedegah, C. de Taisne, J. Norman, S. H. Induction of Antigen-Specific Cytotoxic T Lymphocytes in Humans by a Malaria DNA Vaccine. *Science* **282,** 476–480 (1998).

124. Wang, R. *et al.* Induction of Antigen-Specific Cytotoxic T Lymphocytes in Humans by a Malaria DNA Vaccine. *Sci. AAAS* **282,** (1998).

125. B. Pulendran, S. Li, and H. N. Systems Vaccinology. *Immunity* **33,** 516–29 (2011).

126. Nakaya, H. I. *et al.* Systems biology of immunity to MF59-adjuvanted versus nonadjuvanted trivalent seasonal influenza vaccines in early childhood. *Proc Natl Acad Sci* **113,** 1853–8 (2016).

127. Nakaya, H. I. *et al.* Systems Biology of Seasonal Influenza Vaccination in Humans. *Nat Immunol* **12,** 786–795 (2012).

128. Pirani, A. *et al.* Systems Biology approach predicts immunogenicity of the yellow fever vaccine in humans. *Nat. Immunol.* **10,** 116–125 (2014).

129. Newell, E. W., Sigal, N., Bendall, S. C., Nolan, G. P. & Davis, M. M. Resource Cytometry by Time-of-Flight Shows Combinatorial Cytokine Expression and Virus-Specific Cell Niches within a Continuum of CD8 + T Cell Phenotypes. *Immunity* **36,** 142–152 (2012).

Appendix

Appendix 1: BioMark (Fluidigm) TaqMan Assays (Life Technologies) used for gene expression analysis. 96 TaqMan primers and probes indicating T-cell functions. TF: transcription factor, SLEC: terminally differentiated short lived effector cells (SLEC) Blimp 1, klrg1, tbet, MPEC: memory precursor effector cells. # removed from analysis, CyTOF-1 Mass Cytometer (Fluidigm) (missing: LY6C (^{141}Pr) IL-17a/IL-17f (^{174}Yb), PE (^{156}Gd), CD45 (^{147}Sm)).

CyTOF Metal	Gene Symbol	Function in T cells	Location	TaqMan Assay ID	bp
	ahr	Regulation	TF / Nucleus	Mm00478932_m1	61
	bcl3	Priming	TF / Nucleus	Mm00504306_m1	83
	bcl6	Memory (T_{cm})	TF / Nucleus	Mm00477633_m1	112
	bcl11b	Development	TF / Nucleus	Mm00480516_m1	152
	blimp1	SLEC, homeostasis	TF / Nucleus	Mm00476128_m1	72
	camkiv	Regulation	TF / Nucleus	Mm01135329_m1	65
	eomes	MPEC	TF / Nucleus	Mm01351985_m1	58
	foxo3a	Regulation	TF / Nucleus	Mm01185722_m1	71
	foxp3	Treg	TF / Nucleus	Mm00475162_m1	74
	gata3	Homeostasis and activation	TF / Nucleus	Mm00484683_m1	57
	irf4	Expansion and maintenance	TF / Nucleus	Mm00516431_m1	62
	mki67	Proliferation	TF / Nucleus	Mm01278616_m1	95
	nf-kβ1	Maintenance	TF / Nucleus	Mm00476379_m1	83
	relb	Maintenance	TF / Nucleus	Mm00485664_m1	58
	rorc	Tc17 generation	TF / Nucleus	Mm01261022_m1	54
	stat5a	Memory homeostasis	TF / Nucleus	Mm00839861_m1	69
	tbet	SLEC	TF / Nucleus	Mm00450960_m1	69
	bim	Regulation	Cytoplasm	Mm00437796_m1	64
	gcn2	Regulation	Cytoplasm	Mm00469222_m1	102
	gzma	Cytotoxicity - serine protease A	Cytoplasm	Mm00439191_m1	73
^{148}Nd	***gzmb***	Cytotoxicity - serine protease B	Cytoplasm	Mm00442834_m1	95
	gzmk	Cytotoxicity - serine protease K	Cytoplasm	Mm00492530_m1	86
	itk	Development	Cytoplasm	Mm00439861_m1	70
	mapk8	Transcription regulation	Cytoplasm	Mm00489514_m1	99
^{153}Eu	***perforin***	Pore forming cytolytic protein	Cytoplasm	Mm00812512_m1	95
	spi6	Inhibit cytotoxic apoptosis	Cytoplasm	Mm00777163_m1	125
	traf2	Homeostasis	cytoplasm	Mm00801978_m1	75
	was	Activation of naive $CD8^+$ T cells	Cytoplasm	Mm00494167_m1	137
	klrc1	Prevent apoptosis, preserve $CD8^+$ T-cells	Plasma membrane	Mm01183333_m1	79
	klrd1	Regulate antiviral $CD8^+$ T cells	Plasma membrane	Mm00495182_m1	62

^{167}Er	***klrg1***	SLEC	Plasma membrane	Mm00516879_m1	81
^{158}Gd	***klrk1***	Activation of cytotoxic CD8^{+} T cells	Plasma membrane	Mm00473603_m1	124
	#il-1r	Enhances antigen-driven CD8 T cell responses	Plasma membrane	Mm00434237_m1	63
^{150}Nd	***il-2rα***	Stimulation - differentiation into memory	Plasma membrane	Mm01340213_m1	83
	il-2rγ	Stimulation - differentiation into memory	Plasma membrane	Mm00442885_m1	65
^{175}Lu	***il-7rα***	MPEC seperation of activated Tcells during infection	Plasma membrane	Mm00434295_m1	100
	il-10rα	Insulating of cells from inflammatory signals	Plasma membrane	Mm00434151_m1	66
	il-12r-β1	Essential for resistance to intracellular pathogens	Plasma membrane	Mm00434189_m1	60
	il-21r	Long-term maintenance and functionality	Plasma membrane	Mm00600319_m1	65
^{173}Yb	***ccr4***	Skin/lung homing	Plasma membrane	Mm00438271_m1	65
^{176}Yb	***ccr5***	Memory, lung homing during viral infection	Plasma membrane	Mm01216171_m1	78
^{146}Nd	***#ccr6***	Homing for T_{em} cells - mucosal	Plasma membrane	Mm01323931_m1	78
^{163}Dy	***ccr7***	Lymphatic organ homing	Plasma membrane	Mm01301785_m1	78
	ccr10	Skin/lung homing	Plasma membrane	Mm01292449_m1	72
	cx3cr1	Antiviral homing	Plasma membrane	Mm00438354_m1	70
^{154}Sm	***cxcr3***	Inflammatory homing	Plasma membrane	Mm00438259_m1	58
	cxcr4	Bone marrow homing (T_{cm})	Plasma membrane	Mm01292123_m1	99
	cxcr5	Entry to follicular areas	Plasma membrane	Mm00432086_m1	126
^{169}Tm	***cxcr6***	Entry to inflammmed tissue	Plasma membrane	Mm00472858_m1	90
^{152}Sm	***cd3***	Part of T cell receptor	Plasma membrane	Mm00599683_m1	110
^{145}Nd	***cd4***	Co-stimulatory	Plasma membrane	Mm00442754_m1	78
^{168}Er	***cd8***	Co-stimulatory	Plasma membrane	Mm01182108_m1	67
^{172}Yb	***lfa1***	Co-stimulatory migration and activation	Plasma membrane	Mm00801807_m1	119
	cd19	B-lymphocyte antigen	Plasma membrane	Mm00515420_m1	69
^{166}Er	***cd27***	Co-stimulatory maintenance and survival	Plasma membrane / TNFRSF	Mm01185212_g1	87
	cd28	Co-stimulatory antiviral immunity	Plasma membrane	Mm00483137_m1	68
	vla4b	VLA4 complex, directed into inflammed tissue	Plasma membrane	Mm01253230_m1	75
^{171}Yb	***cd44***	Antigen mature activated cells	Plasma membrane	Mm01277163_m1	83
	vla4a	VLA4 complex, directed into inflammed tissue	Plasma membrane	Mm00439770_m1	69
^{164}Dy	***cd62l***	Stimulation and entry into LN	Plasma membrane	Mm00441291_m1	101
^{143}Nd	***cd69***	Homing	Plasma membrane	Mm01183378_m1	76
	itgae	Lung homing after viral infection w. CD69	Plasma membrane	Mm00434443_m1	69
	itgb7	Gut homing	Plasma membrane	Mm00442916_m1	79
	lamp1	Degranulation	Plasma membrane	Mm00495262_m1	76
	ox40	Co-stimulatory recall memory responses	Plasma membrane / TNFRSF	Mm00442037_g1	64
	41bb	Co-stimulatory survival	Plasma membrane / TNFRSF	Mm00441899_m1	71
	ctla4	Regulates effector functions of CD8^{+} T cells	Plasma membrane	Mm00486849_m1	71
	cd160	Co-inhibitory function	Plasma membrane	Mm00444462_m1	99
	selplg	inflammation/resting cell homing to lympnoid	Plasma membrane	Mm01204601_m1	91
	btla	co-inhibitory molecules (cancer)	Plasma membrane	Mm00616981_m1	71
	icos	Co-stimulatory activation	Plasma membrane	Mm00497600_m1	65
^{159}Tb	***pd1***	Exhaustion, supression and terminally differentially	Plasma membrane	Mm00435532_m1	65
	gitr	Co-stimulatory survival & function	Plasma membrane / TNFRSF	Mm00437136_m1	89
	s1p1	Migration in lymphoid tissues post infection	Plasma membrane	Mm00514644_m1	133
	tim3	Exhaustion (with pd1) during chronic viral infection	Plasma membrane	Mm00454540_m1	98
	tlr2	Proliferation, survival, effector	Plasma membrane	Mm00442346_m1	69
	tlr4	Generating memory CD8^{+} T cells	Plasma membrane	Mm00445273_m1	87
	notch2	Clearance of acute infection with influenza virus	Plasma membrane	Mm00803077_m1	84
	ccl4	Immune modulation	Extracellular space	Mm00443111_m1	70
	#cd70	Co stimulator, ligand for CD27	Extracellular space	Mm00441914_m1	66
	cd40l	Inducer of proliferation, activation	Extracellular space / TNFSF	Mm00441911_m1	120

^{142}Nd	***fasl***	Proliferation and homeostasis (cell death inducer)	Extracellular space / TNFSF	Mm00438864_m1	84
^{144}Nd	***il-2***	Activation	Cytokine	Mm99999222_m1	91
	#il-4	Th0 cells to Th2 cells	Cytokine	Mm00445259_m1	79
	#il-5	Eosiniophil mediated inflammation	Cytokine	Mm00439646_m1	62
	#il-9	Regulating inflammatory immunity	Cytokine	Mm00434305_m1	81
	#il-10	Anti-inflammatory	Cytokine	Mm00439614_m1	79
	#il-13	Th0 cells to Th2 cells	Cytokine	Mm00434204_m1	56
	il-21	Control of persistent viral infections	Cytokine	Mm00517640_m1	67
	#il-22 (Iltifb)	Pro-inflammatory	Cytokine	Mm00444241_m1	86
	#mmp2	Regulate T-cell activation	Extracellular space	Mm00439498_m1	62
	mmp9	Regulate T-cell activation	Extracellular space	Mm00442991_m1	76
^{165}Ho	***ifn-γ***	Stimulation during acute viral infection	Cytokine	Mm01168134_m1	100
^{159}Tb	***tgf-β1***	Regulation	Cytokine	Mm01178820_m1	59
^{162}Dy	***tnf***	Regulation of antiviral T-cell response	Cytokine	Mm00443260_g1	61
^{149}Sm	***traiL***	Killing of virally infected cells	Extracellular space / TNFSF	Mm00437174_m1	83

Appendix 2: CyTOF-1 Mass Cytometry (Fluidigm) 32 metal-labeled antibodies (Ab).

Marker	Isotope	Metal	Vendor	Conjugation	Staining
anti-PE (pentamer)	156Gd	Gadolinium	DVS	DVS pre-conjugated	Extracellular 1
CD3	152Sm	Samarium	DVS	DVS pre-conjugated	Extracellular 1
CD4	145Nd	Neodymium	DVS	DVS pre-conjugated	Extracellular 1
CD8	168Er	Erbium	DVS	DVS pre-conjugated	Extracellular 1
CD11a (LFA1)	172 Yb	Ytterbium	eBiosciense	In house conjugated	Extracellular 2
CD25 (IL-2Rα)	150 Nd	Neodymium	DVS	DVS pre-conjugated	Extracellular 2
CD27	166Er	Erbium	Pharmingen	In house conjugated	Extracellular 2
CD44a	171Yb	Ytterbium	DVS	DVS pre-conjugated	Extracellular 2
CD45	147Sm	Samarium	DVS	DVS pre-conjugated	Extracellular 1
CD62L	164Dy	Dysprosium	DVS	DVS pre-conjugated	Extracellular 1
CD69	143Nd	Neodymium	DVS	DVS pre-conjugated	Extracellular 1
IL-7Rα (CD127)	175Lu	Lutetium	DVS	DVS pre-conjugated	Extracellular 2
FasL (CD178)	142Nd	Neodymium	BioLegend	In house conjugated	Extracellular 2
GzmB	148Nd	Neodymium	eBiosciense	In house conjugated	Intracellular
IFN-γ	165Ho	Holmium	DVS	DVS pre-conjugated	Intracellular
Perforin	153Eu	Europium	eBiosciense	In house conjugated	Intracellular
TNF-α	162Dy	Dysprosium	DVS	DVS pre-conjugated	Intracellular
TGF-β1	170 Er	Erbium	BioLegend	In house conjugated	Intracellular
TRAIL (CD253)	149Sm	Samarium	Pharmingen	In house conjugated	Extracellular 2
KLRK1 (CD314)	158Gd	Gadolium	Pharmingen	In house conjugated	Extracellular 1
KLRG1	167 Er	Erbium	BioXCell	In house conjugated	Extracellular 1
PD1 (CD279)	159 Tb	Terbium	DVS	DVS pre-conjugated	Extracellular 1
IL-2	144Nd	Neodymium	DVS	DVS pre-conjugated	Intracellular
IL-17A	174Yb	Ytterbium	DVS	DVS pre-conjugated	Intracellular
IL-17F	174Yb	Ytterbium	eBiosciense	In house conjugated	Intracellular
Ly6C	141Pr	Praseodymium	BioLegend	In house conjugated	Extracellular 2
CXCR3	154 Sm	Samarium	eBiosciense	In house conjugated	Extracellular 2
CXCR6	169 Tm	Thulium	R&D	In house conjugated	Extracellular 2
CCR4	160Gd	Gadolium	Biolegend	In house conjugated	Extracellular 1
CCR5	176Yb	Ytterbium	eBiosciense	In house conjugated	Extracellular 2
CCR6	146Nd	Neodymium	BioLegend	In house conjugated	Extracellular 2
CCR7 (CD197)	163Dy	Dysprosium	eBiosciense	In house conjugated	Intracellular

Appendix 3.A: Differentially expressed genes (DEG) in T_{EFF} cells at d10p1 and d10p2. Significant genes found in scatterplots (figure 4.4) are shown as bar plots, to observe the frequency of cells expressing the significant genes in aMIV and SAM(H1) groups. Fisher's test, *$p \leq 0.05$, **$p \leq 0.001$.

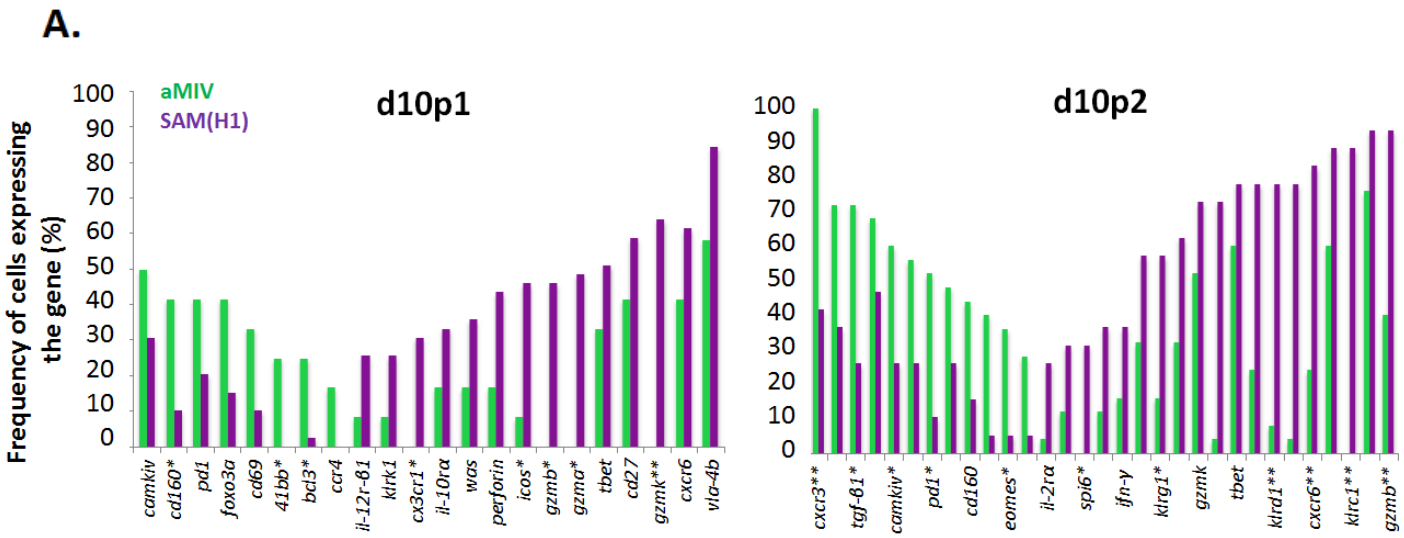

Appendix 3.B: Differentially expressed genes (DEG) in T_{EM} cells at all timepoints. Significant genes found in scatterplots (figure 4.5) are shown as bar plots, to observe the frequency of cells expressing the significant genes in aMIV and SAM(H1) groups. Fisher's test, *$p \leq 0.05$, **$p \leq 0.001$.

B.

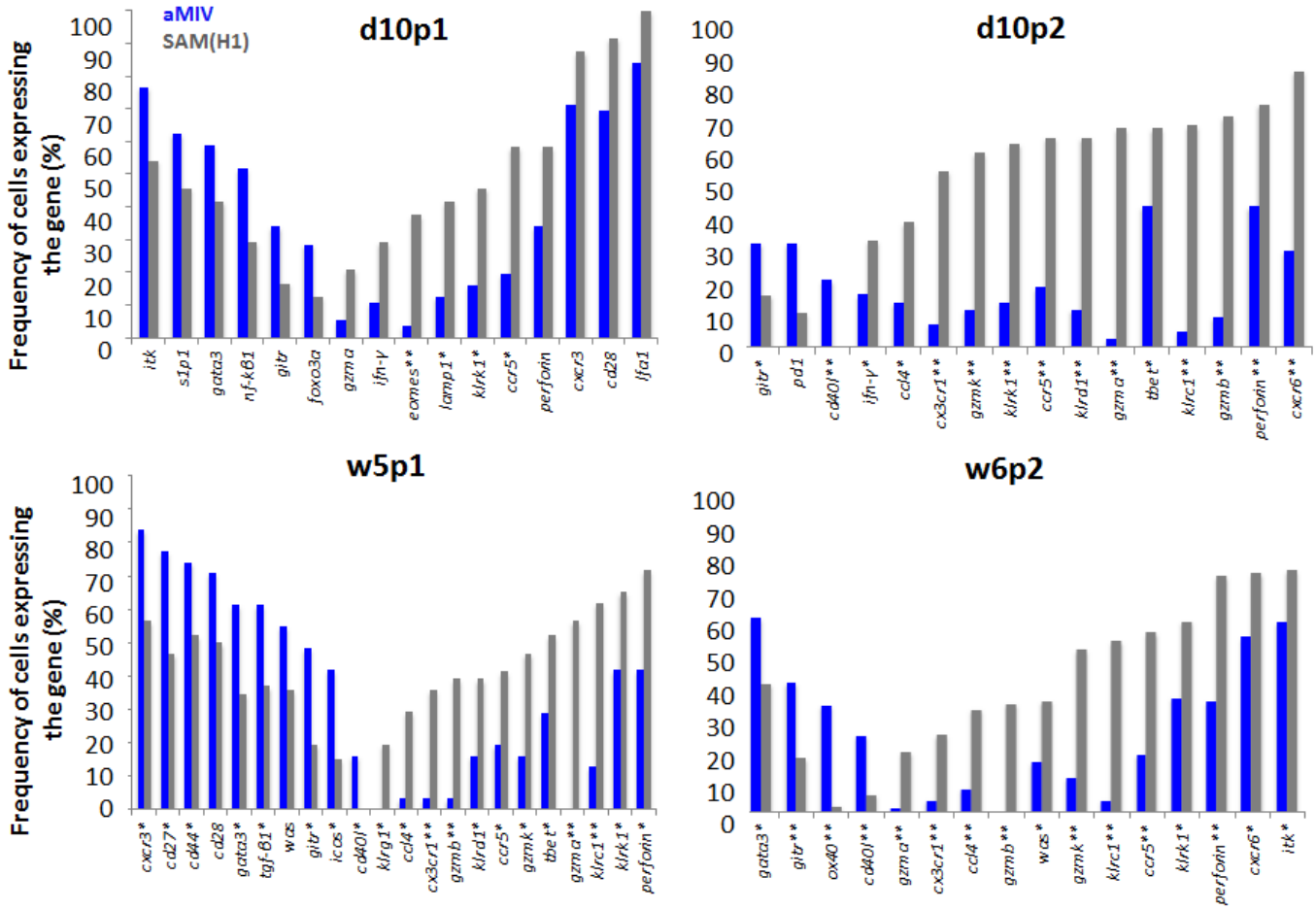

Appendix 3.C: Differentially expressed genes (DEG) in T_{CM} cells at all timepoints. Significant genes found in scatterplots (figure 4.6) are shown as bar plots, to observe the frequency of cells expressing the significant genes in aMIV and SAM(H1) groups. Fisher's test, *$p \leq 0.05$, **$p \leq 0.001$.